ABSTRACT

Title of Document:	SCALE MODELING OF STATIC FIRES IN A COMPLEX GEOMETRY FOR FORENSIC FIRE APPLICATIONS.
	Allison C. Carey, M.S., 2010
Directed By:	John L. Bryan Chair Professor James G. Quintiere, Department of Fire Protection Engineering

Scale modeling can allow fire investigators to replicate specific fire dynamics at a dramatically reduced cost. A gas burner, liquid pool, wood crib, and polyurethane foam block are used to represent the wide range of fuels that investigators encounter. These fuels are classified into two groups: the burner and liquid pool that reach a semi-immediate steady state (static fires) and the crib and foam that have a fire spread and growth period (dynamic fires). This research examines the proposed scaling method for the static fires. The enclosure consists of a large corridor that provides an interesting challenge due to the presence of partitions at the ceiling. The design fires and the model enclosure are designed based on Froude scaling derived from conservation equations. The eight various sized fires demonstrate acceptable scaling results in the prediction of flame height and temperature at various elevations in the enclosure.

SCALE MODELING OF STATIC FIRES IN A COMPLEX GEOMETRY FOR FORENSIC FIRE APPLICATIONS.

By

Allison C. Carey.

Thesis submitted to the Faculty of the Graduate School of the
University of Maryland, College Park, in partial fulfillment
of the requirements for the degree of
Masters of Science
2010

Advisory Committee:
Professor James G. Quintiere, Chair
Professor Andre Marshall
Professor Peter Sunderland

Acknowledgements

I would like to thank the Department of Justice for funding this research. The past five years as an undergraduate and graduate student in the Department of Fire Protection Engineering has been the most rewarding time of my life. Thank you to all the professors who have helped shape my future at the University of Maryland, especially my committee members Dr. Peter Sunderland and Dr. Andre Marshall. A special thanks and appreciation goes to my advisor, Dr. James Quintiere. The countless hours with Dr. Quintiere not only helped my research efforts, but they also formed my deep understanding of fire dynamics and principles. His unrelenting patience and support has molded so many professionals in the past, and I am lucky to be his student. Thank you to the Bureau of Alcohol, Tobacco, Firearms, and Explosives, especially Dr. Dave Sheppard, for allowing us to share their lab space and experimental data.

I would also like to thank my fellow students. It was a pleasure to share the full scale experiments with Charles Chan and Tom Layton. Their impeccable attention to detail and observation made replicating these experiments that much easier. Constructing my precise model and conducting my experiments would have been impossible without the help of Justin Worden, thank you!

Finally, I would not be where I am today without my amazing family. Mom, Dad, Matt, and Shelly have provided me with unwavering love and support. All of my hard work is a credit to everything they have done for me. I love you all.

Table of Contents

Nomenclature

A_s	Area of Thermocouple Bead
A_o	Exposed Surface Area of the Wood Crib
A	Vertical Shaft Area within the Wood Crib
c_p, c	Specific Heat
c_w	Specific Heat of Boundary
C	Material Constant for Wood Crib Design
D	Diffusivity
D_c	Diameter of the Wood Crib Sticks
E	Full Scale Values (for Uncertainty)
ΔE	Full Scale Temperature Rise
Fr	Froude Number
g	Gravity
Gr	Grashof Number
H	Enclosure Height
ΔH_c, Δh_c	Heat of Combustion
h_c	Convective Heat Transfer Coefficient
k	Conductivity of Gas
k_w	Conductivity of Boundary
ℓ	Dimensionless Length Scale
l	Length of the Wood Crib
M	Scale Model Values (for Uncertainty)
ΔM	Scale Model Temperature Rise
m	Mass
$\dot{m}$	Mass Flow Rate
$\dot{m}''$	Mass Flow Rate per Unit Area
$\dot{m}_f^*$	Dimensionless Mass Flow Rate of Fuel
Nu	Nusselt Number
n	Number of Sticks in the Wood Crib
P	Porosity
Pr	Prandtl Number
p	Pressure
p_R	Reference Pressure
$\hat{p}$	Dimensionless Pressure
$\dot{Q}$	Heat Release Rate
Q^*	Dimensionless Heat Release Rate
q_R''	Radiative Heat Flux
Re	Reynold's Number
s	Spacing Between Sticks
T	Gas Temperature
T_w	Boundary Temperature
T_∞	Ambient Temperature

ΔT	Gas Temperature Difference
t	Time
t_R	Reference Time
$\hat{t}$	Dimensionless Time
Δt	Sampling Period
u	Flow Velocity
u_R	Reference Flow Velocity
$\hat{u}$	Dimensionless Flow Velocity
V	Volume
x	Linear Distance
x_w	Boundary Distance
$\hat{x}$	Dimensionless Linear Distance
$\hat{x}_w$	Dimensionless Boundary Distance
Y_i	Species Yield
$Y_{i,\infty}$	Ambient Species Yield

Greek

μ	Dynamic Viscosity
υ	Kinematic Viscosity
κ	Absorption Coefficent
Π_i	Dimensionless Pi Group
σ	Stephan-Boltzmann Constant
ε	Emissivity
ε_g	Gas Emissivity
θ	Dimensionless Temperature
ρ	Density
ρ_w	Boundary Density
ρ_∞	Ambient Density
$\hat{\rho}$	Dimensionless Density
τ	Dimensionless Time
δ_w	Boundary Thickness

List of Tables and Figures

1. Introduction

In past decades, scale models have been utilized in numerous fields. From civil to aerospace engineering, scale models demonstrate how a final product may perform. Models have been used to visualize interactions between various parts of a design, to experiment with different design ideas, and to improve the overall product [1]. They offer engineers an additional way to analyze and understand phenomena. In order to create a representative scale model, equations applying the conservation of mass, momentum, chemical species, and energy are reviewed. Dimensionless parameters are extracted to show the relationship between the actual and the scaled model. These dimensionless groups are the key to building an accurate model. If they do not encompass the physics of the full scale prototype, the model will not accurately predict the desired phenomena. Additionally, not every dimensionless group can be satisfied simultaneously. The main idea of scale modeling is to obtain reasonable accuracy from practical approaches. This is the art of scaling [2]. Errors may arise in scale modeling because it is impossible to match all dimensionless groups. By minimizing these errors through the art of partial scaling, the scale model becomes a more accurate way to predict behavior in the full scale scenario.

Scale modeling has been applied in transportation, power, structural, material, and environmental areas. For example, wind tunnel tests are used to examine the dynamic effects of wind-induced vibrations on long-span bridges and high-rise buildings [3]. It has also been utilized in fire research. In this research, scale modeling has been used to characterize static fires in a complex geometry. Fires have the ability to cause severe damage to manmade structures, especially when contained in an

enclosure. There is a growing need to further understand enclosure fire dynamics, particularly in complex geometries. Full scale research is costly when trying to simulate fires in large buildings or with extensive fuel loads. By using scale modeling, fire can be studied without the significant time or monetary cost limitations. Additionally, scale modeling can be applied where the building or enclosure no longer remains. Forensic fire investigation can benefit from scale modeling by allowing fire investigators to replicate and study the fire dynamics within a particular enclosure. Using various scaling techniques, the fire can be characterized and the effects on the surrounding enclosure can be observed.

One of the earliest examples of fire scaling in research can be traced to Rosin [4] in 1939, who used dimensionless groups to physically model domestic fireplaces. Other notable scientists have discussed the merits of scale modeling: Spalding [5] indicated the benefit of partial scaling in combustion, Williams [6] noted more than 28 independent dimensionless groups apply in combustion, and Thomas [7] emphasized that scaling in fire is an art of selecting the proper groups to characterize the fire. Enclosure fires are of particular interest to this study since the overall goal is to apply physical scaling methods for fire investigations. In particular, scale modeling can be used to reproduce burning rates, temperatures, heat fluxes, and gaseous species.

Modeling requires an in depth understanding of fire physics. Scaling a particular fire begins with assessing the governing conservation equations and selecting the appropriate dimensionless groups. One major obstacle is the extent of existing information about the fire. If the fire size, or heat release rate of the fire, is

known, then certain dimensionless groups can be used with ease. The engineer will scale the fire based on this heat release rate. However, many fires exhibit a growth period where the exact heat release rate as a function of time is unknown. The burning of the fuel can change with oxygen concentration, radiation effects, the area of the fire, and the specific fuel properties; all of these factors complicate how a fire is scaled [8]. An investigator would need to understand the fire dynamics involved with their case to select the dimensionless groups that would characterize that specific fire. For example, a static fire such as a liquid fuel spill can be modeled based on the heat release rate where radiation is neglected. However, radiation plays a key role in dynamic fires where flame spread and re-radiation from the enclosure occurs, such as the flame spread across a mattress. Therefore, the dimensionless groups considered in each of these cases would vary.

This work will serve as a foundation for fire investigators to use scale modeling as a research tool in their cases and litigation efforts. First, static fires where the heat release rate is known will be examined and scaled. In this portion of the research, full scale experiments with various fuels were conducted. The full scale experiments were conducted in a wide, complex geometry at the Bureau of Alcohol, Tobacco, Firearms, and Explosives in Beltsville, MD. Partitions extended 0.6 meters down from the ceiling throughout the enclosure to create a total of twenty bays. This configuration limited the spread of hot gases and smoke since the ceiling jet was contained in the bays. The general scaling methodology presented addresses the key roles of convection in the full scale experiments. This research concentrates on the scaling of a gas burner and a liquid pool fire. These simple, static fires are used as a benchmark

for developing a scaling theory that can be used for fire investigations. They also serve as controlled fuels that may be similar to fuels found at a fire scene. Full scale data has also been collected for a wood crib and blocks of polyurethane foam. In the full scale High-Bay test series at ATF, temperature, velocity, optical density, and smoke detection were measured.

Early convection played a role in this research. After the full scale experiments, a scale model was constructed based on the selected dimensionless groups. The fires were replicated in the small scale. After the static fire scale theory has been successfully applied, dynamic fires including flame spread will be explored in the same complex geometry. Finally, the scaling theory will be applied to various configurations, including an enclosure that eventually reaches flashover. Additional full scale data is available for complex geometries, such as a two-story building and a room reaching flashover. A two-story configuration would be used to develop conduction and convection models and a post-flashover room can develop radiation scaling for various scenarios. These examples may be used in future research efforts.

This research presents a review of scaling theory used in fire research. Scaling rules for design fires and enclosure material boundaries are derived and presented. Full scale testing of a gas burner, heptane pool fire, pine wood crib, and polyurethane foam is described. The scaling theory is applied to the full scale scenario and a ⅛ scale compartment is constructed. The gas burner and pool fires tests are run in the scale model. The accuracy of the scale model compared to the full scale data is discussed.

2. Background

The following discusses various fuels used in scale modeling and their relevance to fire investigators. Successful past examples of scaling theory are outlined and later related to the theory presented in this paper. In addition, suggestions for the fire investigator with respect to scaling are provided.

2.1 Importance of Fuel Packages

2.1.1 Previous Fuels Used in Modeling

The key to scale modeling is to understand and represent the fire dynamics. This can become very complex depending on the type of fire. The size, flame height, heat flux, soot production, and growth rate of the fire are all aspects that must be considered. The interaction between the fire and the surroundings is also important. A deep concrete slab could act as a heat sink whereas a sooty wall may increase re-radiation. In general, scale modeling must try to match the heat release rate of a fire. This is done depending on the fuel, but it generally leads to similar fire behavior. The duration of the fire trial is important between the full scale and the model. Some modeling efforts keep time the same between the large and small scales while others shorten the time for the scaled model. All of these parameters are selected according to the scaling methodology and the researcher with some approximations. With so many variables to account for, scale modeling becomes an art of accurately representing the full scale fire.

Scale modeling uses various fuels to represent the specific load as accurately as possible. For example, an office building with boxes and papers may be

represented using wood cribs, but this is a challenge. A gas burner could also be used, but controlling the mass flow rate of the gas becomes very important. Fires can be modeled using a wide variety of scenarios. The key to selecting the fuel is to choose fuels that are representative of the fire size and flame temperatures in the actual fire. This way, the scale model has the highest probability of reproducing the same temperatures, heat fluxes, burn patterns, etc. as the full scale [6]. Gas burners, liquid fuel, and wood cribs have all been used in successful examples of scale modeling. It is important to realize each fuel is applied to the scaling theory in a different way, but the overall concepts are the same. In the method of scaling used for this research, the dimensionless heat release rate is matched between the full scale and the model scale. A gas burner can be scaled geometrically; the size of the burner acts linearly with the scale of the model. The flow rate of the gaseous fuel is adjusted based on a dimensionless heat release rate that is calculated using the full scale data. The heat release rate of a pool of flammable liquid is dependent on both the diameter of the pool and the amount of fuel (depth). The diameter is scaled based on the dimensionless mass loss rate of the fuel and the amount of fuel is calculated using the diameter and the dimensionless heat release rate. Wood cribs are also scaled to a dimensionless heat release rate, but the primary factors that change are the spacing of the sticks, the size of the sticks, and the number of sticks. When scaling wood cribs, it is important to consider the porosity of the wood crib. If the sticks are too far apart, they will burn individually. However if they are too close together, the crib will not have proper ventilation to achieve pyrolysis of the sticks. Gross and Robertson [9]

experimented with scaling wood cribs. They attempted to match the Froude number based on their recognition that the fire plume flow was governed by buoyancy.

$$Fr = \frac{u}{\sqrt{g\ell}} \tag{2.1}$$

The compartment was geometrically scaled, but the boundary materials remained the same between the full scale and model. This became a source of error later in the research when their results from various scales did not compare well [9]. This is a prime example of the necessity to select appropriate dimensionless groups. Proper scaling of wood cribs will be explored in future experiments. Polyurethane foam has not been widely used in scale modeling. It is important to capture the behavior of the foam and the resulting fire dynamics through the dimensionless groups.

2.1.2 Relevance of Fuels to Fire Investigators

Fire investigators must understand the relationship between various scaling fuels and the fuels found in their specific cases. This can be very difficult, especially at a scene where the majority of the fuel has been consumed by the fire or destroyed by fire fighting measures. Instead of trying to scale the numerous types of fuels that can be found in enclosures, it is up to the investigator to determine which reliable scaled fuels can be used to represent the fuel load. For example, an armchair can be represented using a wood crib designed to reach a specific heat release rate. If the heat release rate of armchair is known, a wood crib can be designed based on this parameter. An investigator needs to decide which aspect of the fire is the priority in scale modeling. While a wood crib may produce a similar fire size, the products of combustion would surely be different between the foam armchair and the wood.

The scope of this project includes scaling gas burners, flammable liquid pools, wood cribs, and blocks of polyurethane foam (PU foam). A gas burner provides a standard to check the scaling theory, a liquid pool can represent an accelerant used in arson, a wood crib is similar to furniture, and PU foam promotes spread and growth comparable to a mattress or sofa. Given the tools in this project and future research, a fire investigator can apply scaling theory to recreate some fire scenarios.

2.2 Successful Examples of Scale Modeling

These examples of scale modeling describe how various researchers have applied the dimensionless groups. It is interesting to note that, while some slight differences exist; most studies have applied dimensionless groups similar to the general scaling theory. The type of fire and environmental conditions do play a role in the selection of the dimensionless groups, which generally address position, velocity, time, heat generated (or heat release rate), the boundary behavior, the fuel behavior, and radiation.

In most laboratory experiments, the heat release rate of the full scale experiment is known. In a forensic setting, the materials in the fire must be researched and modeled in order to accurately model the burning rate.

2.2.1 Corridor Fire Conditions

Quintiere, McCaffery, and Kashiwagi [10] scaled a corridor subjected to a room fire. The experiments consisted of a $1/7^{th}$ geometric scale with a gas burner as the fuel source. Over the course of the 30 minute experiment, the heat release rate of the burner was manually adjusted to maintain the same fire behavior as in the full scale

experiment. The duration of the experiment was the same in the full and model scale experiments. Manually adjusting the heat release rate ensured the fire events occurred at the same time in both size enclosures. This method is appropriate in this case because early convection is not imperative to the overall study. Overall, the gas temperature and the velocity scaled well (see Figure 2.1).

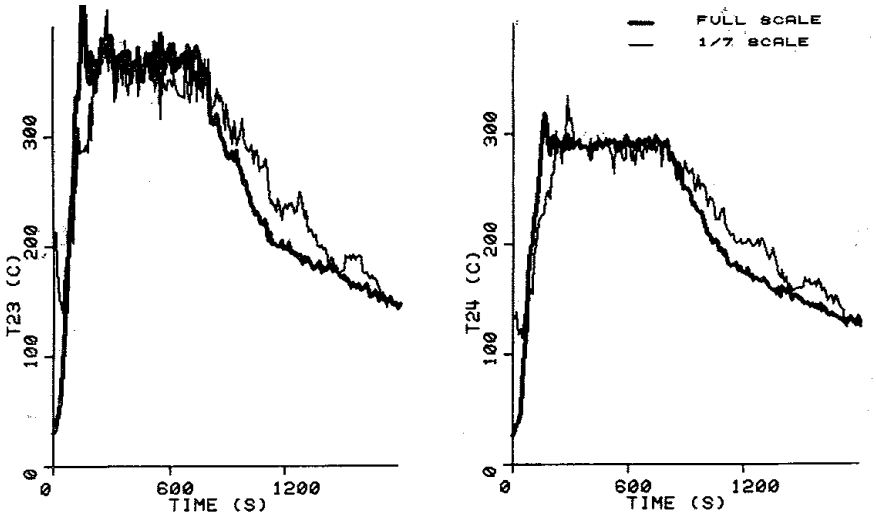

Figure 2.1: Quintiere, McCaffery, and Kashiwagi Gas Temperatures [10].

The gas velocity measured in the scale model was slightly higher than the velocity measured in the full scale experiments. When time is scaled as a burn time, time lags due to flow are not accounted for in the scale model. This had minimal impact in this experiment; however it could play a large role in tests where automatic detection and suppression are factors. The velocities depicted in Figure 2.2 are considered to agree reasonably well for a scale model.

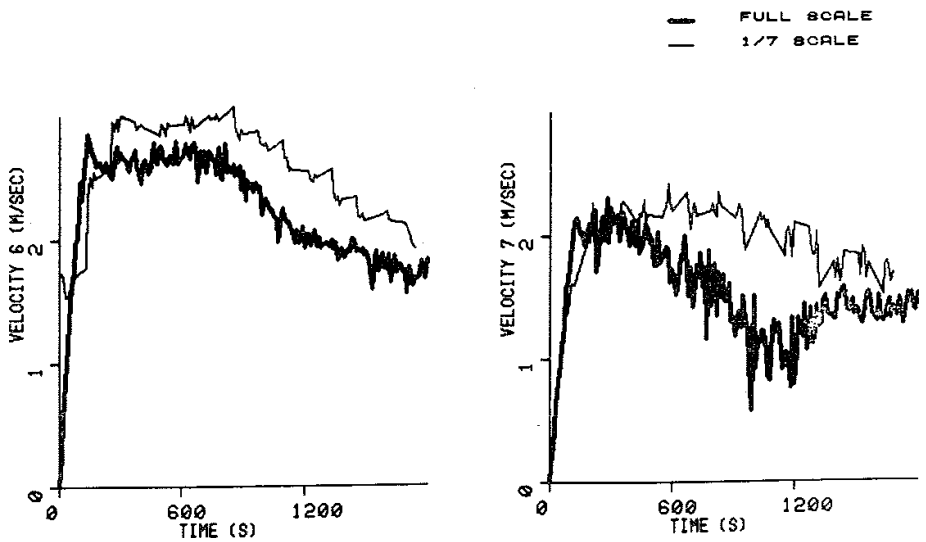

Figure 2.2: Quintiere, McCaffery, and Kashiwagi Gas Velocities [10].

While the temperatures of the gas in the enclosure scaled well, the surface temperatures were higher by a factor of two in the full scale test than in the scale model (see Figure 2.3). Additionally, the total heat flux measurements were higher in the full scale test than in the model.

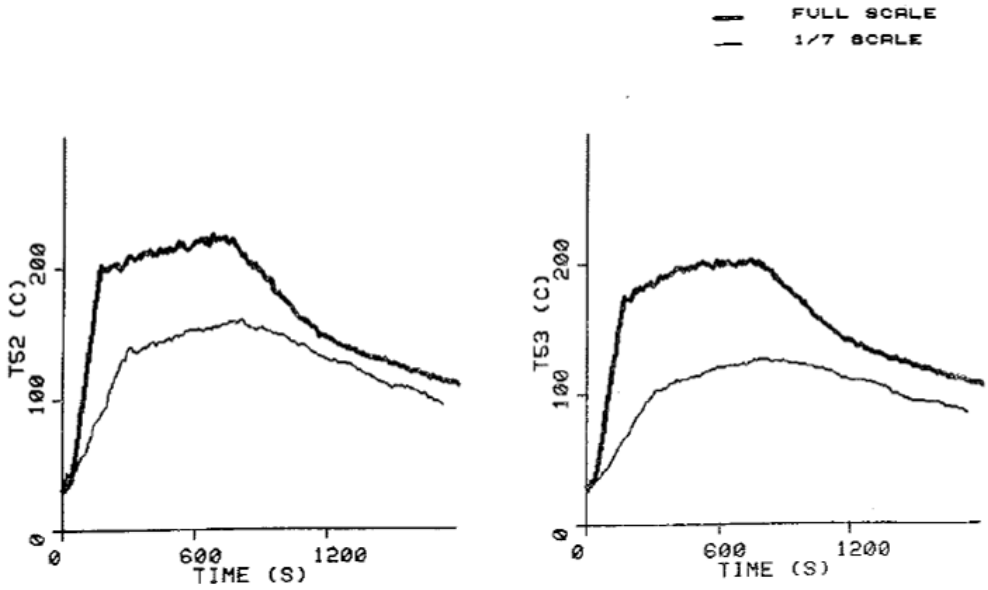

Figure 2.3: Quintiere, McCaffery, and Kashiwagi Surface Temperatures [10].

The fact that the fire was larger over the same period of time in the full scale experiment meant that more flame and smoke radiation affected the surrounding enclosure.

2.2.2 Initial Ceiling Jet

Heskestad [11] conducted a study of initial convective flow generated by a fire. The main goal of this research was to apply scaling to fire detection. Only turbulent flows were considered. The experiments observed steady fires, where fire growth to steady-state was almost instantaneous, and quasi-steady fires, where the heat release rate varies either slowly with time or as a function of time to the n^{th} power. Liquid pools were used to model the steady fires. Wood cribs were used to model the quasi-steady fires. The tests were conducted in two different enclosures. One enclosure had 0.31 meter partitions at the ceiling. The other configuration had a flat ceiling. Similar to Quintiere, McCaffery, and Kashiwagi [10], time remained the same between the full scale and model experiments. Heskestad developed a scaling theory where the velocity and temperature were scaled based on the heat release rate. This method is valuable since his equations can be applied to various scale sizes, along with the full scale experiment. The data collapses using these equations and direct comparisons can be made. Figure 2.4 employs Heskestad's dimensionless groups. Several measurements under diverse conditions are well correlated.

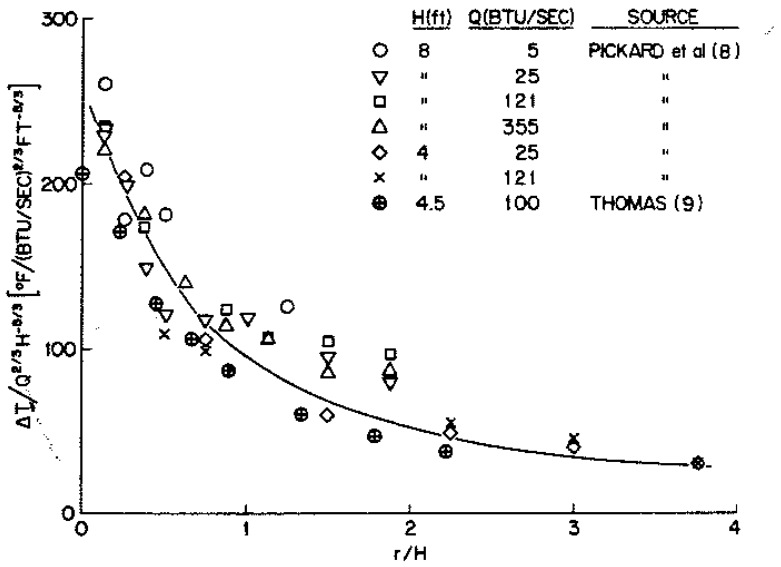

Figure 2.4: Heskestad's Dimensionless Groups Applied to Various Fires [11].

In this application, Heskestad does not include boundary scaling or radiation. In some cases, radiation and boundary scaling are an important part of the modeling process to ensure similar heat transfer in the model when compared to the full scale experiment. Other parameters that scaled well include the velocity of the gas and the concentration of various products of combustion. The ceiling contours did affect the detection response in the scale models for steady fires. It was observed that the initial smoke front arrival time in the ceiling bays were insensitive to fire size for the power-law fires.

2.2.3 Wood Crib in an Enclosure

Heskestad [12], and later, Croce and Xin [13], scaled wood crib fires in enclosures. In these studies, peak averages were used, so transient data was not presented. However, the burn time (defined by t_R) of the wood crib was included in the dimensionless groups pertaining to boundary scaling. The time in these experiments was the same between the full and model scales. One influential scaling factor is the porosity of the crib, which had a direct impact on the heat release rate

produced. Block developed the concept of porosity using the theory of burning of densely packed wood cribs [14]. Porosity is a measure of stick spacing and placement, with an optimal value of about 0.06. The porosity can be defined as:

$$P = (sD_c)^{1/2}\frac{A_o}{A} \tag{2.2}$$

Where s is the stick spacing, D_c is the diameter of the stick, A_o is the exposed surface area of the crib, and A is the vertical shafts area within the crib. Figure 2.5 displays the crib porosity and burning rate results from Croce's experiments.

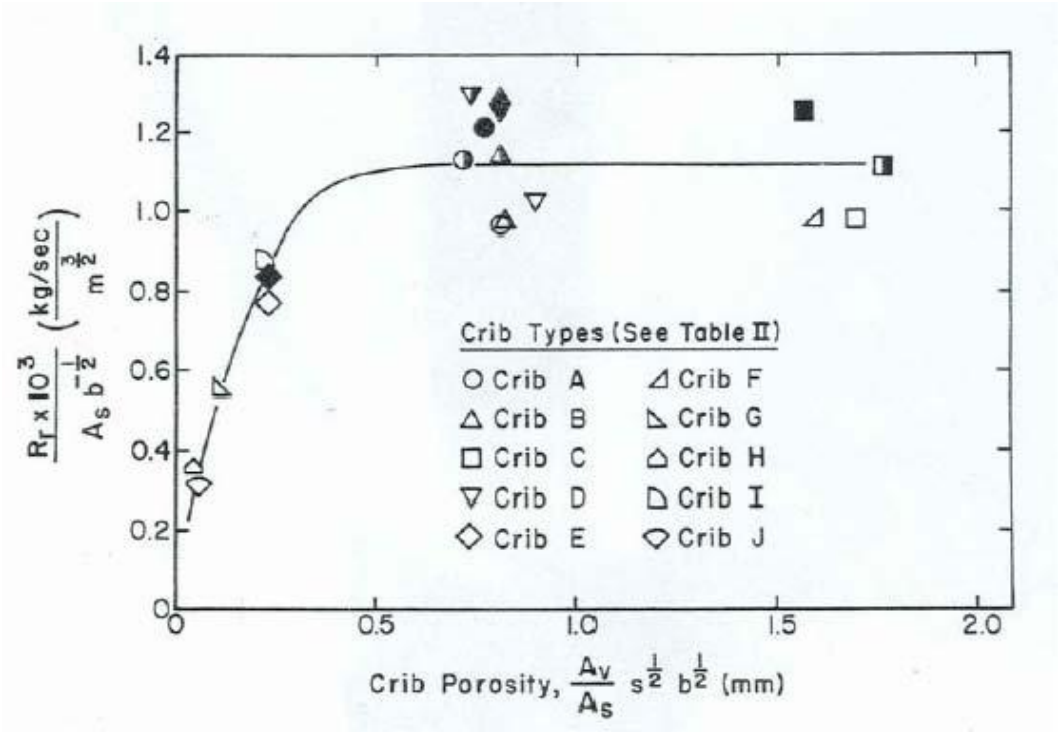

Figure 2.5: Croce's Crib Porosity and Burning Rate Experimental Results [13].

If the sticks were too close together, the fire would not sustain on the crib as a whole due to underventilation. If the sticks were too far apart, the sticks would burn individually instead of as an entire crib. The free burning rate of wood cribs was found to be related to the porosity factor [2]:

$$\frac{\dot{m}}{A_o D_c^{1/2}} = f(P) \tag{2.3}$$

Since ventilation factors changed the burning behavior, only scenarios with large ventilation factors were studied. The dimensionless groups used by Heskestad and Croce are outlined below. Radiation is ignored. The burn time follows $t_R \sim b^{3/2}$, where b is the thickness of the sticks in the wood crib. The general scaling laws of the research can be described by:

$$\left[\frac{T-T_\infty}{T_\infty}, Y_i, \frac{\dot{m}_{crib}}{\dot{m}_{free}}\right] = \left[\frac{x}{\ell}, \frac{t}{t_{burn}}, P, \frac{k_w t_{burn}}{\delta^2 \rho_w c_w}, \frac{T_\infty k_w}{\dot{q}''_{wall} \delta_w}\right] \tag{2.4}$$

where the temperature, species, and mass loss ratio are dependent on the position, time, crib porosity, and thermal boundary scaling. The equations used by Heskestad and Croce to scale the thermal properties of the boundaries are:

$$\frac{\ell^{19/8}}{\delta_w \rho_w c_w} = \text{constant} \tag{2.5}$$

$$\frac{k_w}{\delta_w \ell^{1/2}} = \text{constant} \tag{2.6}$$

Heskestad and Croce's enclosure had a vent opening, which also affected the burning of the crib through ventilation. For ¼ scale, ½ scale, and full scale, the dimensionless groups yielded generally well correlated results for both gas temperatures (Figure 2.6) and wall temperatures (Figure 2.7).

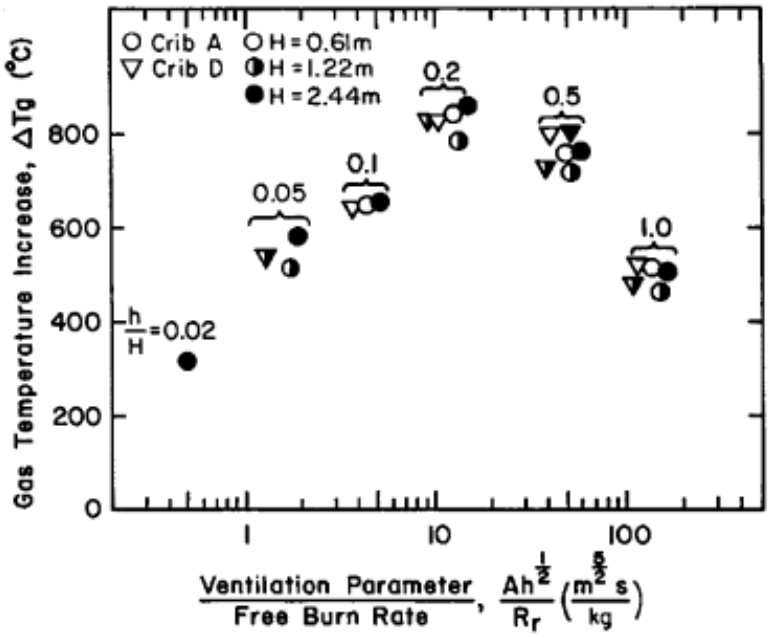

Figure 2.6: Heskestad and Croce's Gas Temperature Increase for Various Scales [13].

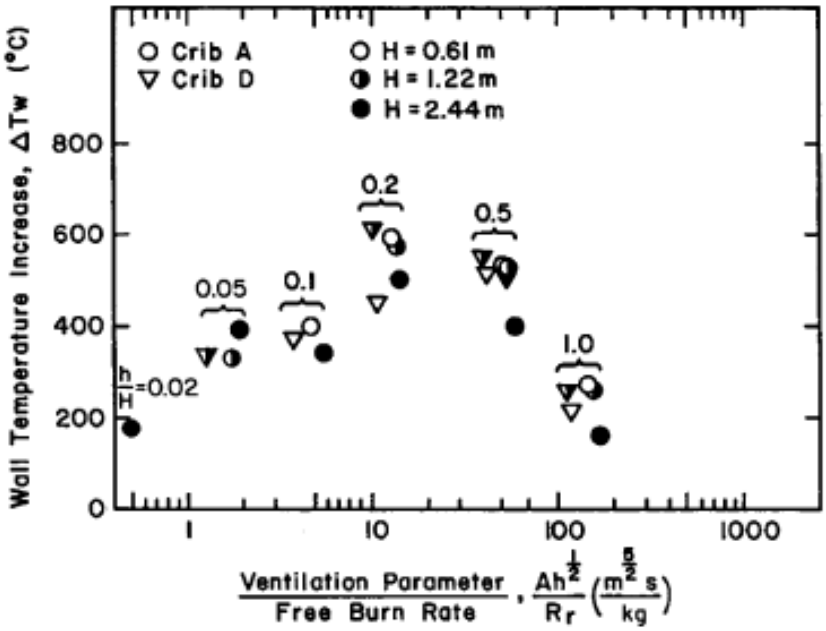

Figure 2.7: Heskestad and Croce's Wall Temperature Increase for Various Scales [13].

Good agreement between the model and full scale experiments were also recorded for concentration of oxygen, carbon monoxide, and carbon dioxide. The inaccurate scaling of the wall thickness affected some of the results.

2.2.4 Wood Cribs in an Enclosure II

Perricone [15] studied wood cribs in an enclosure and the response of structural elements in a fire. He conducted ⅛, ¼, and ⅜ scale model experiments where additional scaling of insulated loaded structural frames provided an estimate of thickness and thermal conductivity of structural fire proofing. Perricone reduced the duration of the scaled experiments by a factor of $t \sim \ell^{1/2}$ in order to accurately capture flow behavior in the experiments. This treatment of time is referred to as flow time scaling. The boundaries used by Perricone were scaled in terms of thickness, conduction, and convection. The following equations were used to scale the boundaries.

$$\Pi_{w,\delta} = \frac{\delta g^{1/4}}{\left(k/\rho c\right)_w^{1/2} \ell^{1/4}} \tag{2.7}$$

$$\Pi_{w,c} = \frac{h_c \ell^2 T_\infty}{\rho_\infty c_p T_\infty \sqrt{g}\, \ell^{5/2}} \tag{2.8}$$

$$\Pi_{w,k} = \frac{\left(\frac{k\rho c}{t_R}\right)^{1/2} \ell^2 T_\infty}{\rho_\infty c_p T_\infty \sqrt{g}\, \ell^{5/2}} \tag{2.9}$$

Perricone assigned $h_c \sim \ell^{1/5}$. This assumes turbulent behavior since the convective heat transfer coefficient is found through the relationship of the Nusselt number to the turbulent Reynold's number. Radiation was considered through scaling the emissivity of the gas compared to black body radiation. This played a significant role since Perricone was not only trying to replicate the fire dynamics, but also the response of the structural elements around the fire. In general, Perricone's scaling methods

yielded good agreement in the results. He found that the key to transient scaling is the direct link between the characteristic time and the characteristic length scale [15]. As seen in Figure 2.8, the gas temperatures were matched very well between various scales. His success supports the use of flow time as an independent variable for the modeling of various fuels in enclosures.

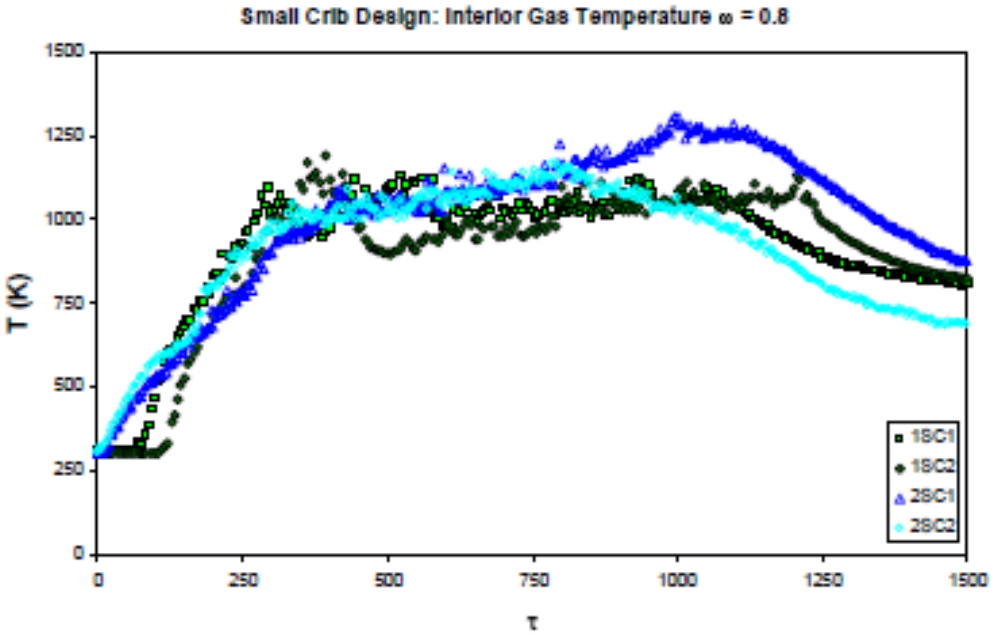

Figure 2.8: Perricone's Gas Temperature Increase for Various Scales [15].

Perricone also achieved good results for the mass loss of the crib, the incident radiant heat flux to the boundaries, and the temperature of the structural elements.

2.2.5 Conclusions from Past Experiments

Numerous scaling methods have been successful in the past. The type of fire dictates which scaling methods will yield the most accurate results. The selection of the various dimensionless groups presented above should be considered based on the full scale situation. For example, pool fires provide a relatively constant heat flux to the enclosure, but their size affects the optimal scaling method. For smaller diameter fires, the burning rate of buoyancy-controlled turbulent pool fires is governed by

natural convection rather than by radiation [16]. Therefore, these studies can be compared to the general scaling methodology for convection driven fires. However, large diameter pool fires are controlled by radiation and therefore require additional scaling of the emissivity terms. It has been shown that a burn time scaling is successful for enclosure fires where a small time lag will not affect results and radiation plays a role in the fire development. Flow time scaling is ideal when the primary mode of heat transfer is convection and the flow of gases throughout the enclosure can be considered turbulent. In the following sections, a flow time scaling method is applied to various fuels to develop an optimal scaling method of static fires for fire investigators.

2.3 Scale Modeling for the Investigator

Physical scale modeling is a science applied to a scaled structure to predict full scale parameters. It has been used to predict temperature rise, heat release rate, detection behavior, and suppression response, among others, for a large scale fire. Scaled models can utilize fire and saltwater experimental results to calculate the full scale values. In this discussion, physical fire scale modeling is described for various scenarios to display how to use basic modeling principles in a related forensic setting. Note that this discussion is limited to non-spreading enclosure fires. Additional information for modeling fire spread within an enclosure is currently being researched.

Using scale modeling to represent full scale fire behavior requires a general understanding of the variables matched between the full scale experiment and the model test. Dimensionless groups are utilized in this process. They are used to obtain

variables for the full scale based on the small scale model and vice versa. It is impossible to keep all of these groups consistent between the full scale and small scale experiments. Instead, a few key groups are chosen depending upon the fire scenario. These dimensionless groups are used as a correlation between the full and model scale experiments. Values from the full scale or the model scale must be known to apply these relationships. For example, the thickness of the boundaries is scaled using the thermal properties and the characteristic length scale of the full scale and the model:

$$\frac{\delta_{\text{model}}}{\delta_{\text{full}}} = \frac{\left(\frac{k}{\rho c}\right)_{\text{model}}^{1/2} \ell_{\text{model}}^{1/4}}{\left(\frac{k}{\rho c}\right)_{\text{full}}^{1/2} \ell_{\text{full}}^{1/4}} \tag{2.10}$$

The conductivity, k, and the density, ρ, are material properties that vary similarly with the scale factor. The specific heat, c, remains the same since most materials have a specific heat of about 1. Therefore, using a ⅛ scale, the thickness of the boundaries in the model related to the boundaries in the full scale experiment becomes the ratio of ℓ_{mod} to ℓ_{full}, or $\ell^{¼}$ where ℓ is ⅛:

$$\delta_{\text{model}} = 0.594\delta_{\text{full}} \tag{2.11}$$

The principles in this example can be applied to the dimensionless Π groups when scaling as long as the assumptions are stated. The type of fire can limit the use of this general application of dimensionless groups.

a. Convection Driven

Convection driven fires are predominant for localized burning of a room pre-flashover [16]. The fire may be limited to a burner or piece of furniture. This includes

enclosure fires leading up to flashover. Convection plays a large role in the flame height and energy release of the fire. These models are simpler to scale than radiation driven fires. However, the fuel source must be analyzed precisely to simulate full scale behavior. This can be done using various fuels in order to obtain the most accurate results. The general description of scaling can be applied to convection driven fires. This research describes convection driven fires fueled by natural gas burners and heptane liquid pools burning in an enclosure.

b. Radiation Driven

Radiation driven fires describe global burning of a room. This includes pre-flashover and post-flashover fires. The radiative components of fire spread include radiation from the fire to the surrounding environment, the emissivity of various components of the fire (enclosure walls, smoke layer, etc.), and re-radiation to the fire. The biggest challenge in modeling radiation driven fires is the changing the emissivity of various components, such as the smoke layer and the enclosure boundaries [8]. The emissivity, ε, is a function of the absorption coefficient, κ, of the flame, as seen in the following relationship [8]:

$$\varepsilon \approx 1 - e^{-\kappa \ell} \tag{2.12}$$

This relationship can be applied for the gas or flame. Convection driven scaling methods require the temperature of the fuel surface and the gas temperature to remain the same as the scale changes. However, the emissivity of the flame and smoke change with scale, making the fuel and gas temperature inconsistent with one another. This transition means radiation must be taken into account and the emissivity requires its own dimensionless relationship. Without knowing how to scale emissivity, the

radiation effects of the fire to the surrounding environment are unknown. Even a general approach to scaling emissivity does not account for the view factor between the fuel and the surrounding boundaries. A view factor represents the proportion of radiation that leaves one surface and strikes another [17]. Realistically, the view factor between a fire and the surrounding environment is not close to one. The emissivity correlation discussed above assumes that the radiation and re-radiation between the environment and the fire is equal. In other words, the fire and the environment act as two parallel infinite plates. The fact that this does not occur in actual fires makes it even more difficult to scale emissivity in a forensic fire setting. The view factors must be represented as an additional dimensionless group when modeling radiation [18]. Therefore, fires that are driven by flame spread and radiation cannot be scaled using the general scaling relationships.

3. Scaling Methodology

The methodology for developing the scaling relationships and relevant dimensionless groups follows an analysis of the full governing equations and boundary conditions. This approach follows the basic equations as presented in Quintiere [16]. The principal features and assumptions of the scaling procedure are stated below:

- The Reynolds number (*Re*) is maintained large enough to assure turbulent flow, and terms associated with $1/Re$ in the equations are ignored in the body of the flow field. The requirement to insure turbulent flow in natural convection is $Re > 10^5$ [17].

- Construction of solid combustible materials will be scaled to preserve appropriate heat transfer behavior.
- Fire power and flow rates will be scaled according to gravity and time.
- The inertia and buoyant forces dictated by the Froude number are dominant and the viscous forces dictated by the Reynold's number are considered negligible. This is called Froude modeling.

Scale modeling is developed from the full governing conservation and state equations with particular attention to the initial and boundary conditions. By approximately making these equations dimensionless, the scaling relationships emerge. In general, scaling seeks to reproduce the flow field velocities, temperatures, and species in a fire at corresponding positions and times. Somehow the dynamics of the fire release of energy and species must be reproduced. The approach here is to consider the governing equations in their simplest form. The dimensionless variables are scaled in terms of fixed reference volumes and geometric scale length, ℓ. This scale factor is used in the dimensionless equations as a ratio between the full and model scale. For instance, a ⅛ scale model has a geometric scale length of 1 for the full scale and 8 for the model scale. The length scale to compare the full scale to the model scale is therefore ⅛. In the following sections, each partial differential equation is made dimensionless using this scale length to reveal the dimensionless groups, labeled as Π groups. A select number of Π groups are used in physical scale modeling depending on the scenario being modeled. For this research, the scenario includes static gas burner and liquid pool fires where the heat release rate of the fire is known. The dependent and independent dimensionless variables are listed below.

Dependent Dimensionless Variables

Temperature: $\theta = \frac{T - T_\infty}{T_\infty}$

Density: $\hat{\rho} = \frac{\rho - \rho_\infty}{\rho_\infty}$

Pressure: $\hat{p} = p / p_R$

Velocity: $\hat{u} = u / u_R$

Mass Fraction of Species *i*: Y_i

These dependent variables are the measured outputs in the scale model. They will vary based on the independent variables of time and position. The relationship between the scale model values and the full scale values of these variables depends on assumptions made when deriving the dimensionless groups. In most scale modeling experiments, the temperature is the same between scales. In other words, the temperature rise in the scale model should be comparable to the temperature rise in the full scale. The temperature distribution should also be similar, where variations in temperature occur at the same position and time as in the full scale model.

Independent Dimensionless Variables

Coordinates: $\hat{x} = \frac{x}{\ell}, \hat{y} = \frac{y}{\ell}, \hat{z} = \frac{z}{\ell}$

Time: $\hat{t} = t / t_R$

The reference time, t_R, can vary based on the time scaling used by the researcher. Flow time or burn time scaling is applied using this parameter.

Initial Conditions

Along with a consideration of the governing equations, the following initial conditions are indicated. They are the values of the ambient surroundings, e.g. the air. These conditions are applied in the balance equations in order to obtain the dimensionless groups. Previous scaling methods may have assumed other initial conditions, which would slightly change the dimensionless groups used in physical scaling. Assumptions made later include the treatment of the reference velocity and reference time.

Temperature: $T = T_\infty$

Density: $\rho = \rho_\infty$

Velocity: $u = u_\infty$

Pressure: $p = p_\infty$

Mass Fraction of Species i: $Y_i = Y_{i,\infty}$

The conservation equations are considered in one space dimension without a loss in generalization. Source terms are represented in a global sense.

3.1 Conservation of Mass

The conservation of mass is the simplest governing equation. It ultimately defines the time scaling [8]. Only one dimension is considered here because it is sufficient to represent this form of scaling.

$$\frac{\partial \rho}{\partial t} + \frac{\partial}{\partial x}(\rho u) = 0 \tag{3.1}$$

Make the equation dimensionless by selected normalizing factors: reference time t_R, reference velocity u_R, and characteristics length scale ℓ. ℓ represents the length, width,

and height. Since geometric similarity is maintained, ℓ is proportional to each dimension.

$$\frac{\rho_\infty}{t_R}\frac{\partial\hat{\rho}}{\partial\hat{t}}+\frac{u_R\rho_\infty}{\ell}\frac{\partial\hat{\rho}\hat{u}}{\partial\hat{x}}=0 \tag{3.2}$$

Rearranging,

$$\frac{\partial\hat{\rho}}{\partial\hat{t}}+\Pi_1\frac{\partial\hat{\rho}\hat{u}}{\partial\hat{x}}=0 \tag{3.3}$$

As all terms are dimensionless, the first dimensionless group emerges. Π_1 relates the velocity, time, and geometric length scale. It is the ratio of time to the fluid flow time. This Π group determines the treatment of the reference time. One way to select a reference time is to force: [8]

$$\Pi_1=\frac{u_R t_R}{\ell}=1 \quad or \tag{3.4}$$

$$t_R=\frac{\ell}{u_R} \tag{3.5}$$

then t_R has the physical meaning of a flow time. This means it is the time required for a fluid particle to travel ℓ. This selection insures that scaled time matches the flow time. Events at a corresponding scaled position will occur at the same scaled time. However, other plausible reference times could be selected. This is the art and style of scale modeling. Such choices lead to indications of the importance of phenomena and whether such phenomena might be dominant or negligible.

The relationship defined by the flow time is explored further using the reference velocity. This simple derivation plays a key role in physical modeling where the scaled

time is reduced and fire events occur earlier in the scale model relative to the full scale experiments. To compare the model results to the full scale experiments, the time is converted back to full scale time and plotted against the original data.

3.2 Conservation of Momentum

Conservation of momentum applied to include the effects of gravity yields relationships pertaining to velocity and pressure [8]. The conservation of momentum is:

$$\rho\left(\frac{\partial u}{\partial t}+u\frac{\partial u}{\partial x}\right)=\mu\frac{\partial^2 u}{\partial x^2}-\frac{\partial p}{\partial x}-\rho g \quad . \tag{3.6}$$

The partial differential equation is made dimensionless by utilizing the normalizing parameters mentioned earlier.

$$\frac{\rho_\infty u_R}{t_R}\hat{\rho}\frac{\partial \hat{u}}{\partial \hat{t}}+\frac{\rho_\infty u_R^2}{\ell}\hat{\rho}\hat{u}\frac{\partial \hat{u}}{\partial \hat{x}}=\frac{u_R}{\ell^2}\mu\frac{\partial^2 \hat{u}}{\partial \hat{x}^2}-\frac{p_R}{\ell}\frac{\partial \hat{p}}{\partial \hat{x}}-\rho_\infty g\hat{\rho} \tag{3.7}$$

After dividing each term by $\frac{\rho_\infty u_R^2}{\ell}$, the dimensionless Π groups can be extracted. Note that Π_1 is seen again in the conservation of momentum.

$$\frac{\ell}{u_R t_R}\frac{\partial \hat{u}}{\partial \hat{t}}+\hat{\rho}\hat{u}\frac{\partial \hat{u}}{\partial \hat{x}}=\frac{\mu}{\rho_\infty u_R \ell}\frac{\partial^2 \hat{u}}{\partial \hat{x}^2}-\frac{p_R}{\rho_\infty u_R^2}\frac{\partial \hat{p}}{\partial \hat{x}}-\frac{g\ell}{u_R^2}\hat{\rho} \tag{3.8}$$

$$\frac{1}{\Pi_1}\frac{\partial \hat{u}}{\partial \hat{t}}+\hat{\rho}\hat{u}\frac{\partial \hat{u}}{\partial \hat{x}}=\frac{1}{\Pi_2}\frac{\partial^2 \hat{u}}{\partial \hat{x}^2}-\Pi_3\frac{\partial \hat{p}}{\partial \hat{x}}-\frac{1}{\Pi_4}\hat{\rho} \tag{3.9}$$

Where the dimensionless groups are defined and named as follows:

$$\Pi_2=\frac{\rho_\infty u_R \ell}{\mu},\ \text{Reynolds Number, Re}\sim\left(\frac{\text{momentum}}{\text{viscous force}}\right) \tag{3.10}$$

$$\Pi_3 = \frac{p_R}{\rho_\infty u_R^2}, \quad \text{Euler Number, Eu} \sim \left(\frac{\text{pressure force}}{\text{momentum}} \right) \tag{3.11}$$

$$\Pi_4 = \frac{u_R^2}{g\ell}, \quad \text{Froude Number, Fr} \sim \left(\frac{\text{momentum}}{\text{gravity force}} \right) \tag{3.12}$$

All of these groups cannot normally be matched between the model and full scale. For example, if Π_2 and Π_4 are sought to be preserved between a model and prototype in air under normal gravity, the Π_2 requires that $u_R \sim \ell^{-1}$ and Π_4 requires $u_R \sim \ell^{1/2}$. Both cannot be done. However, Π_2 governs turbulence and a criterion for turbulent flow is $Re > 10^5$ [17]. The turbulence in the scale model should be verified once the characteristic scale length has been selected. The dimensionless group Π_3 is the Euler number [19]. It relates the pressure in the scale model to the kinetic energy per volume. It is used to characterize losses in the flow. A perfect frictionless flow is achieved when the Euler number is equal to 1. Allowing $\Pi_3 = 1$ yields $p_R = \rho_\infty u_R^2$ giving a way to select p_R in terms of the reference velocity. Π_4 is the dimensionless Froude number. A reference velocity can be selected by allowing $\Pi_4 = 1$. This is done when there is no clear prescribed velocity for reference and the flow is induced by gravity. This Π is proportional to the ratio of momentum to gravity forces. If $\Pi_4 = 1$, then $u_R = \sqrt{g\ell}$. This resulting relationship is appropriate for buoyancy driven flows. The selected reference velocity also impacts the choice of t_R as the of flow time from Π_1. Substituting for u_R, the reference time is now:

$$t_R = \frac{\ell}{u_R} \tag{3.13}$$

$$t_R = \frac{\ell}{\sqrt{g\ell}} = \sqrt{\frac{\ell}{g}} \tag{3.14}$$

Therefore, time is related to scale as $t_R \sim \ell^{1/2}$. This means that the scale model experimental time is calculated by reducing the full scale experimental time:

$$\frac{t_{model}}{t_{full}} = \left(\frac{\ell_{model}}{\ell_{full}} \right)^{1/2} \tag{3.15}$$

This selection of u_R could change based on the full scale scenario. If there is a wind present with a specific velocity u_∞, then u_∞ could be selected for u_R. The Froude number will then remain as $\Pi_4 = \frac{u_R^2}{g\ell} = \frac{u_\infty^2}{g\ell}$.

3.3 Conservation of Energy

Conservation of energy yields the dimensionless groups pertaining to firepower and fuel behavior [8]. The governing equation and its boundary conditions account for conduction, convection, and radiation.

$$\rho c_p \left(\frac{dT}{dt} + u\frac{dT}{dx} \right) = k\frac{\partial^2 T}{\partial x^2} - \frac{\partial \dot{q}_R''}{\partial x} + \frac{\partial p}{\partial t} + \dot{m}''' \Delta h_c \tag{3.16}$$

The source term on the right hand side is dimensionally represented in terms of the overall heat release rate, $\dot{Q}$. The overall heat release rate is convenient since it is commonly known in some experiments. In some cases the heat release depends on the phenomena of fire growth where the mass loss rate depends on external factors, i.e. oxygen concentration, radiation, fuel, etc. [8]. As the volume can be represented using ℓ^3 since the enclosure dimension is geometrically scaled, the heat generation term can be represented as:

$$\dot{m}''' \Delta h_c = \dot{q}'''_{comb} \sim \frac{\dot{Q}}{\ell^3} \quad . \tag{3.17}$$

Additionally, the radiation transfer term is represented in terms of the absorption coefficient of the fluid media, κ:

$$\dot{q}''_R \sim \kappa \sigma T^4 \tag{3.18}$$

The dimensionless conservation of energy equation is easily manipulated by dividing each term by $\frac{\rho_\infty T_\infty u_R}{\ell}$ to reveal additional dimensionless groups.

$$\rho_\infty \hat{\rho} c_p \left(\frac{T_\infty}{t_R} \frac{d\hat{T}}{d\hat{t}} + \frac{u_R T_\infty}{\ell} \hat{u} \frac{d\hat{T}}{d\hat{x}} \right) = \frac{T_\infty}{\ell^2} k \frac{\partial^2 \hat{T}}{\partial \hat{x}^2} - \kappa \sigma T_\infty^4 \hat{T}^4 + \frac{p_R}{c_p t_R} \frac{\partial \hat{p}}{\partial \hat{t}} + \frac{\dot{Q}}{\ell^3 c_p} \tag{3.19}$$

$$\hat{\rho} \left(\frac{\ell}{u_R t_R} \frac{d\hat{T}}{d\hat{t}} + \hat{u} \frac{d\hat{T}}{d\hat{x}} \right) = \frac{k}{\rho_\infty c_p \ell u_R} \frac{\partial^2 \hat{T}}{\partial \hat{x}^2} - \frac{\kappa \sigma T_\infty^4 \hat{T}^4 \ell}{\rho_\infty T_\infty u_R c_p} + \frac{p_R \ell}{c_p t_R \rho_\infty T_\infty u_R} \frac{\partial \hat{p}}{\partial \hat{t}} + \frac{\dot{Q}}{\ell^2 T_\infty \rho_\infty c_p u_R} \tag{3.20}$$

The Π groups are once again extracted from the dimensionless equation.

$$\hat{\rho} \left(\frac{1}{\Pi_1} \frac{d\hat{T}}{d\hat{t}} + \hat{u} \frac{d\hat{T}}{d\hat{x}} \right) = \frac{1}{\Pi_5} \frac{1}{\mathrm{Re}} \frac{\partial^2 \hat{T}}{\partial \hat{x}^2} - \Pi_6 \Pi_7 \hat{T}^4 + \Pi_8 \frac{\partial \hat{P}}{\partial \hat{t}} + \Pi_9 \tag{3.21}$$

$$\Pi_5 = \mathrm{Pr} = \frac{\mu c_p}{k} = \frac{\upsilon}{\alpha}, \left(\frac{\text{viscous diffusion}}{\text{thermal diffusion}} \right) \tag{3.22}$$

Let $t_R = \ell / u_R$, $u_R = (g\ell)^{1/2}$:

$$\Pi_6 = \left[\frac{\sigma T_\infty^3}{\rho_\infty c_p \sqrt{g\ell}} \right], \left(\frac{\text{radiant energy}}{\text{thermal flow energy}} \right) \tag{3.23}$$

$$\Pi_7 = [\kappa \ell], \left(\frac{\text{physical length}}{\text{radiant absorption depth}} \right) \tag{3.24}$$

$$\Pi_8 = \frac{g\ell}{c_p T_\infty}, \left(\frac{\text{potential energy}}{\text{enthalpy}} \right) \tag{3.25}$$

$$\Pi_9 = Q^* = \frac{\dot{Q}}{\rho_\infty c_p T_\infty \sqrt{g}\,\ell^{5/2}}, \left(\frac{\text{firepower}}{\text{enthalpy rate}} \right) \tag{3.26}$$

Here Π_5, the Prandtl number, is included through the scaling of the convective heat transfer coefficient. Groups Π_6 and Π_7 pertain to the radiative heat losses in the fire and the enclosure. Π_8 defines an important linear relationship between the temperature and the dimensionless length scale. Π_9 is called the Zukoski number [8]. It describes the dimensionless heat release rate. This group is used in all fuel scaling to match the full scale Q* to the model Q*. Since the acceleration of gravity does not change with scale and g~ℓ^0, the heat release rate is scaled as $\ell^{5/2}$ [2].

3.4 Conservation of Species

Fuel behavior is defined using conservation of species. In particular, the diffusivity and the fuel flow are defined.

$$\rho\left(\frac{\partial Y_i}{\partial t} + u\frac{\partial Y_i}{\partial x} \right) = \rho D \frac{\partial^2 Y_i}{\partial x^2} + \dot{m}_i''' y_i \tag{3.27}$$

When the governing equation is made dimensionless, mass flux is selected as the mass flux of the fuel.

$$\frac{\rho}{t_R}\frac{\partial Y_i}{\partial \hat{t}} + \frac{\hat{u}u_R}{\ell}\frac{\partial Y_i}{\partial \hat{x}} = \frac{\rho_\infty D}{\ell^2}\frac{\partial^2 Y_i}{\partial \hat{x}^2} + \frac{\dot{m}_{fuel,\sup} y_i}{\ell^3} \tag{3.28}$$

After each term is divided by (u_R/ℓ) , the dimensionless groups are extracted.

$$\frac{\rho_\infty \ell}{\rho_\infty u_R t_R}\frac{\partial Y_i}{\partial \hat{t}} + \hat{u}\frac{\partial Y_i}{\partial \hat{x}} = \frac{\mu\rho_\infty D\ell}{\mu\ell^2 u_R \rho_\infty}\frac{\partial^2 Y_i}{\partial \hat{x}^2} + \frac{\ell}{u_R}\frac{\dot{m}_{fuel,\sup} y_i}{\ell^3} \tag{3.29}$$

$$\frac{1}{\Pi_1}\left[\frac{\partial Y_i}{\partial t} + u\frac{\partial Y_i}{\partial x} \right] = \frac{1}{\Pi_2}\frac{1}{\Pi_{10}}\frac{\partial^2 Y_i}{\partial x^2} + \Pi_{11} y_i \tag{3.30}$$

$$\Pi_{10} = \frac{\upsilon}{D} = \frac{\mu}{\rho_\infty D}, \left(\frac{\text{viscous}}{\text{diffusion}}\right) \tag{3.31}$$

$$\Pi_{11} = \dot{m}^*_{F,\text{sup}} = \frac{\dot{m}_{F,\text{sup}}}{\rho_\infty \sqrt{g}\,\ell^{5/2}}, \left(\frac{\text{fuel flow}}{\text{advection}}\right) \tag{3.32}$$

Note that y_i is a yield given as mass of species to mass of fuel gases released or supplied. These groups will play a significant role for fuels with unsteady burning characteristics. The fuel characteristics of steady fires with a known heat release rate are included in the scaling of the heat release rate found in Π_9.

3.5 Boundary Conditions

The thermal boundary conditions are used to determine the heat transfer scaling and the selections of the construction materials. The following Π groups apply to the boundary conditions of the enclosure. The thickness, δ, and thermal properties of the enclosure walls may be modified so the heat exchange rate between the hot gas layer and the boundaries scales directly with the convective heat transfer in the enclosure. This analysis begins with a heat transfer equation describing conduction and convection. The heat conduction equation governs the boundary construction material.

$$\rho_w c_w \frac{\partial T}{\partial t} = k_w \frac{\partial^2 T}{\partial x_w^{\,2}} \tag{3.33}$$

The equation is now made dimensionless.

$$\frac{T_\infty \rho c}{t_R} \frac{\partial \hat{T}}{\partial \hat{t}} = \frac{T_\infty k}{\delta_w^{\,2}} \frac{\partial^2 \hat{T}}{\partial \hat{x}_w^{\,2}} \tag{3.34}$$

where

$$\hat{x}_w = \frac{x_w}{\delta_w} \tag{3.35}$$

The coefficient on the right hand side can be combined with the left hand side in order to extract the dimensionless group.

$$\frac{\rho_w c_w \delta_w^{\,2}}{k_w t_R}\frac{\partial \hat{T}}{\partial \hat{t}} = \frac{\partial^2 \hat{T}}{\partial \hat{x}_w^{\,2}} \tag{3.36}$$

$$\Pi_{12} = \frac{\rho_w c_w \delta_w^{\,2}}{k_w t_R}, \left(\frac{\text{thickness}}{\text{thermal length}}\right) \tag{3.37}$$

The heat transfer to the construction material is based on the thermal length and reference time. This is a representative analysis used to obtain the dimensionless groups. The next equation balances conduction with convection, radiation from the gas, and radiation from the surface. At the solid surface (x=0):

$$-k_w \frac{\partial T}{\partial x_w} = h_c(T - T_w) + \varepsilon_g \sigma T^4 - \varepsilon\sigma T_w^{\,4} \tag{3.38}$$

This equation is now made dimensionless.

$$-\frac{k_w}{\delta_w}\frac{\partial \hat{T}}{\partial \hat{x}_w} = h_c(\hat{T} - \hat{T}_w) + T_\infty^3 \varepsilon_g \sigma \hat{T}^4 - T_\infty^3 \varepsilon\sigma \hat{T}_w^{\,4} \tag{3.39}$$

The ratio of conductivity to thermal thickness is moved to the right hand side of the equation.

$$\frac{\partial \hat{T}}{\partial \hat{x}_w} = \frac{h_c \delta_w}{k_w}(\hat{T} - \hat{T}_w) + \frac{T_\infty^3 \varepsilon_g \sigma \delta_w}{k}\hat{T}^4 - \frac{T_\infty^3 \varepsilon_g \sigma \delta_w}{k_w}\hat{T}_w^{\,4} \tag{3.40}$$

$$\frac{\partial \hat{T}}{\partial \hat{x}_w} = \Pi_{13}(\hat{T} - \hat{T}_w) + \Pi_{15}\hat{T}^4 - \Pi_{14}\hat{T}_w^{\,4} \tag{3.41}$$

Convection and radiation are described at the solid surface. The convective heat transfer coefficient changes throughout the experiment. Therefore, it is related to the Reynold's number and Prandtl number by the following [17]:

$$Nu = \frac{h_c \ell}{k} \sim \mathrm{Re}^{4/5}\,\mathrm{Pr}^{1/3} \quad \text{for turbulent flow} \tag{3.42}$$

$$\mathrm{Re}^{4/5} \sim \left(\frac{\sqrt{g\ell}\,\ell}{\upsilon} \right) \tag{3.43}$$

$$h_c \sim \left(\frac{\left(\ell^{3/2}\right)^{4/5}}{\ell} \right) \sim \ell^{1/5} \tag{3.44}$$

Using this relationship for the convective heat transfer coefficient, substitutions can be made in Π_{13}.

$$\Pi_{13} = \frac{h_c \delta_w}{k_w} \sim \left(\frac{g^{2/5} k_g}{\upsilon^{4/5}} \right) \frac{\ell^{1/5} \delta_w}{k_w}, \left(\frac{\text{convection}}{\text{conduction}} \right) \tag{3.45}$$

$$\Pi_{14} = \frac{\varepsilon \sigma T_\infty^3 \delta_w}{k_w}, \quad \left(\frac{\text{surface radiation}}{\text{conduction}} \right) \tag{3.46}$$

Π_{13} relates the thermal properties of the boundaries, particularly conductivity. Since conductivity and density are scaled similarly, this can also be used to calculate the density in the scale model boundaries [8]. Π_{14} and Π_{15} address the radiation from the gas and boundary surfaces. As mentioned earlier, accurately scaling the emissivity poses a significant challenge as the fire changes throughout the experiment.

Note that the Π group pertaining to the gas radiation scaling is not included.

$$\Pi_{15} = \frac{\varepsilon_g \sigma T_\infty^3 \delta}{k} \tag{3.47}$$

This group addresses the emissivity of the gas, ε_g. This value can be represented by the following relationship:

$$\varepsilon_g \sim 1 - e^{-\kappa \ell} \tag{3.48}$$

Π_7 describes $\kappa \ell$, therefore Π_{15} does not need to be included.

3.6 The Dimensionless Groups

This section describes the dimensionless groups derived from the governing conservation equations in Section 3.5. The following Π groups rely on the general assumptions and initial conditions stated above with regard to time, velocity, and pressure. These groups form the basis of this scaling method.

$$\Pi_1 = \frac{u_R t_R}{\ell} \tag{3.49}$$

$$\Pi_2 = \mathrm{Re} = \frac{\rho_\infty u_R \ell}{\mu}, \left(\frac{\text{inertia}}{\text{viscous}} \right) \tag{3.50}$$

$$\Pi_3 = Euler = \frac{p_R}{\rho_\infty u_R^2} \tag{3.51}$$

$$\Pi_4 = Fr = \frac{u_R^2}{g \ell} \tag{3.52}$$

Some groups in Π_5 through Π_{14} include assumptions for the reference time and velocity. These are based on Π_1=1 (flow time) and Π_4=1 (gravity speed).

$$\Pi_5 = \mathrm{Pr} = \frac{\mu c_p}{k}, \left(\frac{\text{viscous diffusion}}{\text{thermal diffusion}} \right) \tag{3.53}$$

The following Π groups apply to the fire source behavior and interactions with the surrounding enclosure. Relationships to the geometric scale length are also provided.

These would only be used if the dimensionless groups are included in the scaling methodology.

$$\Pi_6 = \left[\frac{\sigma T_\infty^3}{\rho_\infty c_p \sqrt{g\ell}}\right], \left(\frac{\text{radiant energy}}{\text{thermal flow energy}}\right) \quad T_\infty \sim \ell^{1/6} \tag{3.54}$$

$$\Pi_7 = \kappa\ell, \quad \left(\frac{\text{physical length}}{\text{radiant absorption depth}}\right) \quad \kappa \sim \ell^{-1} \tag{3.55}$$

$$\Pi_8 = \frac{g\ell}{c_p T_\infty}, \quad \left(\frac{\text{potential energy}}{\text{enthalpy}}\right) \tag{3.56}$$

$$\Pi_9 = Q^* = \frac{\dot{Q}}{\rho_\infty c_p T_\infty \sqrt{g}\,\ell^{5/2}}, \left(\frac{\text{firepower}}{\text{enthalpy rate}}\right) \quad \dot{Q} \sim \ell^{5/2} \tag{3.57}$$

$$\Pi_{10} = \frac{\upsilon}{D} = \frac{\mu}{\rho_\infty D}, \left(\frac{\text{viscous}}{\text{diffusion}}\right) \tag{3.58}$$

$$\Pi_{11} = \dot{m}^*_{F,\text{sup}} = \frac{y_i \dot{m}_{F,\text{sup}}}{\rho_\infty \sqrt{g}\,\ell^{5/2}}, \left(\frac{\text{fuel flow}}{\text{advection}}\right) \tag{3.59}$$

$$\Pi_{12} = \frac{\delta_w^{\,2}}{(k/\rho c)_w (\ell/g)^{1/2}}, \left(\frac{\text{thickness}}{\text{thermal length}}\right) \quad \delta_w \sim \ell^{1/4} \tag{3.60}$$

The thickness of the thermal boundaries is related to the geometric length scale by assuming that the density and conductivity of the boundaries scale similarly. It also assumes the specific heat does not change between scales. This results in $\delta_w^{\,2}/\ell^{1/2}$, so $\delta_w \sim \ell^{1/4}$. Proportionalities for Π_{13} also rely on these assumptions.

$$\Pi_{13} = \frac{h_c \delta_w}{k} \sim \left(\frac{g^{2/5} k_g}{\upsilon^{4/5}}\right) \frac{\ell^{1/5} \delta_w}{k_w}, \left(\frac{\text{convection}}{\text{conduction}}\right) \quad k \sim \ell^{9/20}, \rho \sim \ell^{9/20} \tag{3.61}$$

$$\Pi_{14} = \frac{\varepsilon\sigma T_\infty^3 \delta}{k}, \left(\frac{\text{surface radiation}}{\text{conduction}}\right) \tag{3.62}$$

3.6.1 Strategy of Partial Scaling

Complete scaling would preserve all fourteen dimensionless groups simultaneously. This is not possible. For example, the preservation of the Froude number Π_4, which describes buoyancy of the plume flow, and the Reynold's number Π_2, which describes turbulence of the plume flow, is difficult to implement.

$$\Pi_4 = F_r = \frac{u_R^2}{g\ell} = 1 \tag{3.63}$$

When the Froude number is one, the reference velocity becomes equal to the square root of gravity times the length scale. Substituting the reference velocity into the Reynold's number yields:

$$\Pi_2 = \mathrm{Re} = \frac{\rho_\infty u_R \ell}{\mu} = \frac{\rho_\infty \sqrt{g}\,\ell^{3/2}}{\mu} \tag{3.64}$$

This relationship suggests that Re is proportional to $\ell^{3/2}$. In other words, by changing the length scale, ℓ, the turbulence in the bulk flow also changes. The partial differential equations used to derive the dimensionless groups assume that the Reynold's number is large. Π_2 is not included in the scaling theory since $\mathrm{Re} > \mathrm{Re}_{turb}=10^5$ is optimal. The Froude number is used and the Reynold's number is assumed to be turbulent in both the full and scale models [8]. This is one example of the application of partial scaling. A scale model serves to preserve certain factors in a full scale prototype so a reasonable level of accuracy is achieved. Partial scaling uses the Π groups that describe dominant fire effects and omits Π groups that are negligible under typical conditions [2]. A deep

understanding of fire phenomena and the particular fire scenario is important when selecting the appropriate dimensionless groups.

The full scale experiments describe static fires with known heat release rates. Static fires reach an almost immediate steady-state while dynamic fires have a growth period before reaching steady state. Convection and conduction play an important role due to the large vents in the enclosure and the numerous partitions at the ceiling. Radiation is present, but it is not explicitly scaled due to the difficulty of accurately representing the changing emissivity in the corridor. Instead, the radiation present in the full scale fires is assumed to be accounted for through the boundary and design fire scaling. Since early convection is a factor, time is scaled using a flow time approach. The Reynold's number is assumed to be turbulent in the scaled model since the full scale experiment exhibited turbulent flow behavior. This assumption allows the Froude number to describe the buoyancy of the flow in the scale model. As a result of these experimental characteristics, this research employs Π_1, Π_4, Π_9, Π_{11}, Π_{12}, and Π_{13}. The dimensionless groups can be related to the dependent dimensionless parameters.

$$\left[\frac{u}{u_R}, \frac{T-T_\infty}{T_\infty}, \frac{p}{P_R}, Y_i\right] = f\left[\frac{x}{\ell}, \frac{t}{t_R}, \Pi_1, \Pi_4, \Pi_9, \Pi_{11}, \Pi_{12}, \Pi_{13}\right] \tag{3.65}$$

$$\Pi_1 = \frac{u_R t_R}{\ell} \sim 1 \text{ specified so that } \quad t_R = \frac{\ell}{u_R} = \sqrt{\frac{\ell}{g}}, \quad t \sim \ell^{1/2} \text{ (gravity scaling)} \tag{3.66}$$

$$\Pi_4 = Fr = \frac{u_R^2}{g\ell} = 1 \quad \text{specified so that } \; u_R = \sqrt{g\ell}, \quad u \sim \ell^{1/2} \tag{3.67}$$

$$\Pi_9 = Q^* = \frac{\dot{Q}}{\rho_\infty c_p T_\infty \sqrt{g}\,\ell^{5/2}}, \left(\frac{\text{firepower}}{\text{enthalpy rate}}\right) \quad \dot{Q} \sim \ell^{5/2} \tag{3.68}$$

$$\Pi_{11} = \dot{m}^*_{F,\sup} = \frac{y_i \dot{m}_{F,\sup}}{\rho_\infty \sqrt{g}\,\ell^{5/2}}, \left(\frac{\text{fuel flow}}{\text{advection}}\right) \tag{3.69}$$

$$\Pi_{12} = \frac{\delta_w{}^2}{(k/\rho c)_w (\ell/g)^{1/2}}, \left(\frac{\text{thickness}}{\text{thermal length}}\right) \quad \delta_w \sim \ell^{1/4} \tag{3.70}$$

$$\Pi_{13} = \frac{h_c \delta_w}{k} \sim \left(\frac{g^{2/5} k_g}{\upsilon^{4/5}}\right) \frac{\ell^{1/5} \delta_w}{k_w}, \left(\frac{\text{convection}}{\text{conduction}}\right) \quad k_w \sim \ell^{9/20}, \rho_w \sim \ell^{9/20} \tag{3.71}$$

Other scenarios for localized burning in a convection driven cases may use other groups presented here or other scaling methodologies. Fire exhibiting significant growth, spread, or flashover should account for radiation in the scale model. The selection of dimensionless groups is left up to the researcher's understanding of the fire scenario to be modeled. Further guidance is given in Section 2.3. Table 3.1 lists the calculated dimensionless groups for the full scale and scale model used in this research. This is done to visualize the representation of the full scale experiments. Note that for some Π groups, there is a large difference between scales since not all were included in the partial scaling. The groups that are equal to one are based on the assumptions made during the derivation. Π_9 and Π_{10} change with fire size. These values have been calculated and matched between scales, as seen in Section 4.2. Π_{12}, Π_{13}, Π_{14} and are calculated for the partitions at the ceiling. These calculations were also performed for the walls and floor in the enclosure. The fire investigator should see that not every group needs to match in order to build a representative scale model. Groups with large values that are located in the denominator in the derivations, such as Π_2, and with small values that are located in the numerator, such as Π_{10}, can be ignored.

Table 3.1: Calculated Dimensionless Groups

Dimensionless Group	Full Scale Value	⅛ Scale Value
$\Pi_1 = \frac{u_R t_R}{\ell}$	1	1
$\Pi_2 = \mathrm{Re} = \frac{\rho_\infty u_R \ell}{\mu}$	217144	9596
$\Pi_3 = Euler = \frac{p_R}{\rho_\infty u_R^2}$	1	1
$\Pi_4 = Fr = \frac{u_R^2}{g\ell}$	1	1
$\Pi_5 = \mathrm{Pr} = \frac{\mu c_p}{k}$	0.721	0.721
$\Pi_6 = \left[\frac{\sigma T_\infty^3}{\rho_\infty c_p \sqrt{g\ell}}\right]$	0.00043	0.0011
$\Pi_7 = \kappa\ell$	0.8	0.1
$\Pi_8 = \frac{g\ell}{c_p T_\infty}$	0.0326	0.2676
$\Pi_9 = Q^* = \frac{\dot{Q}}{\rho_\infty c_p T_\infty \sqrt{g}\,\ell^{5/2}}$	Varies	Varies
$\Pi_{10} = \frac{\upsilon}{D} = \frac{\mu}{\rho_\infty D}$	0.0000154	0.0000144
$\Pi_{11} = \dot{m}^*_{F,\mathrm{sup}} = \frac{y_i \dot{m}_{F,\mathrm{sup}}}{\rho_\infty \sqrt{g}\,\ell^{5/2}}$	Varies	Varies
$\Pi_{12} = \frac{\delta_w^{\ 2}}{(k/\rho c)_w (\ell/g)^{1/2}}$	2154	1632
$\Pi_{13} = \left(\frac{g^{2/5} k_g}{\upsilon^{4/5}}\right)\frac{\ell^{1/5}\delta_w}{k_w}$	323	268
$\Pi_{14} = \frac{\varepsilon\sigma T_\infty^3 \delta}{k}$	105	122

3.6.2 Harmonization with Past Research

The examples of scale modeling discussed in Section 2 can be related to this derived scaling theory. It is important to keep in mind that various assumptions made

by the researcher can change the dimensionless groups. There is no single way to scale a fire. The main difference between the scaling method used by Quintiere, McCaffery, and Kashiwagi and the method presented here is that time is scaled as a burn time instead of a flow time, meaning events occurred at the same time in the scale model and in the full scale [10]. The other Π groups remained the same. Heskestad [11] also used burn time scaling. Additionally, his dimensionless groups were modified by a factor of the dimensionless heat release rate. This is valuable since it allows data from various size scales to be compared. The data collapses due to the Q* parameter that is included in each Π group. Heskestad did not include boundary scaling or radiation scaling in his derivation. The research completed by Heskestad [12] and later Croce and Xin [13] also employs the use of burn time scaling. This burn time follows $t_R \sim b^{3/2}$, where b is the thickness of the sticks in the wood crib. Heskestad and Croce also decided to scale the convective heat transfer coefficient differently in their boundary condition scaling. The relationship between convection and enthalpy is scaled as $h_c \sim \ell^{1/2}$. This is a direct result of a laminar flow behavior instead of a turbulent flow behavior in the experiments. The heat release rate and fuel behavior were scaled similarly to the methodology presented above. Finally, Perricone [15] conducted experiments using a scaling theory that is most similar to the general scaling theory. The most noteworthy similarity is the use of a scaled flow time instead of a burn time. Scaling the velocity, heat release rate, and fuel behavior are also the same as the Π groups above. Table 3.1 compares the experiments and dimensionless groups of the past research to the scenario present in this research.

While seemingly varied, the basis of scale modeling in each of these examples is the same basis formed in this research. The dominant dimensionless groups remain generally the same for different fire scenarios. While some research chose to omit boundary scaling or radiation scaling, the foundation of scale modeling can be seen through past research. Time and flow velocity assumptions are left to the researcher. The Froude number is used to characterize buoyancy while the Reynold's number is assumed to remain turbulent. When the heat release rate is known, the Zukoski number is matched between the full and small scales. The boundaries are scaled with respect to convection and conduction. Sometimes radiation is included, but it requires a more complex dimensionless group to represent the emissivity. With such a wide range of research based on these simplified scaling laws, a fire investigator would most likely find scale modeling very useful.

Table 3.2: Past and Present Scaling Comparisons

Researcher	Design Fire/ Set-up	Time	Differing Π Groups	Comments
Quintiere, McCaffery, and Kashiwagi [10]	Gas Burner in a Room with Adjacent Corridor 1/7 Scale 300 to 1500 kW Fires	Burn Time Scaling 30 Minute Duration	All Groups Remain the Same Except Π_1: $t_{model} = t_{full\ scale}$ $t \sim \ell^0$	• Time Lags Not Included • Radiation Groups Ignored • Good Results for Convective Processes (T_{gas}, u_{gas}, $\dot{q}''_{conv}$) • $T_{surface}$: model< full scale • $\dot{q}''$: model< full scale • Flame Heights Not Scaled
Heskestad [11]	Initial Convective Flow Attempt to Apply Scaling to Fire Detection Only Turbulent Flows are Considered Pool Fires and Wood Cribs Partitioned and Flat Ceilings	Burn Time Scaling	(Includes Q* Factor) $\Pi_{time} = \frac{t_R}{Q^{*1/3}} = \frac{\Pi_1}{Q^{*1/3}}$ $\Pi_{velocity} = \frac{u/\sqrt{g\ell}}{Q^{*1/3}} = \frac{\Pi_4}{Q^{*1/3}}$ $\Pi_{tempersature} = \frac{\Delta T/T_\infty}{Q^{*2/3}}$ $\Pi_{fuel} = \frac{Y_i}{\left(\frac{y_i c_p T_\infty}{\Delta h_c}\right) Q^{*2/3}}$	• No Boundary or Radiation Scaling • Ceiling Contours Affect Detection Scaling • Including Q* Factor Allows Various Scales to Collapse • Good Results: T_{gas}, u_{gas}, Y_i • Initial Smoke Front Arrival Time is Insensitive to Size for Power-Law Fires

Heskestad [12] Croce and Xin [13]	Wood Cribs in Enclosures Laminar Flow: $h_c \sim \ell^{1/2}$ Two Sizes of Enclosures Compared at ¼, ½, Full Scale Ventilation Factors Played a Key Role	Burn Time Scaling Based on Crib: $t_R \sim b^{3/2}$	$P = (sD_c)^{1/2}\frac{A_o}{A}$ $\Pi_{time} = t_R \sim b^{3/2}$ $\Pi_{conv} = \frac{T_\infty k_w}{q\delta} = \frac{k_w}{h_c\delta} = \frac{1}{\Pi_{13}}$ $\Pi_{boundary} = \frac{k_w t_R}{\delta^2 \rho_w c_w} = \frac{t_R}{\Pi_{12}\left(\ell/g\right)^{1/2}}$	• Good Results: T_{gas}, $T_{surface}$, Y_{O2}, Y_{CO}, Y_{CO2} • Agreement between Burning Rate Factor and Ventilation Factor • Inaccurate Scaling of Wall Thickness Affected Results • Radiation Groups Ignored • Only Large Ventilation Factors were Examined
Perricone [15]	Wood Cribs and Structural Loads Laminar Flow: $h_c \sim \ell^{1/5}$ ⅛, ¼, ⅜ Scale	Flow Time Scaling: $t \sim \ell^{1/2}$	$\Pi_{w,\delta} = \frac{\delta g^{1/4}}{\left(k/\rho c\right)_w^{1/2}\ell^{1/4}} = \sqrt{\Pi_{12}}$ $\Pi_{w,c} = \frac{h_c \ell^2 T_\infty}{\rho_\infty c_p T_\infty \sqrt{g}\,\ell^{5/2}}$ $\Pi_{w,k} = \frac{\left(\frac{k\rho c}{t_R}\right)^{1/2}\ell^2 T_\infty}{\rho_\infty c_p T_\infty \sqrt{g}\,\ell^{5/2}}$ $\Pi_{13} \sim \frac{\Pi_{w,c}\Pi_{w,\delta}}{\Pi_{w.k}}$	• Transient Data Comparisons • Ventilation of the Wood Crib is Important • Good Results: T_{gas}, $\dot{m}''$, $\dot{q}''_{rad}$, $T_{Structural\ Elements}$ • Radiation Considered Through Gas Emissivity Scaling (Π_e)

4. Design and Experimentation

4.1 Full Scale Experiments

To confirm the validity of the scaling method presented in Section 3, a series of full scale experiments was conducted at the Bureau of Alcohol, Tobacco, Firearms, and Explosives in Beltsville, MD. The experiments were conducted in a 4.5 meter high enclosure with joist-like partitions at the ceiling. Figure 4.1 is a representation of the facility.

The walls of the structure were constructed of 2x4 lumber, spaced 60.9 cm on center and sheathed with a layer of 1.6 cm thick gypsum wallboard. A series of 19 ceiling bays were created using oriented strand board (OSB) plywood partitions and 2x4 lumber. These partitions extended about 0.6 meters down from the ceiling. As seen in Figure 4.1, two smaller corridors extended off of the main area corridor of the enclosure. The ends of the corridor were open to the ambient air in the laboratory space. Temperature, flame height, smoke detector response, velocity, and smoke obscuration were measured throughout the test series. A load cell was used to measure the mass loss in the wood crib and polyurethane (PU) foam tests. Flame height was visualized with the aid of a metal stand marked off every 0.25 meters. This stand was located 1.78 meters away from the east wall and centered with the test specimen. The exact dimensions of the enclosure, the partitions, and the location of the instrumentation can be seen in Appendix A.

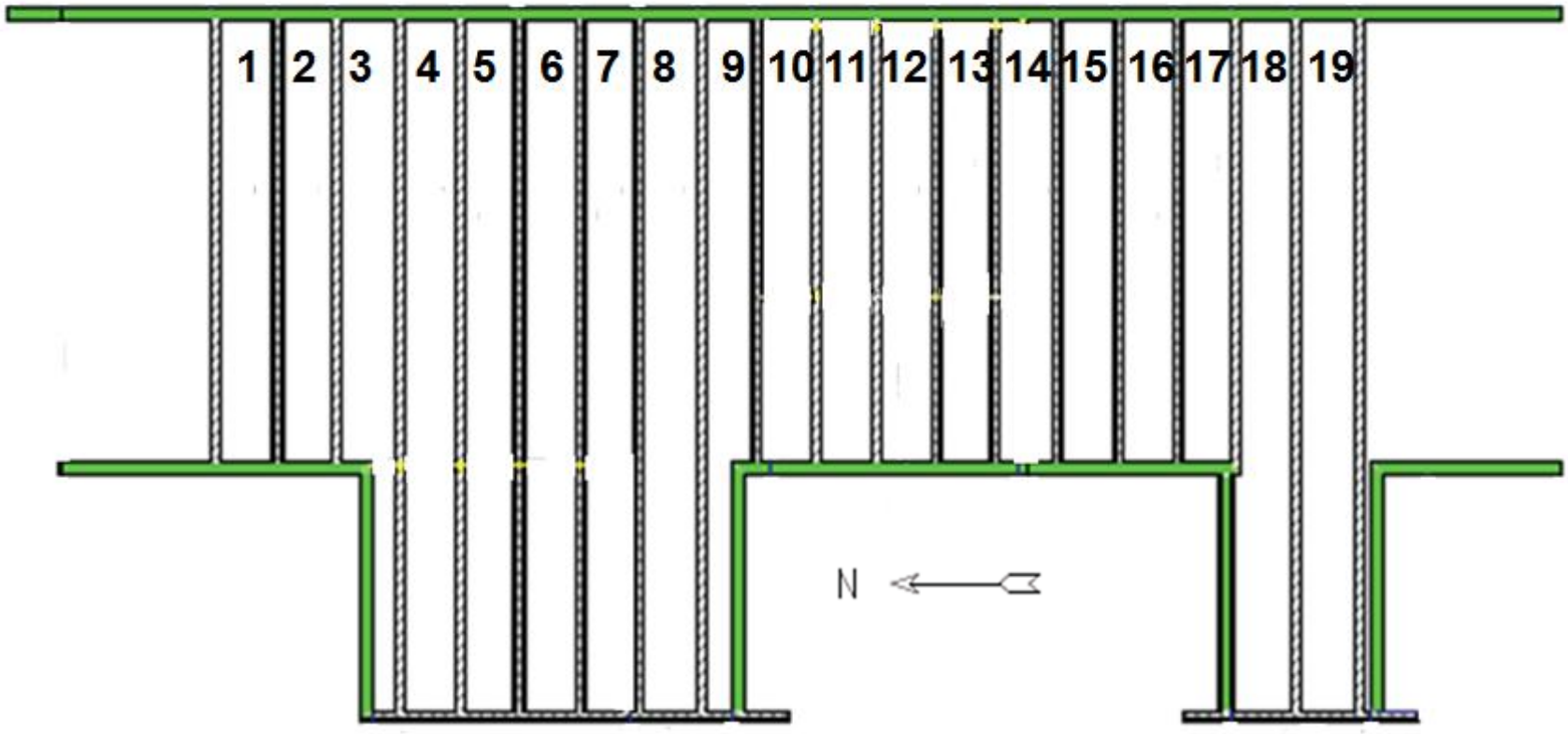

Figure 4.1: Plan View of ATF High-Bay Corridor Facility.

In general, instrumentation included thermocouples, hot wire anemometers, ionization detectors, photoelectric detectors, and optical density meters. A vertical thermocouple tree was located in every bay with thermocouples 5.1 cm, 15.2 cm, and 45.7 cm below the ceiling. Select bays were also instrumented with a horizontal thermocouple tree oriented parallel to the partitions. The tree was 30.5 cm below the ceiling with a thermocouple located every foot. The fuel in each test was positioned in "Location 2", as labeled in Figure 4.2. The smaller square represents the stand used to indicate flame height. Video cameras and still cameras were used to document the tests.

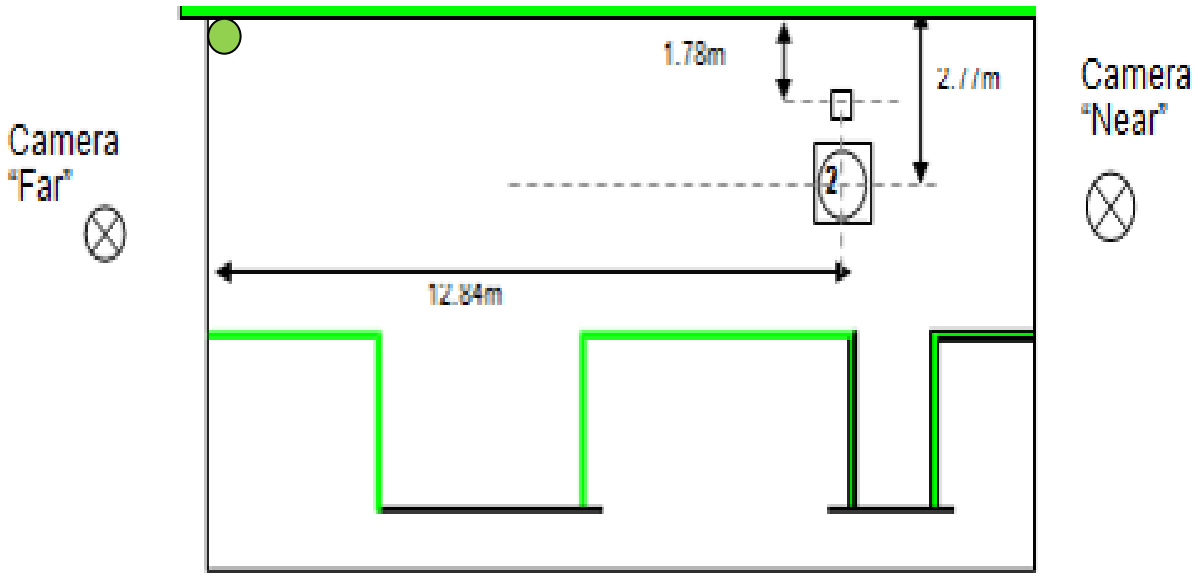

(a) Plan View of Fire Location.

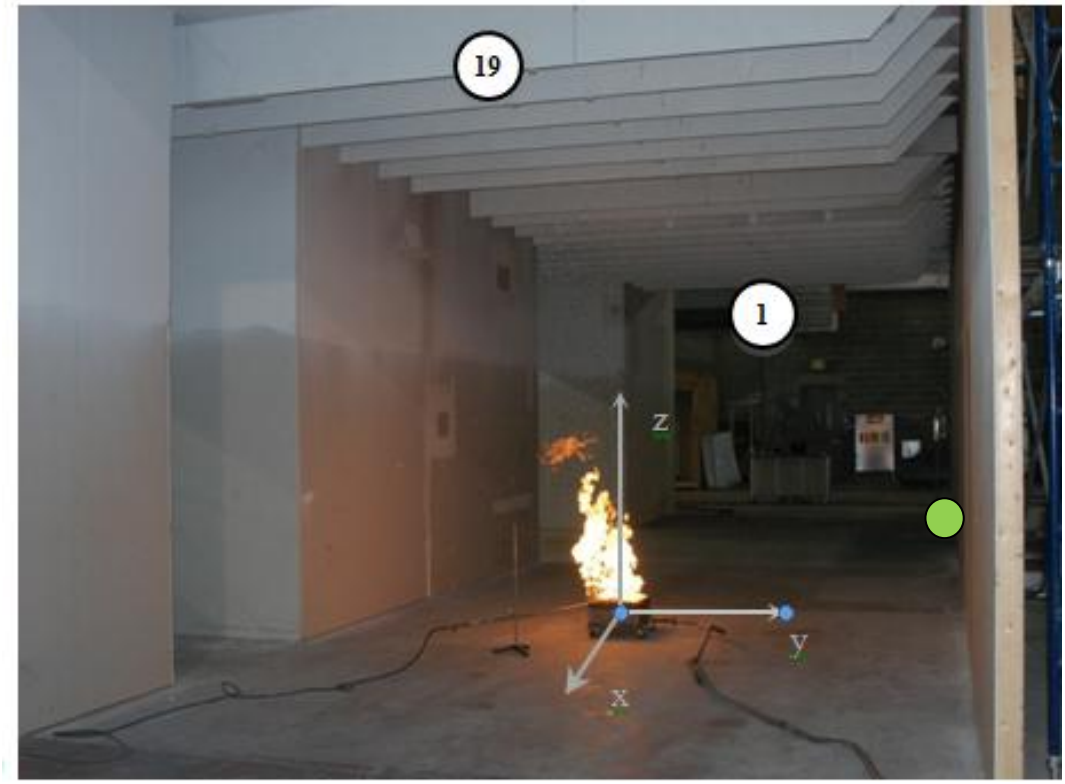

(b) Actual View of Fire Location.

Figure 4.2: Fire Location Within the ATF Enclosure.

A natural gas burner, a heptane pool, pine wood cribs, and polyurethane foam (PU foam) blocks were used as the fuel sources. This research encompasses the scaled tests for the gas burner and heptane pool fires. Future work with this project will address scaling the wood cribs and the PU foam. The maximum heat release rate was calculated based on expected temperature rise in the enclosure. The height of the enclosure was 4.42 meters. The ambient temperature read by the thermocouples in the enclosure was 27°C, however this varied slightly throughout the enclosure. In preliminary tests, the natural gas burner was set at a heat release rate of 150 kW. The measurements in the enclosure did not vary greatly with respect to location with this size fire. It was decided that smaller heat release rates using the box burner would cause more of a variance in temperature, optical density, and velocity relative to

position. This is ideal for physical modeling in order to test the accuracy of the scaling. A few larger gas burner fires were also included in the interest of gathering a wide range of data. In summary, data was collected for burners with a maximum heat release rate of 25 kW, 50 kW, 75 kW, 150 kW, 250 kW, and 300 kW over a 15 minute time period for each test. Most of these trials used a ramp function to prescribe the flow rate of the natural gas. One trial with no growth ramp was conducted for each fire size. The scale model is compared to these semi-immediate steady-state trials.

Heptane was burned in metal pans for the liquid fuel portion of the test series. 30.5 cm, 45.7 cm, and 61 cm round pans were each filled with heptane. These are referred to as small, medium, and large pool fires for this research. The amount of heptane was calculated using the burning rate based on the diameter of the pan. Water was poured into the pans before testing to create a level surface for the fuel to promote even burning. The pans were placed on a piece of gypsum wallboard to protect the concrete floor. All dimensions and liquid levels were measured prior to burning the heptane. The heptane was left to burn until self extinction, which occurred three to five minutes after ignition.

The wood cribs were designed using a relationship presented by McCaffery [8], which described the relationship between the temperature rise in the enclosure, the height of the enclosure, and the heat release rate of the fire [18]. This was used to predict the heat release rate based on an expected temperature rise. The maximum heat release rate was determined to be between 380 kW and 730 kW. These

maximum anticipated fire sizes and the enclosure properties were used to design the wood cribs. The heat release rate is defined as:

$$\dot{Q} = \dot{m}\Delta h_c \tag{4.1}$$

where the heat of combustion for pine wood is about 12 kJ/g [16]. The mass loss rate is calculated based on the characteristics of the wood crib:

$$\dot{m} = Cn(4lD_c^{1/2}) \tag{4.2}$$

Where C is a material constant, about 1 mg/ $cm^{1.5}$s for pine, n is the number of sticks in the crib, l is the length of one stick, and D_c is the diameter of one stick. The availability of wood sticks is limited. The length and diameter are predetermined and the resulting number of sticks is calculated using the mass loss rate.

$$\dot{m} = n\ (1)(4)(76.2cm)(2cm)^{1/2} \tag{4.3}$$

$$\dot{m} = (0.431n\ )g/s$$

Using the heat of combustion and the optimal heat release rate of 400 kW, the number of sticks is determined to be 77 for the wood crib.

$$\dot{Q} = (5.172n\ )kW = 400kW \tag{4.4}$$

$$n = 77.33 \sim 77 sticks$$

The crib was organized into 11 layers with 7 sticks per layer. The spacing of the sticks was calculated based on the total length on one stick.

$$l = (\#sticks/layer)D_c + [(\#sticks/layer) - 1]s \tag{4.5}$$

Where l is the length, D_c is the diameter, and s is the spacing between sticks.

$$76.2cm = (7)(1.9cm) + [(7) - 1]s$$

$$s = 10.5cm$$

An optimal porosity of the crib is needed for proper burning characteristics [14]. The porosity for this crib design is 0.065, which is in the optimal range.

$$P = (sD_c)^{1/2} \frac{A_o}{A} = 0.065 \quad (4.6)$$

The wood crib sticks were 1.9 cm square. Ultimately, the wood crib was designed to have a heat release rate of ~400 kW. A total of 77 sticks were used in the crib, with 11 layers of 7 sticks. The sticks were spaced 10.5 cm apart. Each stick was 76.2 cm long. The cribs were assembled using 2.54 cm metal staples. Figure 4.3 shows a wood crib before testing.

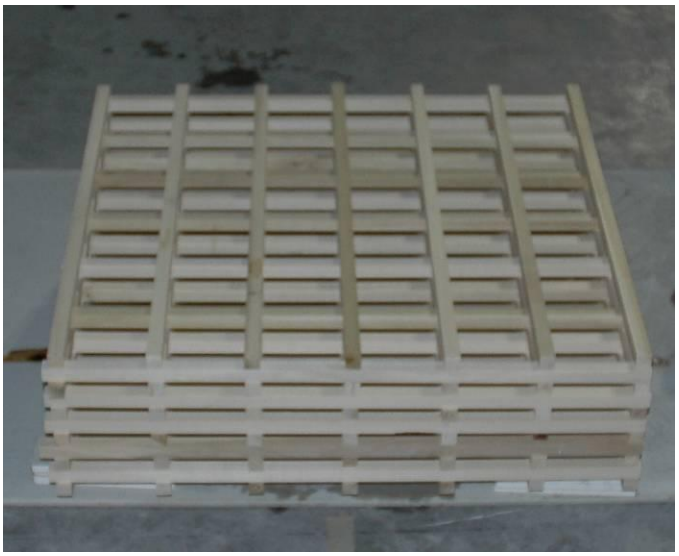

Figure 4.3: A Wood Crib Before Testing.

Three trials were conducted in the test series. A pan filled with heptane was placed under the wood crib to promote even ignition. The wood cribs were stored in an air conditioned room with a 17.4°C ambient temperature and 68% relative humidity. Each crib burned for about five minutes.

The PU foam was cut to be 76.2 centimeters on a side and 12.7 centimeters high. Cardstock was glued to the sides of the foam to prevent the fire from spreading faster at the edges. A 12.7 cm by 12.7 cm grid was drawn on the top face of the foam

in order to track flame spread. A 2.54 cm wide arc groove was cut out in one corner of the foam, as seen in Figure 4.4. Fifty milliliters of heptane were poured into this groove. This was intended to ignite the foam and spread the fire uniformly from the corner.

Figure 4.4: Arc Groove in the Polyurethane Foam.

The PU foam was placed on a piece of gypsum board, which rested on top of the load cell. A pilot light ignited the heptane after it was poured into the foam groove. The test time began when the heptane ignited and ended when the foam had almost completely burned out. A CO_2 extinguisher was used after the test ended. Three foam tests were run in this series, with individual test times of about three to five minutes each. Table 4.1 outlines the complete experimental series for all of the fuels.

Table 4.1: The ATF High-Bay Experimental Series.

FUEL	FREQUENCY	DESIGN FIRE
Natural Gas Burner	1 Trial Each	25 kW, 50 kW, 75 kW, 150 kW, 250 kW, 300 kW
Heptane Liquid Pool	2 Trials 4 Trials 2 Trials	30.5 cm round (70 kW) 45.7 cm round (150 kW) 61 cm round (400 kW)
Pine Wood Crib	3 Trials	7 sticks per layer with 11 layers 1.9 cm square pine 76.2 cm sticks 400 kW
PU Foam Blocks	3 Trials	76.2 cm x 76.2 cm x 12.7 cm high 400 kW

4.2 Model Fuel Scaling

The fuels used in the full scale experiments were scaled to ⅛ model size using the general scaling laws. Heat loss was ignored. The model was considered to be an inviscid, unsteady flow. All experimental times were scaled according to Π_1, where the ratio of the time for model experiments to time for full scale experiments is proportional to $\ell^{1/2}$.

$$t_{model} = t_{full}\left(\frac{\ell_{model}}{\ell_{full}}\right)^{1/2} \tag{4.7}$$

$$t_{model} = 0.35355 t_{full}$$

The times for the completed experiments in this research effort are summarized in Table 4.2.

Table 4.2: The Full Scale and Model Experiment Times.

FUEL	FIRE SIZE	FULL SCALE TIME (sec)	MODEL SCALE TIME (sec)
Natural Gas Burner	All	900	~320
Heptane Liquid Pool	Small Medium Large	~260 ~300 ~200	90-95 100-120 70-75

4.2.1 Natural Gas Burner

The natural gas burner was scaled geometrically using a ⅛ scale. The dimensions of the model burner were 6.4 cm x 6.4 cm x 3.8 cm high. The burner was machined out of an aluminum block. A mesh screen sat inside the burner 1.9 cm above the bottom. Below this screen, the gas entered the burner through a copper pipe with holes drilled into the sides. This configuration allowed the gas to disperse throughout the entire bottom of the burner. Small stones sat above the screen in order to diffuse the gas to the top surface of the burner. The completed gas burner is depicted in Figure 4.5.

Figure 4.5: The Natural Gas Burner for the Scale Model.

The necessary mass flow of natural gas was calculated using Π_9 and the full scale heat release rates. The ratio of the model heat release rate to the full scale heat release rate is proportional to $\ell^{5/2}$, or $(⅛)^{5/2}$. The mass flow rate of the fuel was calculated using the model heat release rate and the heat of combustion of natural gas, 54 kJ/g [16].

$$\dot{m} = \frac{\dot{Q}_{model}}{\Delta h_c} \tag{4.8}$$

Table 4.3 describes the model gas burner experiments and their relation to the full scale tests.

Table 4.3: The Natural Gas Burner Heat Release Rates and Flow Rates.

FULL SCALE EXPERIMENTS		MODEL SCALE EXPERIMENTS	
HRR (kW)	MFR (g/s)	HRR (kW)	MFR (g/s)
25	0.46	0.14	0.0026
50	0.93	0.28	0.0051
75	1.39	0.41	0.0077
150	2.78	0.83	0.0153
250	4.63	1.38	0.0256
300	5.56	1.66	0.0307

4.2.2 Heptane Pool Fire

In order to scale the pool fires, the diameter of the pan was scaled according to the desired heat release rate. Therefore, unlike the gas burner, the pool fires could not be scaled geometrically. The full scale pool fires were designed using laboratory data from the University of Maryland [8]. This data described the mass loss rate and the heat release rate of heptane burning on ceramic boards as a function of the board diameter. The full scale experiments at ATF provided large diameter pool data to verify the correlations. In order to create a representative trend for pool fires in pans, small diameter experiments were conducted at the University of Maryland. With the data from ATF and the University of Maryland, an additional correlation was created for the mass loss rate and the heat release rate of heptane burning in a pan as a function of the pan diameter. These relationships are shown in Figure 4.6 compared to the existing correlation for heptane burning in a porous ceramic disk.

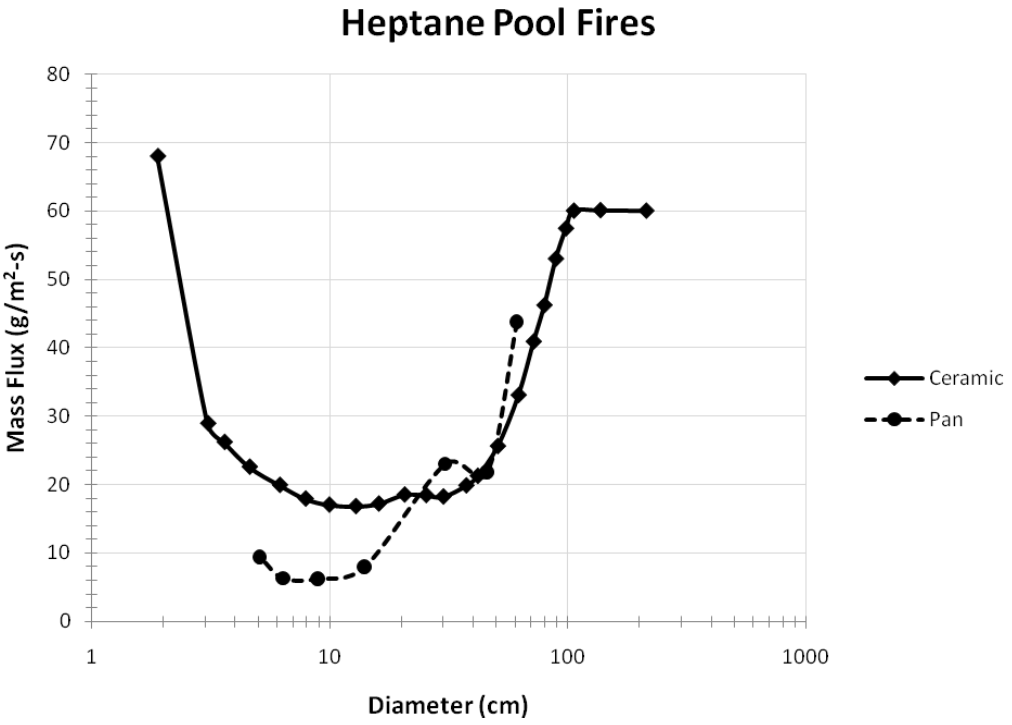

(a)

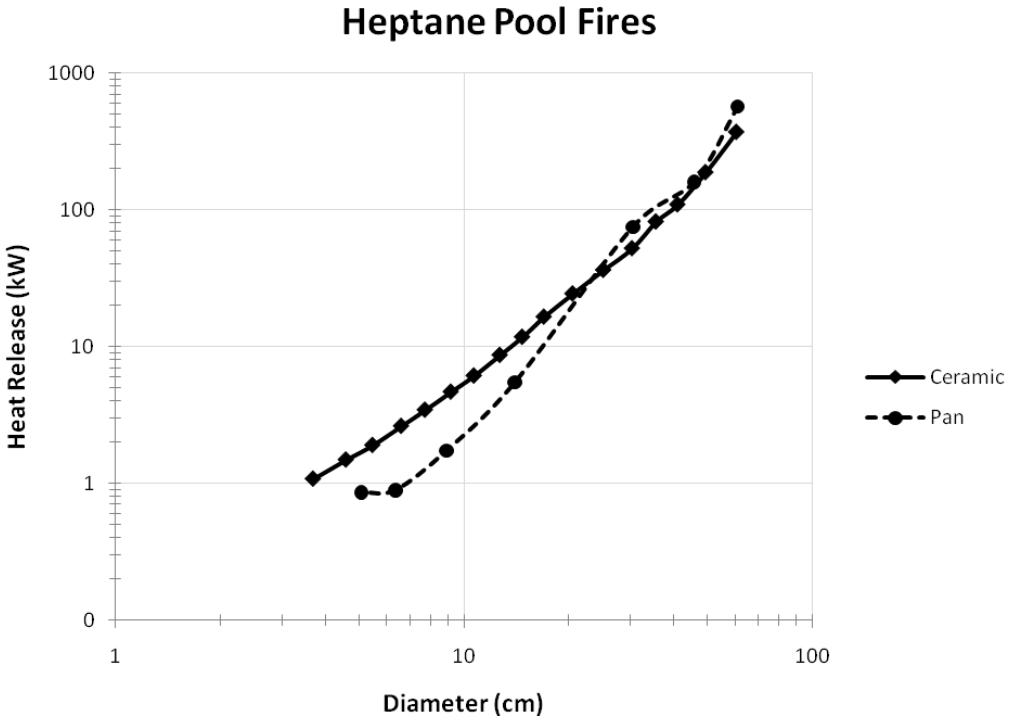

(b)

Figure 4.6: (a) Mass Loss Rate and (b) Heat Release Rate for Heptane.

The results were slightly different than for heptane burning on a ceramic board. Since the fuel was the same in the full scale and the model experiments, the ratio of the model heat release rate to the full scale heat release rate is proportional to $\ell^{5/2}$, or $(1/8)^{5/2}$. The three model size heat release rates were matched using the full scale data and full scale Q*. The appropriate diameter of the pans were found using Figure 4.6. Pans were constructed out of steel to meet the precise diameter requirements. The mass loss rate per unit area was then found from the relationship:

$$\dot{Q} = \dot{m}''\Delta h_c \frac{\pi}{4} D^2 \tag{4.9}$$

Finally, the amount of fuel required for each test was calculated from the known time and mass loss rate.

$$m = \dot{m}\Delta t \tag{4.10}$$

A summary of the scale model heptane experimental set-up and the corresponding full scale experimental set-up is provided in Table 4.4.

Table 4.4: The Heptane Pool Diameters and Initial Masses.

FULL SCALE EXPERIMENTS		MODEL SCALE EXPERIMENTS	
Diameter (cm)	Initial Mass (g)	Diameter (cm)	Initial Mass (g)
30.5	446	4.6	0.83
45.7	1108	6.1	1.91
61	2562	9.9	4.93

4.2.3 Fuel Scaling Concerns

The independence or dependence of the dimensionless heat release rate, Q*, relies on whether or not the heat release rate of the object is known. This is relatively simple to calculate from gas burners and pool fires. However, it becomes more

complicated with other materials, especially when flame spread is introduced. When the heat release rate is known, Q* is considered an independent property and is scaled accordingly. When the heat release rate is unknown, Q* is dependent upon the other scaled parameters in the model. It is up to the researcher to recognize these parameters and match them through the scaling methodology.

4.3 Compartment Design

The selected partial scaling methodology requires some compromise when selecting the materials and thickness of the boundaries in the scale model. The theory results in very precise quantities that need to be rounded or modified based on availability of materials. The following sections describe the dimensionless groups used to design the compartment, some analysis of these groups relative to the scale model, and the construction of the compartment.

4.3.1 Application of Scaling Theory

The heat transfer dynamics that occurred in the full scale experiments must be replicated in the scale model. The heat transfer through the boundaries is especially important since the material thermal properties change with scale according to Π_{12} and Π_{13}. The density and conductivity of the materials scale proportional to $\ell^{9/20}$.

$$\Pi_{13} = \frac{h_c \delta}{k} \sim \left(\frac{g^{2/5} k_g}{\nu^{4/5}} \right) \frac{\ell^{1/5} \delta}{k} \tag{4.11}$$

Gravity, conductivity of the air, and dynamic viscosity of the air are the same in the full and ⅛ scales, this becomes:

$$\Pi_{13} = \frac{h_c \delta}{k} \sim \frac{\ell^{1/5} \delta}{k} \tag{4.12}$$

$$k \sim \ell^{1/5}\delta \tag{4.13}$$

$$\Pi_{12} = \frac{\delta^2}{(k/\rho c)(\ell/g)^{1/2}} \tag{4.14}$$

$$\delta \sim \ell^{1/4} \tag{4.15}$$

By combining these relationships, the conductivity can be scaled using:

$$k \sim \ell^{1/5}\ell^{1/4} \sim \ell^{9/20} \tag{4.16}$$

$$\frac{k_{model}}{k_{full}} = \left(\frac{\ell_{model}}{\ell_{full}}\right)^{9/20} \tag{4.17}$$

This is also used for the density. The specific heat of most materials is about 1 kJ/kg-K, therefore the specific heat does not change for the scale model. Table 4.5 provides the thermal properties of the full scale boundaries along with the scaled values [20].

Table 4.5: The Thermal Properties of the Full and Model Scale Boundaries.

MATERIAL	FULL SCALE			MODEL SCALE		
	k (W/mK)	ρ (kg/m^3)	c (kJ/kgK)	k (W/mK)	ρ (kg/m^3)	c (kJ/kgK)
Concrete	1.7	2400	0.75	0.67	941.5	0.75
OSB Chipboard	0.15	640	1	0.058	251.1	1
Gypsum Board	0.17	600	1.09	0.067	235.4	1.09
2x4 Wood	0.15	530	2.5	0.057	207.9	2.5

It is difficult to find materials that closely match the scaled values. The gypsum and the particle board were relatively close in density and conductivity, Kaowool was used for both in the scale model [21]. Marinite A was selected as the

floor material [22]. Table 4.6 lists the thermal properties for the selected boundary materials in the scale model.

Table 4.6: Thermal Properties of the Selected Material for the Model.

MATERIAL	ACTUAL VALUES		
	k (W/mK)	ρ (kg/m^3)	c (kJ/kgK)
Marinite A	0.28	1041	1.1
Kaowool	0.06	250	1.08

These values do not match the scaled values exactly; however the materials are still acceptable for building a scale model. The thickness of the boundaries scales according to $\ell^{1/4}$.

$$\frac{\delta_{model}}{\delta_{full}} = \left(\frac{\ell_{model}}{\ell_{full}} \right)^{1/4} \tag{4.18}$$

The 1.59 cm walls were scaled to 0.95 cm and the 1.27 cm partitions/ceiling were scaled to 0.74 cm using this relationship. The selected materials are not manufactured in these thicknesses. Therefore, the model walls were selected to be 0.953 cm thick and the model ceiling and partitions were selected to be 0.64 cm thick. The small differences in the boundary thicknesses could be a potential source of future error. The depth of the concrete floor in the full scale experiments was not measured since it was the floor in the lab space. Instead, it was assumed that this deep slab of concrete acted as a heat sink to the fires within the enclosure. The thermal penetration depth was calculated according to the thermal properties and the penetration time.

$$\delta \sim \sqrt{\alpha t} \tag{4.19}$$

$$\alpha = \frac{k}{\rho c} \tag{4.20}$$

For the model, an 8 mm penetration depth was calculated. The Marinite A slab for the floor of the scale model was 1.27 cm thick based on these calculations.

The actual values (thermal properties and thickness) for the boundary materials were compared to the theoretical values by calculating the dimensionless ratios $(\Pi_{12})_{model}/(\Pi_{12})_{full}$ and $(\Pi_{13})_{model}/(\Pi_{13})_{full}$. The closer these ratios are to one, the more accurate the selected material represents the scaling theory. The ratios for all boundary materials are listed in Table 4.7.

Table 4.7: The Comparative Ratios for the Model Physical Boundaries.

BOUNDARY	$(\Pi_{12})_{model}/(\Pi_{12})_{full}$	$(\Pi_{13})_{model}/(\Pi_{13})_{full}$
Concrete	0.77	0.94
Gypsum Board	1.09	1.12
OSB Chipboard	0.69	0.83

From these values, the selected materials are an acceptable representation of the full scale boundaries. The discrepancies between the scaled values and the actual material properties may become a source of error when analyzing the results.

4.3.2 Reynold's Number Specifications

Since the buoyancy flow was preserved in the general scaling methodology, the Reynold's number was assumed to be turbulent at all scales. The Reynold's number was used to verify turbulence in the model.

$$\mathrm{Re} = \frac{\sqrt{g}h^{3/2}}{\upsilon} \tag{4.21}$$

Where h is the height of the enclosure. Since the kinematic viscosity of air varies with temperature, the Reynold's number was calculated at 20°C, 100°C, and 200°C, as seen in Table 4.8. Based on full scale results, the model is not expected to reach temperatures above 200°C.

Table 4.8: Verifying Turbulence for the Scale Model.

TEMPERATURE	REYNOLD'S NUMBER
20°C	0.8×10^5
100°C	0.5×10^5
200°C	0.2×10^5

$Re > 10^5$ is considered turbulent. These values do not account for mixing effects when the plume impinges on the ceiling and partitions; therefore it was assumed that the flows in all experiments remained in the turbulent regime.

4.3.3 ⅛ Scale Compartment Construction

The model was built on top of a drywall and metal stud foundation attached to two rolling tables for mobility around the lab. The Marinite A slab was bolted onto this foundation. The model as a whole was designed to allow relatively easy modification to the structure in case of emergency. The enclosure was constructed separately from the foundation, meaning it could be lifted and modified if necessary. An aluminum channel support system made of 80/20 formed the enclosure. All dimensions of the enclosure were scaled geometrically (ℓ =⅛). Note from Appendix A that the width of each bay varied slightly and some partitions were shorter than others. This was taken into consideration and scaled accordingly. The partitions were angled at the sides. The missing portion formed an isosceles right triangle. The angle

remained the same in the scale model in order to ensure that the same flow characteristics were achieved from bay to bay. The Kaowool panels were measured, cut, and secured to the inside of the 80/20 structure. Seams between panels were filled with liquid Kaowool cement, which had the same material properties as the solid board. The partitions were held at a 90° angle using small clips that extended into the enclosure through the top of the ceiling. The partitions were then secured with the Kaowool cement. Various angles of the model can be seen in Figure 4.7.

Figure 4.7: The Scale Model Compartment.

The dimensions of the finished scale model (main corridor) measured 2.2 meters in length by 0.97 meters in width by 0.56 meters in height. The location of the burner and metal pans were scaled geometrically.

4.4 Measurement and Instrumentation

4.4.1 Scaling the Thermocouples

In the full scale experiments, 28 AWG Type K glass insulated thermocouples were used. The thermocouples were scaled to reduce potential error from a large diameter wire relative to the small bays in the scale model. The scaling methodology considered the diameter of the wire, the flow time in the model, and the velocity of the flow around the thermocouple. Conduction and convection were taken into account to create and additional Π group for thermocouples [8].

$$mc_p \frac{dT}{dt} = hA_s(T_g - T) \tag{4.22}$$

$$\Pi_{TC} = \frac{hA_s}{mc_p} t_R \tag{4.23}$$

$$\Pi_{TC} \sim \left(\frac{\ell^{1/2}}{d} \right)^{3/4} \tag{4.24}$$

The thermocouples for the scale model were matched as closely as possible to the scaled diameter; therefore 40 AWG Type K glass insulated thermocouples were used. The thermocouples wire was not rigid enough to remain in position during the experiments. As a result, small brackets were formed to hold the thermocouples in the desired location, as seen in Figure 4.8. The brackets were coated with liquid Kaowool to ensure the metal did not affect the temperature results. The locations of the thermocouples on the brackets were scaled geometrically based on the full scale thermocouples distance from the ceiling. High temperature resistant RTV silicone was used to hold the thermocouples to the brackets.

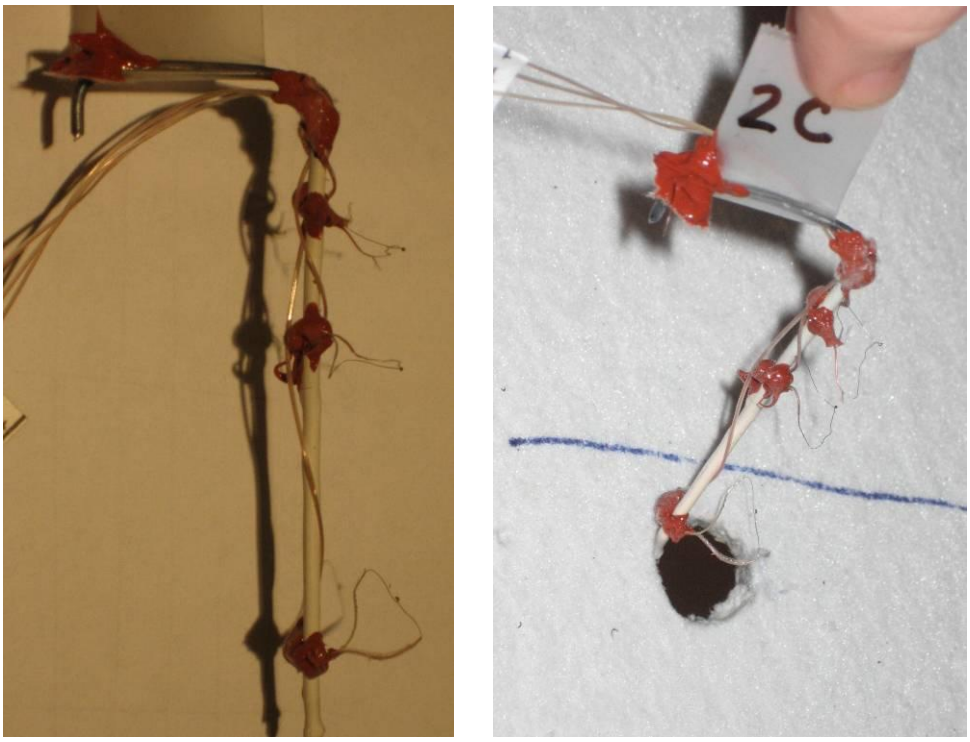

Figure 4.8: The Thermocouples on Brackets.

The full scale enclosure was instrumented with over 60 thermocouples. The ⅛ model used 30 thermocouples. They were chosen based on elevation and distance from the fire. Table 4.9 describes the bay location, orientation, and elevation for the 30 thermocouples used in the scale model. Note: These values list the full scale distances for future comparison purposes.

Table 4.9: Scale Model Thermocouples Locations.

Bay Location	Tree Orientation	Distance From Ceiling (cm)	Distance From East Wall (m)
Bay 2	Vertical	5.1	0.91
Bay 2	Vertical	15.2	0.91
Bay 2	Vertical	45.7	0.91
Bay 4	Vertical	5.1	0.91
Bay 4	Vertical	15.2	0.91
Bay 4	Vertical	45.7	0.91
Bay 6	Vertical	5.1	0.91
Bay 8	Vertical	5.1	0.91
Bay 10	Vertical	5.1	0.91
Bay 10	Vertical	15.2	0.91
Bay 10	Vertical	45.7	0.91
Bay 13	Vertical	5.1	0.91
Bay 15	Vertical	5.1	0.91
Bay 16	Vertical	5.1	0.91
Bay 17	Vertical	5.1	0.91
Bay 19	Vertical	5.1	0.91
Bay 19	Vertical	15.2	0.91
Bay 19	Vertical	45.7	0.91
Bay 2	Horizontal	30.5	0.31
Bay 2	Horizontal	30.5	3.4
Bay 2	Horizontal	30.5	4.6
Bay 4	Horizontal	30.5	0.31
Bay 4	Horizontal	30.5	3.4
Bay 4	Horizontal	30.5	4.6
Bay 10	Horizontal	30.5	0.31
Bay 10	Horizontal	30.5	3.4
Bay 10	Horizontal	30.5	4.6
Bay 19	Horizontal	30.5	0.31
Bay 19	Horizontal	30.5	3.4
Bay 19	Horizontal	30.5	4.6

4.4.2 Future Instrumentation

The pine wood crib and PU foam block experiments will also include a load cell under the fuel. If possible, optical density meters and ionization/photoelectric detectors should be included. Scaling these devices would be beneficial to investigators for analyzing detector response and front arrival times. They would also

assist in modeling toxicity levels due to the presence of smoke as measured by the optical density meters. The full scale ATF test series is an excellent scaling example since a wide range of instrumentation was used.

4.4.3 Data Acquisition

The thermocouples and gas flow meter were connected to two NetDAQ Fluke 2645A data acquisition systems. The systems were interconnected to allow simultaneous scans. Each system was equipped with a terminal block consisting of 20 analog channels to convert transducer signals and relay them to a laptop PC equipped with an Ethernet connection and the *Fluke NetDAQ Logger* software [23]. A single channel was used to collect data from the mass flow meter during the gas burner tests. Measurements were taken at one second intervals.

5. Results and Discussion

5.1 Scaled High Bay Test Series

5.1.1 Comparisons Between ⅛ and Full Scale Models

The goal of scale modeling is to reproduce full scale values or to create an accurate prediction of expected full scale values. The transient data is compared against the full scale time values, meaning the ⅛ scale model time has been increased by a factor of $\ell^{1/2}$. To measure the success of the partial scaling laws applied here, the following data will be examined.

- The temperature results between experimental trials will be compared for the scale model. This will give an indication of the repeatability of the scaled test series.
- The ⅛ scale fires were designed using a target heat release rate from the full scale experiments. The fuel supply rate of the gas and the burning rate of the gas and the heptane will be compared between the full and scale model.
- The uncertainty of the ⅛ model results compared to the full scale temperature values will be assessed. A statistical t-test was also be applied to the data to display the relationship between the full and model data.
- The general temperature rise results are discussed. These results gave an indication of the overall performance and application of the scaling laws for these fires. The transient temperatures will be observed based on fire size, fuel type, and thermocouple location. In particular, the temperature will be

compared between scales for locations close to the ceiling, far from the ceiling, and various axial distances from the fire.

- The flame height and general flame behavior, such as twisting or necking, are compared for the gas burner and the heptane pool fire.
- The temperature rise at steady state will be compared between the ⅛ and full scale models. Steady state was determined by the duration of the test and visual indications during the experiments. Note that both fuels reach steady state relatively fast.

5.1.2 Experimental Procedure

The heptane pool fires were conducted first in this test series. Water was poured into the pans in order to create an even surface for fuel burning. The 4.6 cm diameter and 6.1 cm diameter pans (modeling the 30.5 cm and the 45.7 cm pans) were each filled with 25 mL of water. The 9.9 cm pan (modeling the 61 cm pan) was filled with 50 mL of water. The heptane was measured using a 10 mL graduated cylinder and an eye dropper to ensure accuracy. The amount of fuel for each size was calculated in Section 4.2.2. The 4.6 cm pan required 1.22 mL of heptane, the 6.1 cm pan required 2.82 mL of heptane, and the 9.9 cm pan required 7.3 mL of heptane. For each trial, the pan was positioned in the center of the enclosure under Bay 16. The NetDAQ system was started and allowed to run a few seconds in order to synchronize scans between the two Fluke systems. A video camera was also started at this time. The heptane was lit using a butane lighter and a stop watch was started. Various still camera shots were taken. The heptane was allowed to burn to extinction and the total burn time was recorded. The video camera and data acquisition system were stopped.

The lab hood was turned on to exhaust any gases and assist in cooling down the enclosure. The hood was not used during the tests since the mechanical exhaust had a significant impact on the flame behavior. While the enclosure cooled back to ambient temperature (~20-22°C), the pan was removed, emptied, and refilled with the appropriate amount of water and heptane to ensure the same initial conditions. This process was repeated for each trial. Three trials were conducted for the small pool fires, five trials were conducted for the medium pool fires, and three trials were conducted for the large pool fires.

A mass flow meter was connected to the NetDAQ system for the gas burner tests. Commercial grade methane was used at 137.9 kPa. Small stones were poured into the burner after testing the gas flow. The burner was placed and secured in the center of the enclosure below Bay 16. Due to the precision of the mass flow meter, the 25 kW experiments were not modeled. The scaled flow for the 25 kW fires was not strong enough to sustain a flame. Some flashing did occur, but this was not consistent enough for a comparison with the full scale experiments. Tests were conducted for the 50 kW, 75 kW, 150 kW, 250 kW, and 300 kW fires. In each trial, the NetDAQ system was started and allowed to run a few seconds in order to synchronize scans between the two Fluke systems. A video camera was also started at this time. The flow meter was opened to the prescribed mass flow depending on the size of the fire, as noted in Section 4.2.1. This was done manually. The valve on the flow meter was very sensitive, resulting in some variation from the full scale experiments due to human error. The mass flow meter measured flow in L/min. Table 5.1 displays the mass flow for each fire size.

Table 5.1: The Mass Flow for Each Gas Burner Fire.

Full Scale Fire Size	⅛ Scale Fire Size	Mass Flow (L/min)
50 kW	0.28 kW	0.428
75 kW	0.41 kW	0.642
150 kW	0.83 kW	1.29
250 kW	1.38 kW	2.14
300 kW	1.66 kW	2.57

The burner was lit using a butane lighter and a stop watch was started. Various still camera shots were taken. Each trial burned for 318 seconds. At this time, the valve on the mass flow meter was closed and the flame extinguished immediately. The data acquisition and video camera were stopped. The hood was turned on to exhaust gases and cool down the enclosure to the ambient temperature. Two trials were conducted for each gas burner fire size.

5.1.3 General Observations

The flame in both the gas burner and heptane pool fire tests acted similar to the full scale experiments. As mentioned earlier, the gas burner tests used methane instead of natural gas. Both fuels burn relatively clean, however the smaller scaled experiments (50-150 kW fires) did not produce flames as yellow/orange as the full scale. Additionally, the flame height in the scaled experiments was slightly lower than in the full scale for all tests (see Figure 5.1), whereas the overall shape of the flame was the same between the two scales. The flame height is analyzed further in Section 5.2.

Full Scale **⅛Scale**

Figure 5.1: Visual Flame Height Comparison for 300 kW Gas Burner Tests.

The flame in the ⅛ scale experiments burned evenly across the burner suggesting that the burner design allowed the gas to fully disperse. The burner produced turbulent flames in all tests. It was difficult to capture a turbulent flame on camera for the 50 kW and 75 kW model experiments since the flame tip was a very faint blue. Spinning and leaning of the flame was observed in the experiments due to the burner placement relative to the small corridors. These patterns were also experienced in the full scale test series.

The heptane pool fires were also successful in simulating the full scale fire scenarios. The bright orange heptane flame produced smoke that could be seen exiting the main corridor, as noted in Figure 5.2.

Figure 5.2: Smoke Exiting the Scaled Corridor.

While optical density measurements and smoke detection were not included in the model experiments, the smoke dispersion was visually similar. This is notable due to the complex ceiling geometry created by the partitions. The scaled flame height visually matched the heights from the full scale experiments. The heptane burned steadily in all tests. In the large pool fires, necking of the flame due to air entrainment was observed. This also resulted in a wider turbulent flame farther downstream as noted in Figure 5.3. The flame tips in the ⅛ and full scale large pool fires lifted off of the main body of the flame and extended almost to the height of the partitions.

Full Scale **⅛Scale**

Figure 5.3: Visual Flame Height, Necking, and Turbulence for the Heptane Pool Tests.

The flames in both the model and full scale experiments leaned slightly. Once again, this was due to the location of the fire relative to the two smaller corridors, which provided additional ventilation to the main corridor space. The heptane was allowed to burn until extinction. As the heptane supply diminished, the flame got noticeably smaller and less soot was produced. In some trials, a small portion of the heptane surface kept burning (see Figure 5.4).

Figure 5.4: Flamelet Due to Unevenly Spread Heptane.

These small flamelets were a result of extra heptane pooled at that location. The flamelets only burned an addition 3-5 seconds past the burnout of the rest of the flame, so they had little impact on the overall temperature results.

5.1.4 Repeatability of Scale Model Experiments

Repeatability ensures the test procedure is reliable. To assess the repeatability of the gas burner and heptane pool fires, the temperature rise distribution between trials was compared. Figures 5.5 through 5.9 show trials for each fuel at various sizes and locations.

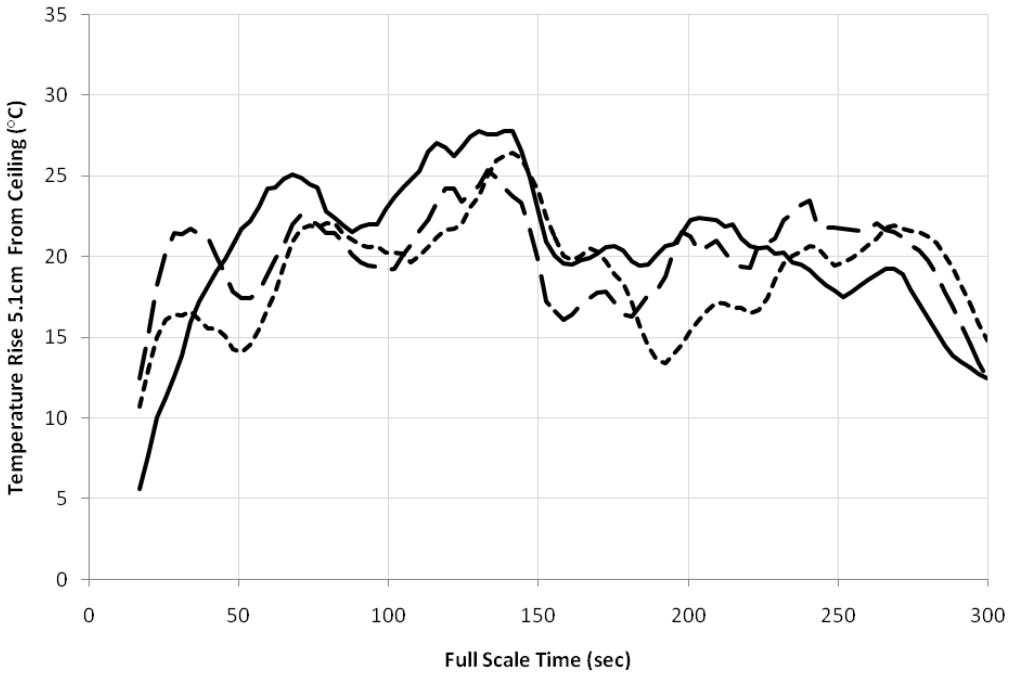

Figure 5.5: ⅛ Scale Small Pool Fire Trials Above Fire

Figure 5.5 displays similar temperature trends and values. Some variation in temperature is acceptable due to human error. Small differences in the water level in the pan or the amount of heptane can result in slight temperature variations. These temperatures were measured directly above the fire where slight changes in flame height or flame trubulence also have an effect on temperature.

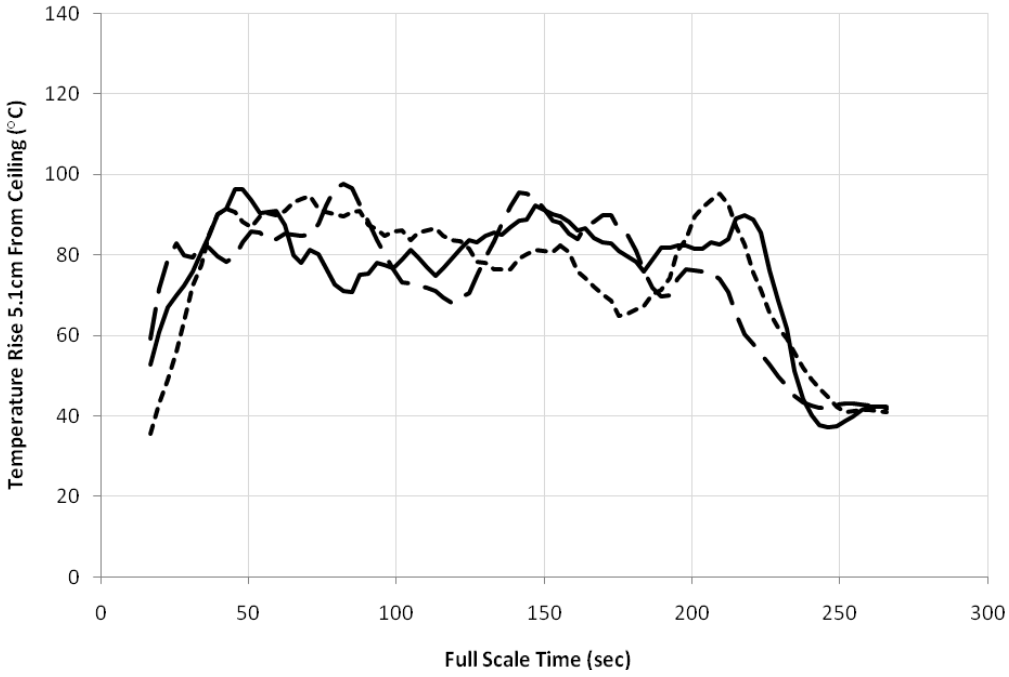

Figure 5.6: ⅛ Scale Large Pool Fire Trials Above Fire

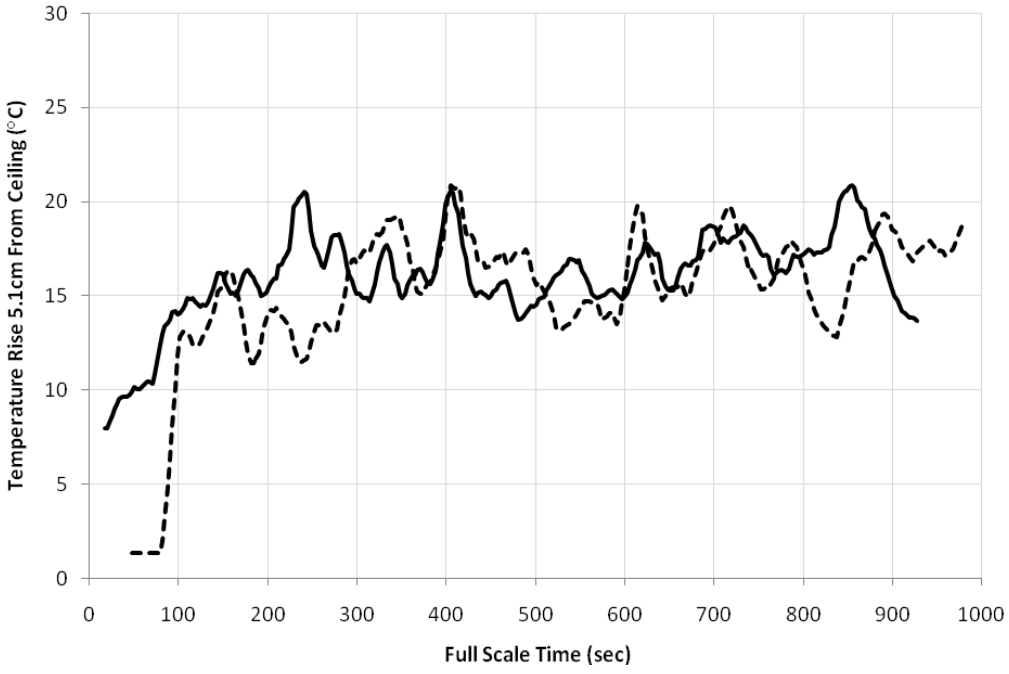

Figure 5.7: ⅛ Scale 50 kW Gas Burner Trials Above Fire

Figure 5.7 shows that the two trials conducted for the 50 kW gas burner measured similar temperatures. There is some discrepancy between the two trials within the first minute of the experiment. This is directly related to human error since the gas

flow meter was very sensitive and the flow was manually adjusted to the prescribed value.

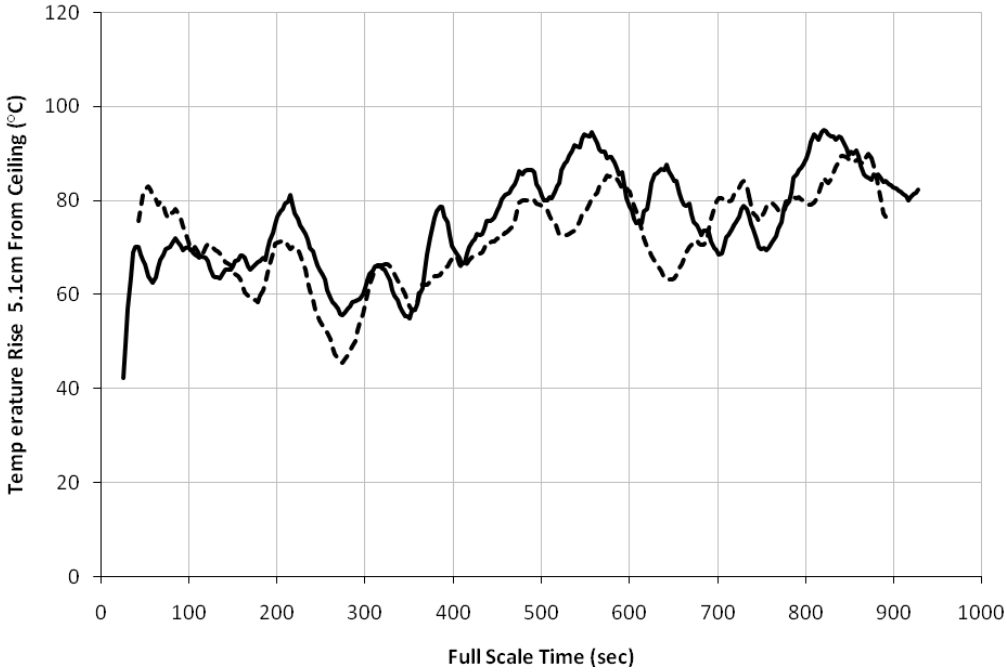

Figure 5.8: ⅛ Scale 250 kW Gas Burner Trials Above Fire

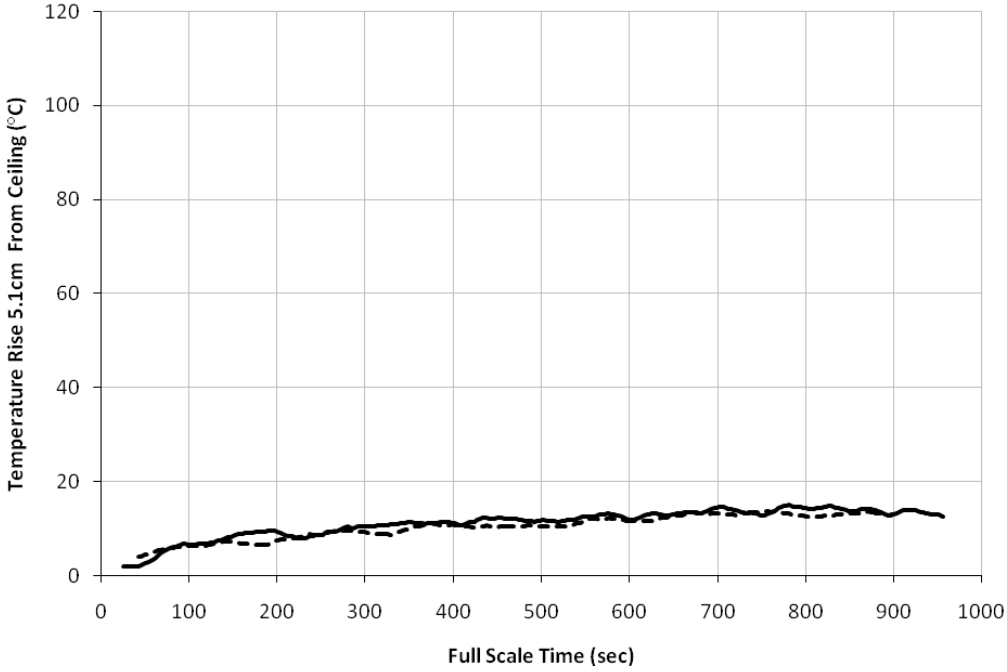

Figure 5.9: ⅛ Scale 250 kW Gas Burner Trials Far From Fire

Figure 5.9 plots the temperatures in Bay 2 for the 250 kW trials. Distance is a factor when comparing the full scale to the ⅛ scale temperature rise data. Bays far from the fire show a greater temperature rise difference from the full scale data. Between trials in the scale model, this is not the case. This graph demonstrates that the boundary materials have the same heat transfer effects between trials, as expected. Both curves follow the same temperature rise trends. Based on the above comparisons, the ⅛ scale model demonstrates repeatability between trials. Temperature rise comparisons between this data and the full scale data are an accuarate representation of this scale model's performance. The slight variations in temperature between trials will contribute to a few degrees of uncertainty. The comparions between full and model scale will be influenced by the trials compared from each test series.

5.1.5 Repeatabilitiy of the Full Scale Experiments

Multiple trials were also conducted for the full scale heptane pool fires experiments. The temperature distributions throughout the enclosure from each trial were compared to assess the repeatability of the full scale experiments. Recall that the mass flow rate was prescribed to grow as a function of time for some trials. One trial for each fire size did not include this ramp function. Since this research focuses on static fires that reach steady-state quickly, only one full scale trial for each fire size is compared to the model experiments. As seen in Figures 5.10-5.12, the full scale trials for the heptane pools demonstrate acceptable repeatibility.

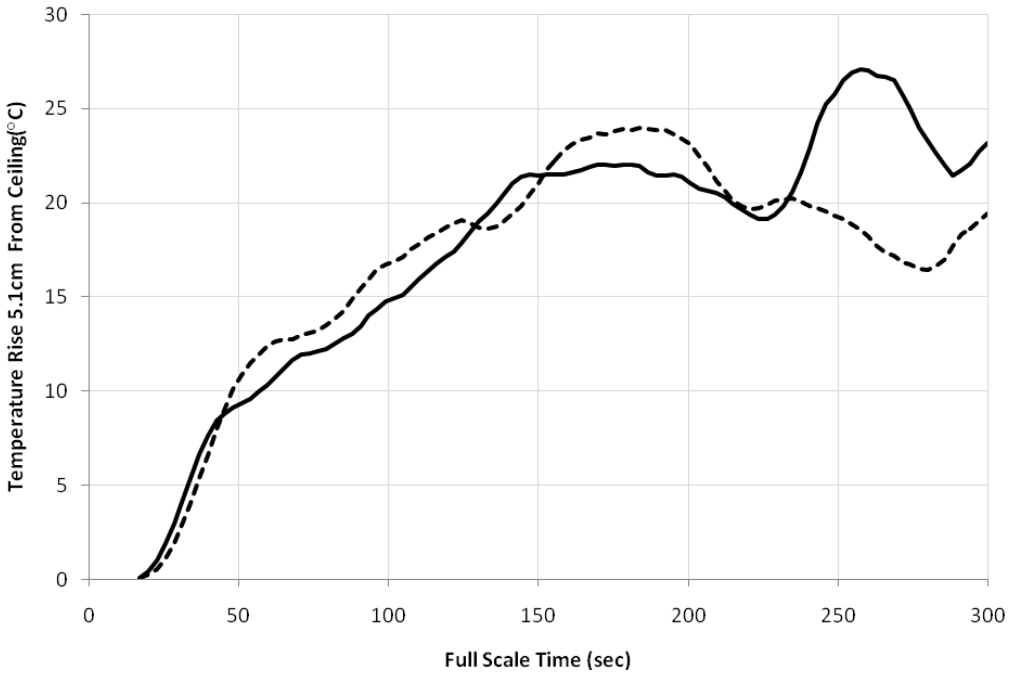

Figure 5.10: Full Scale Small Pool Fire Trials Above Fire

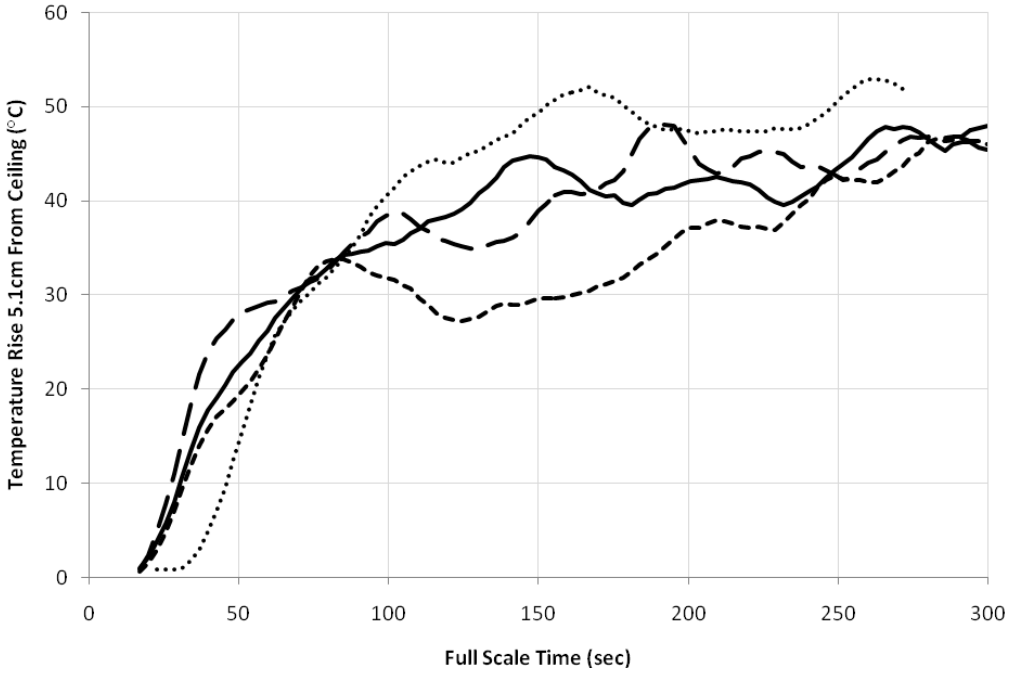

Figure 5.11: Full Scale Medium Pool Fire Trials Above Fire

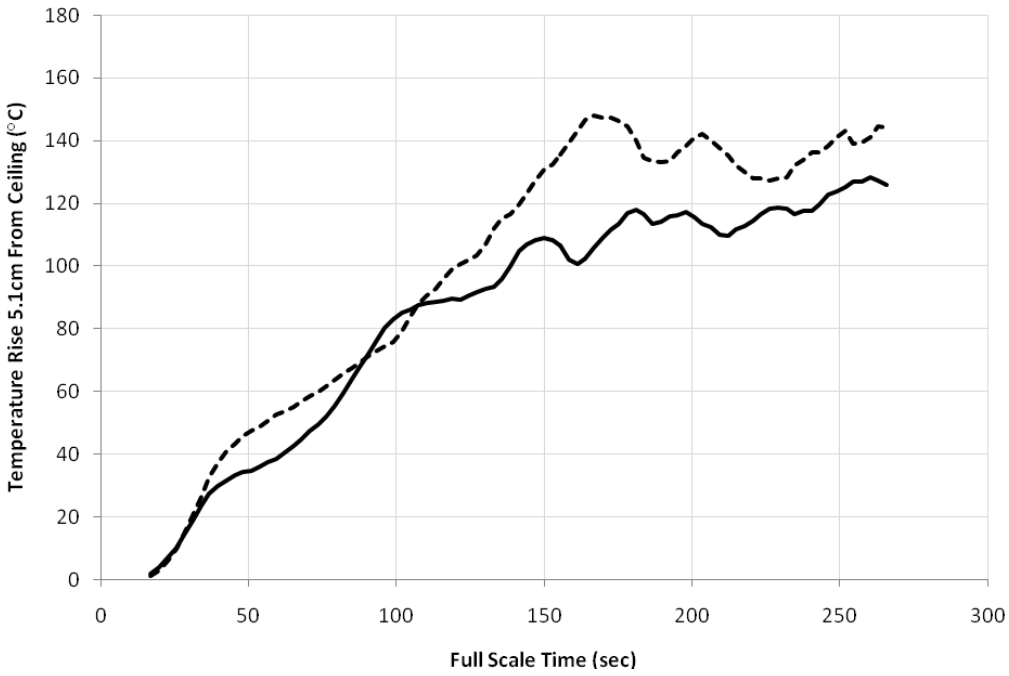

Figure 5.12: Full Scale Large Pool Fire Trials Above Fire

There is more variation between trials in these full scale experiments. This will impact the scale model comparisons. At some times, a 10°C difference is seen between trials with the same fire size. These are especially notable for the medium pool fires. Uncertainty in temperature rise comparions between the full scale and scale model may originate from simple temperature discrpancies between trials.

5.1.6 Fuel Supply Rate and Burning Rate

5.1.6.1 Natural Gas Burner

The fuel supply rate and heat release rate of the natural gas burner were very closely matched between the ⅛ and full scale experiments. To determine the prescribed flow of the ⅛ scale gas burner, the dimensionless heat release rate Q* was matched to the full scale Q*. Some noise is present in the beginning of the model experiments due to the sensitivity of the flow meter and human error. Figure 5.13 shows the heat release rates for the full scale and the model burner at 50 kW, 150 kW,

and 250 kW based on the mass flow data measured during each experiment. Figure 5.13 scales the dimensionless heat release rate values to the full scale fire sizes. The scale model did not have a 50 kW, 150 kW, or 250 kW fire. The proximity to these values is a result of the increasing the model fire size by a factor of $\ell^{5/2}$. It is still an accurate representation of the model dimensionless heat release rate compared to the full scale dimensionless heat release rate.

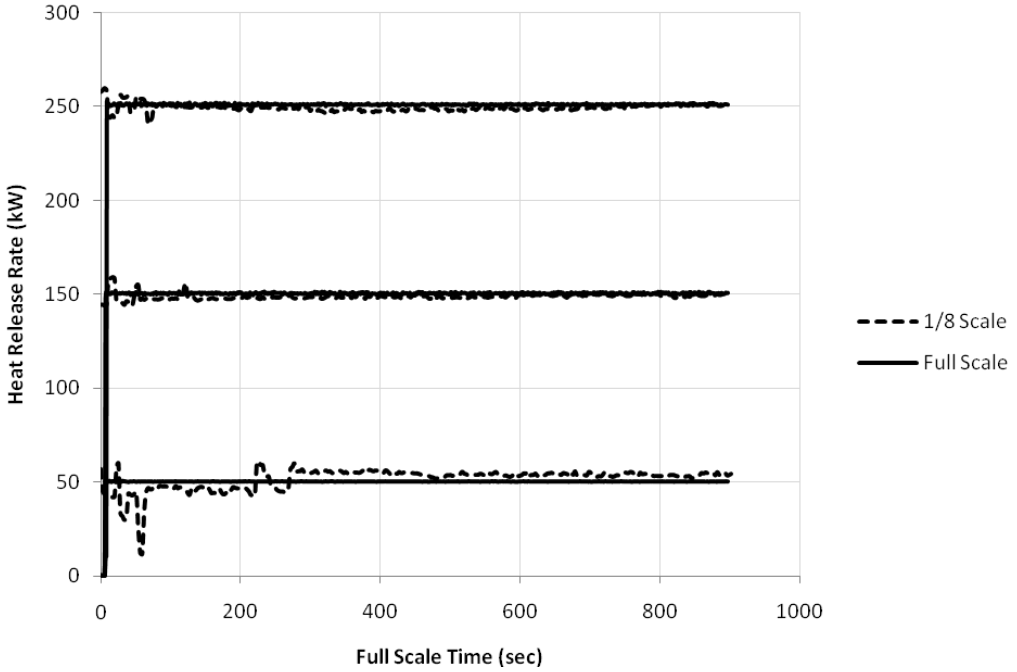

Figure 5.13: Heat Release Rate of Model and Full Scale Gas Burner.

The flow meter was accurate to 0.01 L/min and the flow for each trial was prescribed manually at the beginning of the test. It was especially difficult to adjust the flow meter for the low flows corresponding to the scaled 50 kW and 75 kW experiments.

It is important to verify the prescribed scaling methodology using a controlled fuel. A gas burner is the simplest fuel to scale since there is a constant mass flow and a defined mass loss rate that quickly reaches steady state. This means the actual heat release rate of the burner is close to the theoretical Q values [18, 24]. With other

fuels, radiative heat feedback or fuel depletion can have an effect on the burning characteristics and heat release rate. Therefore, it is suggested that a fuel with a prescribed burning rate, such as a gas burner, is used to reinforce the prescribed scaling methodology.

5.1.6.2 Heptane Pool Fire

The fuel supply rate and dimensionless heat release rate matched reasonably well between the ⅛ and full scale experiments. Since a load cell was not used in either test series, the mass loss rate of the heptane was estimated based on the initial amount of fuel and the elapsed time of the experiment. This was initially done using the full scale (FS) test data in order to calculate Q* and the amount of fuel needed for the scaled experiments. Table 5.2 provides a summary of the average values for the test duration and dimensionless heat release rate for each fire in the ⅛ and full scale models.

Table 5.2: Average Elapsed Time and Q* Comparison.

Fire Size	⅛ Time (sec)	⅛ Q*	FS Time (sec)	FS Q*
Small	99	0.027	93	0.030
Medium	94	0.067	109	0.064
Large	82	0.194	73.5	0.227

The slight differences between the two test series are likely due to the lack of data on the mass loss rate of the fuel. Since the mass loss rate may fluctuate as a function of time, a load cell would allow a more accurate mass loss rate and dimensionless heat release rate to be calculated and applied in the scale model. The faster mass loss rates in the full scale experiments result in a higher heat release rate. Since the ⅛ scale tests burned slightly longer than the full scale tests did, the heat release rate was lower.

This accounts for some of the temperature discrepancies between the model and full scale measurements, as discussed in Section 5.1.4.

5.1.7 General Temperature Results

Overall, the proposed scaling theory provided a good method to predict full scale temperatures using a ⅛ scale model. The best temperature results were measured directly above the fire in Bay 16. Reasonable results were also obtained in the two bays on either side of Bay 16; Bay 13, Bay 15, Bay 17, and Bay 19. The results were assessed using a maximum temperature rise uncertainty, a statistical t-test, and plots of temperature rise as a function of time. For all trials, the temperature rise was used instead of the measured temperature. This was done in order to reduce environmental impacts on the comparison. The full scale experiments were conducted in an open lab in July, where the ambient temperature was ~27°C. The small scale experiments were conducted in a closed lab in January, where the ambient temperature was ~20°C.

5.1.7.1 Maximum Temperature Rise Uncertainty

The maximum temperature rise uncertainty was calculated similar to validation and verification efforts by the Nuclear Regulatory Commission. The method resulted in a percentage of uncertainty based on the peak temperature relative to the ambient temperature. [25]

$$\frac{\Delta M - \Delta E}{\Delta E} x100 = \frac{\left(T_{\max} - T_{\infty}\right)_{\mathrm{mod}\,el} - \left(T_{\max} - T_{\infty}\right)_{full}}{\left(T_{\max} - T_{\infty}\right)_{full}} x100 = \% \qquad (5.1)$$

Where E represents the expected (full scale) values and M represents the model values. This percentage represents the relative difference between the model predictions and the full scale measurements [25]. A maximum value approach was

used since the uncertainty between scales could not be compared as a function of time. The full scale data was collected every second. The ⅛ scale data was collected every second in the experiments, but was then scaled using the $t \sim \ell^{1/2}$ scaling law. This results in fewer data points for the scale model. A transient comparison requires the measurements to have comparable time steps.

Twenty percent was decided to be the highest level of acceptable uncertainty. This would account for any discrepancies between temperature data due to human error, experimental measurement uncertainty, or model sensitivity due to model input uncertainty (such as boundary differences) [25]. If the uncertainty is positive, the full scale temperature difference was higher than the model temperature difference. If the uncertainty is negative, the full scale temperature difference was lower than the model temperature difference. In Figure 5.14 and 5.15, the absolute value of the uncertainty was used to show the uncertainty trends as a function of axial distance from the fire. The fire is located at the origin. Negative distance values represent bay locations north of the fire (Bays 2-15) and positive distance values represent bay locations south of the fire (Bays 17-19).

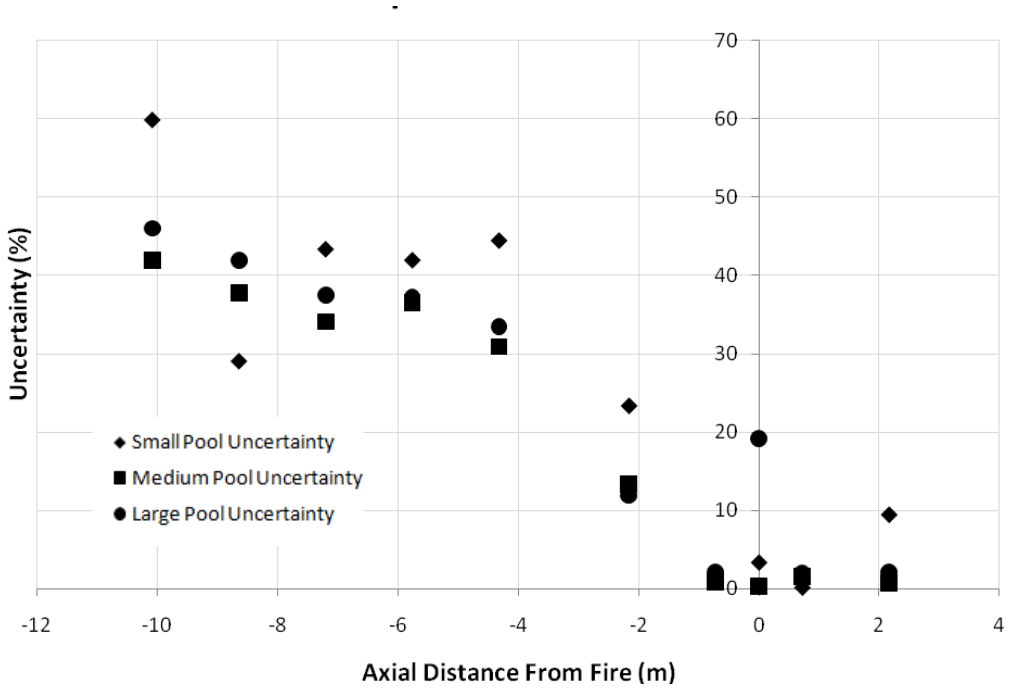

Figure 5.14: Pool Maximum Temperature Rise Uncertainty vs. Distance from Fire

The maximum temperature rise uncertainty increases dramatically for locations far from the fire. In fact, only two locations on either side of the fire have an acceptable level of uncertainty. The same trend occurs for the gas burner fires.

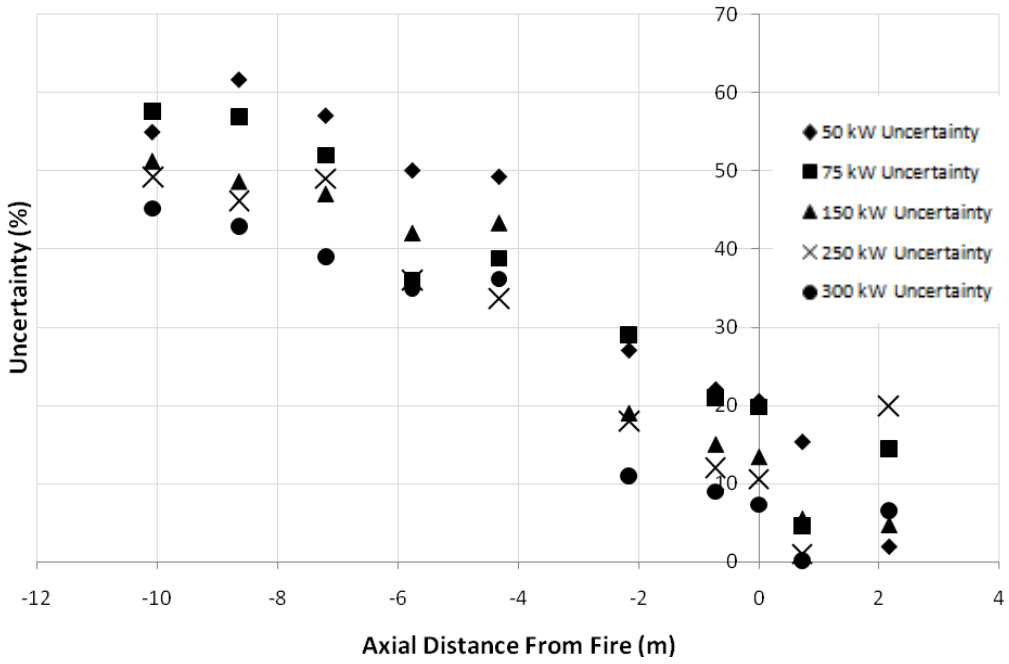

Figure 5.15: Burner Maximum Temperature Rise Uncertainty vs. Distance from Fire

Therefore, based on the maximum temperature rise, only Bays 13, 15, 16, 17, and 19 are reasonably accurate at simulating the full scale fire temperatures. This is directly related to the boundary materials. The discrepancies in the thermal properties of the actual materials compared to the theoretical values cause a variation in the predicted heat transfer properties of the enclosure. In other words, due to the conductivity and density of the Kaowool, the ability of the ⅛ scale temperatures to predict the full scale temperatures decreases with increasing distance from the fire.

5.1.7.2 Statistical T-test

A statistical t-test was performed to show the significance between the ⅛ scale data and the full scale data. Each set of temperature data has its own statistical mean. The t-test measures the means of each test relative to the entire temperature distribution and assigns a p-value which compares the two sets of data. This p-value indicates how likely it is that the scaled results occurred by chance. A low p-value means that the model is a significant representation of the full scale data and vice versa. The t-tests applied for this research assumed unequal variances and independent data sets. A two-tailed approach was used with $\alpha=0.05$. Therefore, a low p-value for these tests is below 0.05. The temperature values were not averaged between trials. Each trial was compared to the full scale data for the heptane pool fires and the gas burner fires. In every case, $p<<0.05$, meaning there is no significant difference between the model and full scale data. Therefore, the ⅛ scale model is representative of the full scale data. [26]

5.1.7.3 Transient Temperature Results

While the maximum temperature rise uncertainty and the t-test provided a good understanding of the relationship between the ⅛ and full scale data, it is important to look at the temperature rise as a function of time. When comparing transient temperature data, it is necessary to consider the time step associated with each set of data. The ⅛ experiments were shorter than the full scale experiments. In order to compare the results as a function of time, the ⅛ scale data was stretched by a factor of $\ell^{1/2}$ to correspond to the full scale time. This means there are significantly fewer data points in the ⅛ scale data. A five point running average was applied to the model data and a ten point running average was applied to the full scale data in order to smooth the temperature rise curves.

Temperature Distribution "Near" the Ceiling

The differences between the full scale and ⅛ scale model temperatures were affected by the location of the thermocouple in the enclosure. Temperatures were measured 5.1 cm, 15.24 cm, and 45.7 cm below the ceiling in the full scale experiments. Figures 5.16-5.18 compare the temperature rise 0.72 meters away from the fire (Bay 17) for the heptane pool fires. These measurements were recorded 5.1 cm below the ceiling.

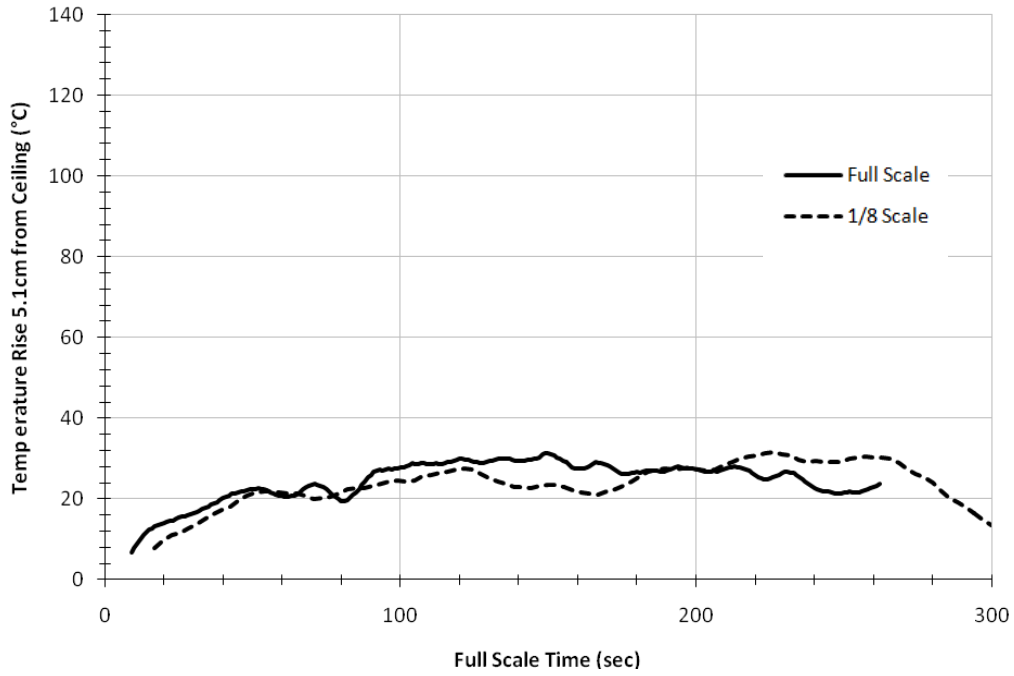

Figure 5.16: Temperature Rise 5.1 cm Below Ceiling in Bay 17 (0.72m away from fire) for Small Pool Fire.

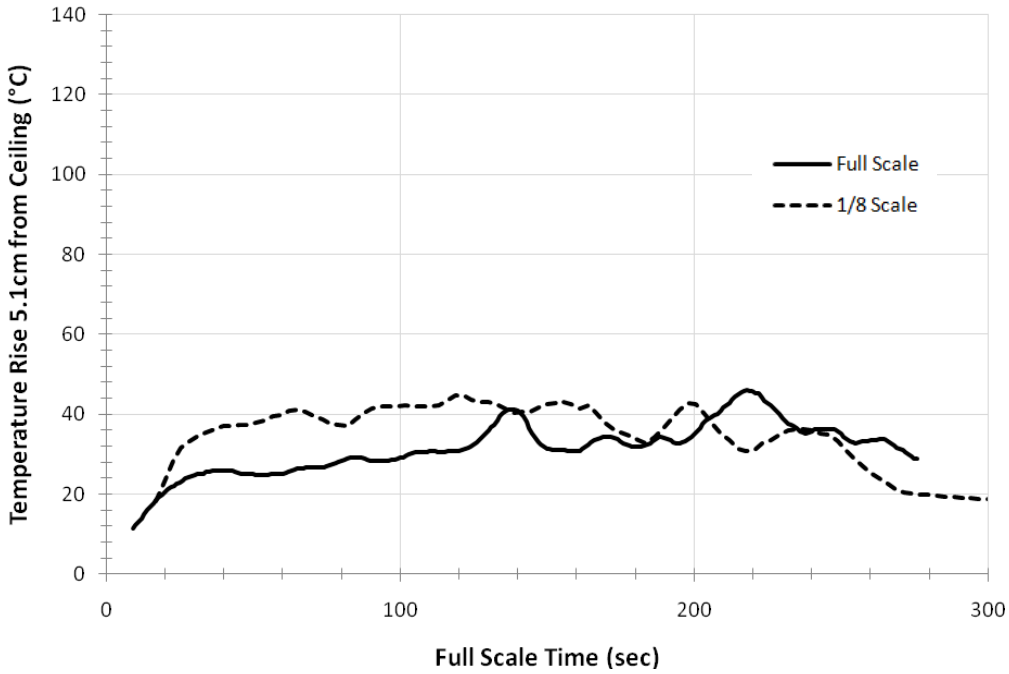

Figure 5.17: Temperature Rise 5.1 cm Below Ceiling in Bay 17 (0.72m away from fire) for Medium Pool Fire.

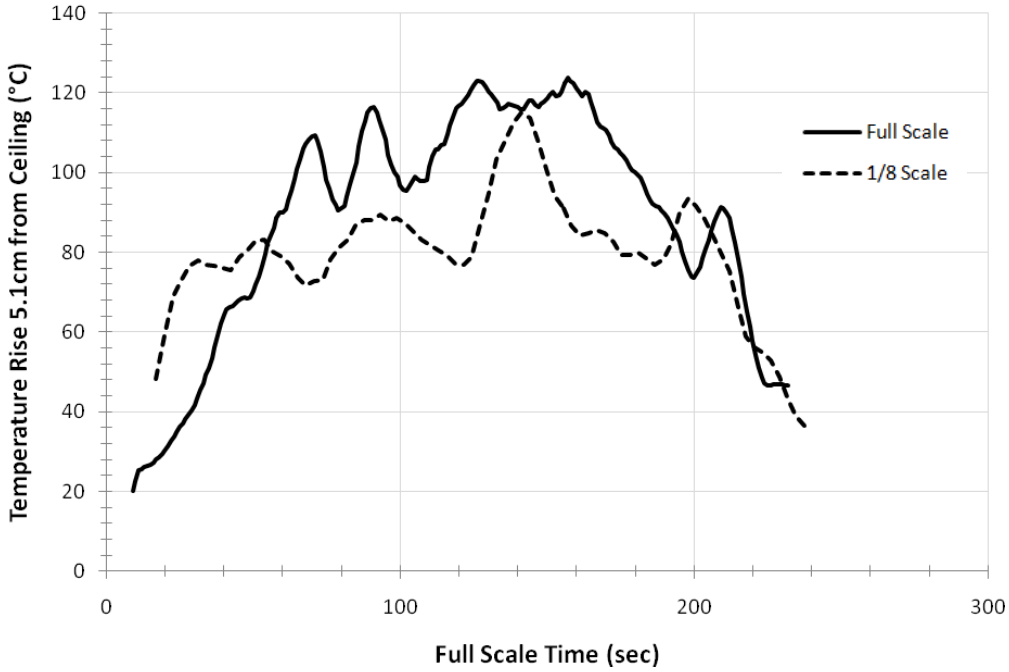

Figure 5.18: Temperature Rise 5.1 cm Below Ceiling in Bay 17 (0.72m away from fire) for Large Pool Fire.

Bay 17 is one bay removed from the fire. There is a slight delay in temperature rise due to the time lag associated with the convective flow. The thermocouples are close to the ceiling, meaning that some fluctuations will occur between models due to the turbulence at that elevation. The partitions and the ceiling cause mixing in the flows close to the boundaries. The 40 AWG thermocouples used in the scale model are sensitive to the temperature variations caused by this turbulence. The ⅛ model data, represented by the dotted line, is within 15°C of the full scale data at all times. Similar trends also occurred for the gas burner, where the ⅛ scale temperatures were within 15°C at Bay 17.

Temperature Distribution "Far" From the Ceiling

The ⅛ scale and full scale temperatures are closer for thermocouples farther from the ceiling. This is because the mixing caused by the boundaries obstructing the flow diminishes. The thermocouples located 45.7 cm below the ceiling show a

steadier temperature distribution. These results did a better job at predicting the full scale temperature data. This is shown in Figures 5.19-5.21, which depict Bay 10 at 45.7 cm below the ceiling for the heptane pool fires. It is important to compare temperature results at various elevations, but there is limited data since vertical thermocouples trees were only placed in Bays 2, 4, 10 and 19 in the scale model. This means that the temperatures 45.7 cm from the ceiling were only measured in a few bays.

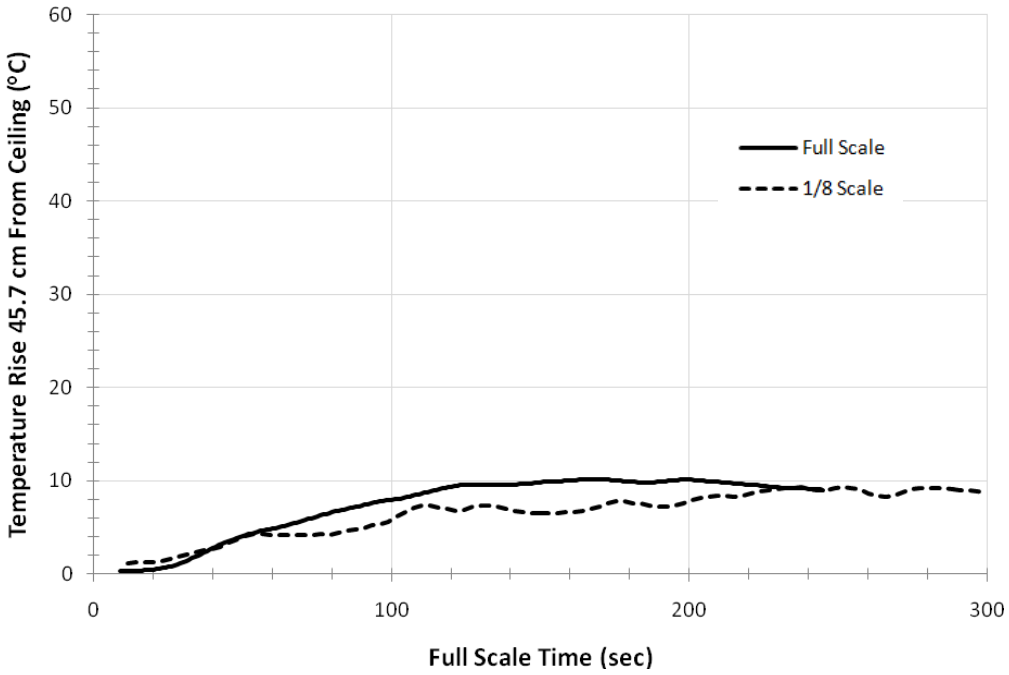

Figure 5.19: Temperature Rise 45.7 cm Below Ceiling in Bay 10 (4.32m away from fire) for Small Pool Fire.

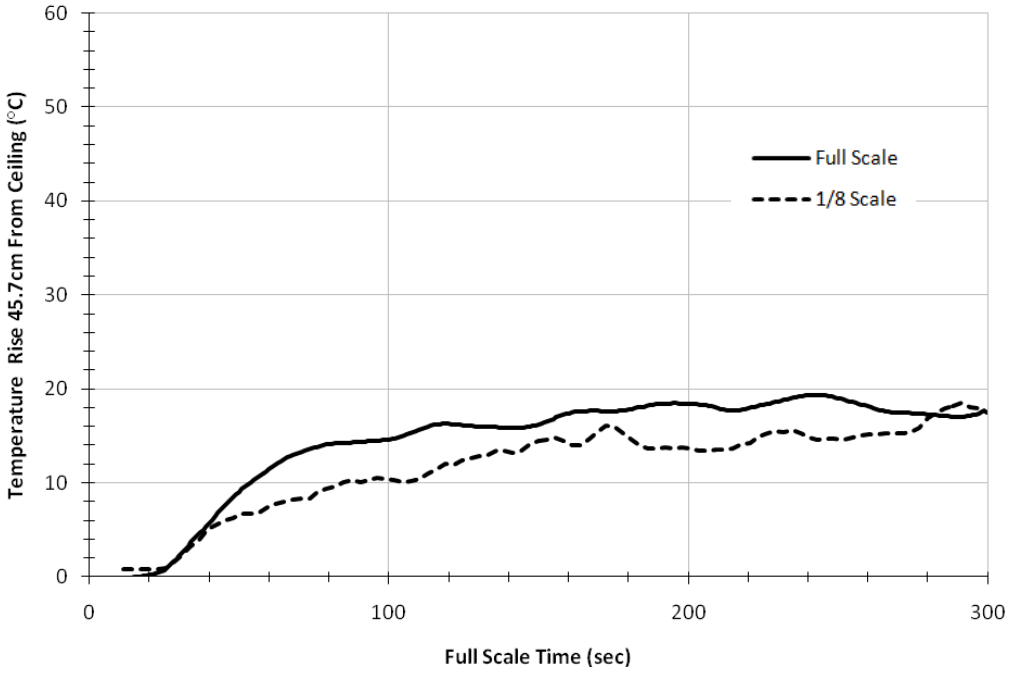

Figure 5.20: Temperature Rise 45.7 cm Below Ceiling in Bay 10 (4.32m away from fire) for Medium Pool Fire.

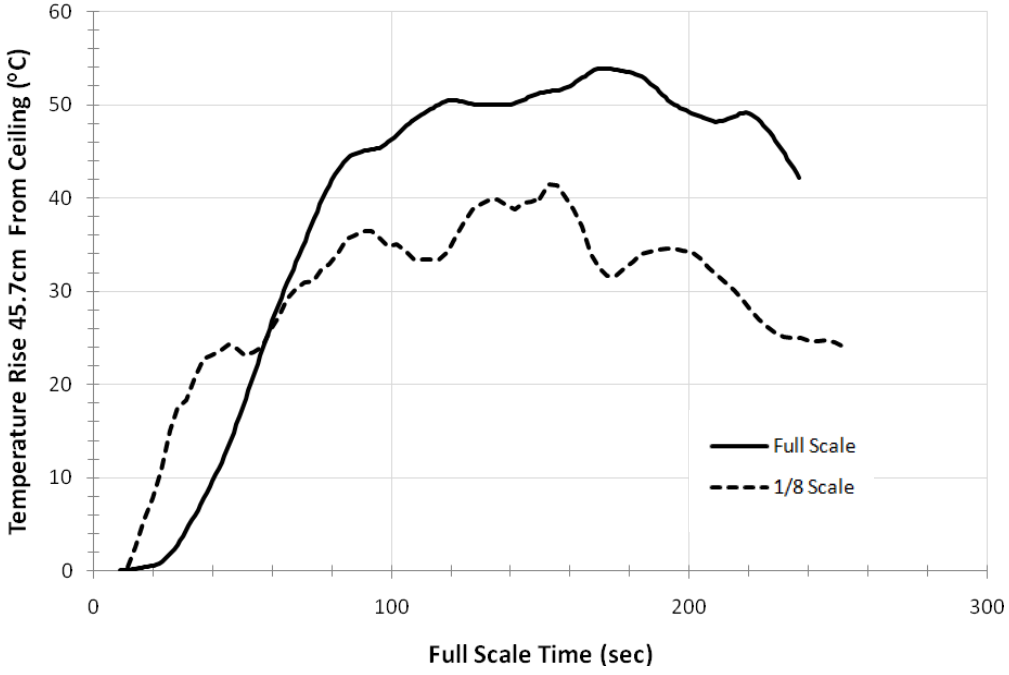

Figure 5.21: Temperature Rise 45.7 cm Below Ceiling in Bay 10 (4.32m away from fire) for Large Pool Fire.

At 45.7 cm below the ceiling, the difference in temperature rise between the full scale and the ⅛ scale is less than the temperature difference at 5.1 cm below the ceiling.

The overall temperature rise growth trend is also a better match farther from the ceiling. This is a result of less turbulence and the development of a layer at a farther distance from the ceiling. The ⅛ scale gas burner tests were also closer to the full scale temperatures at 45.7 cm than at 5.1 cm below the ceiling. Figure 5.18 shows a 15°C difference between scales for the large pool fire; the same difference for temperature close to the ceiling. This introduces the temperature differences based on location from the fire. The 5.1 cm from the ceiling data in Figure 5.15 was only one bay removed from the fire, whereas the 45.7 cm from the ceiling data in Figure 5.18 is six bays removed from the fire. The predictive capabilities of the model are affected by distance due to the material boundaries. This phenomenon is discussed at length in upcoming sections. Obtaining the same temperature difference six bays away shows that more accurate results are achieved at 45.7 cm below the ceiling.

Temperature Distribution Within the Bay

Horizontal thermocouples trees were placed in Bays 2, 4, and 10 in the full scale and ⅛ scale experiments. Bay 2 is 10.08 meters from the fire, Bay 4 is 7.2 meters from the fire, and Bay 10 is 4.32 meters from the fire. The tree was located 30.48 centimeters below the ceiling in each bay. While the larger scale had a thermocouple every 0.31 meters, the small scale experiments only had thermocouples corresponding to the 0.31m, 3.4m, and 4.6m full scale locations. Recall that an isosceles triangle was cut out of the east side of the partitions while the west side remained straight. The 0.31m location was adjacent to the angled side of the partition. This allowed the hot gases to flow freely into the next bay. The 4.6m location was bounded by the Kaowool partitions. The hot gases either had to fill up in the previous

bay and spill over the partition or travel through the angled side of the partition and down the length of the bay in order to reach the 4.6m location. Regardless of how the hot gases reached the thermocouple, there was a significant effect on the heat transfer as a result of the prolonged exposure to the partition material. The temperature rise comparison was very accurate inside of the bays for the large gas burner tests. The smaller gas burner tests matched well at the 0.31m location, but poorly at the 4.6m location. This is a result of the enclosure boundary materials and the configuration of the partitions. Figures 5.22-5.27 show the temperature rise at the 0.31m and 4.6m locations for the 50 kW, 150 kW, and 300 kW fires.

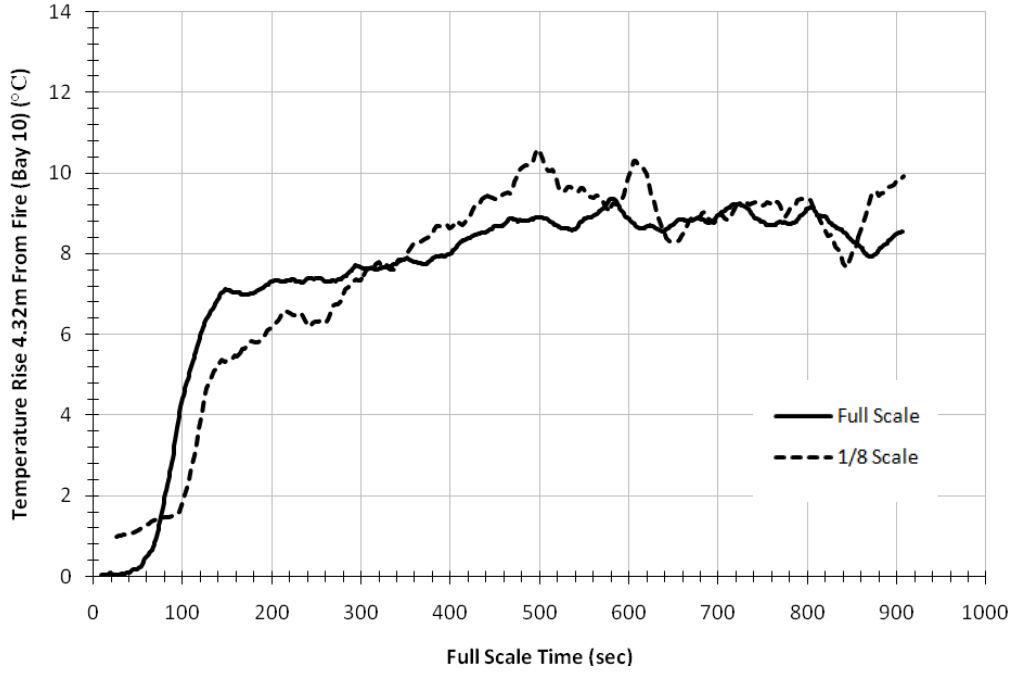

Figure 5.22: Temperature Rise 0.31m from East Wall in Bay 10 for 50 kW Gas Burner.

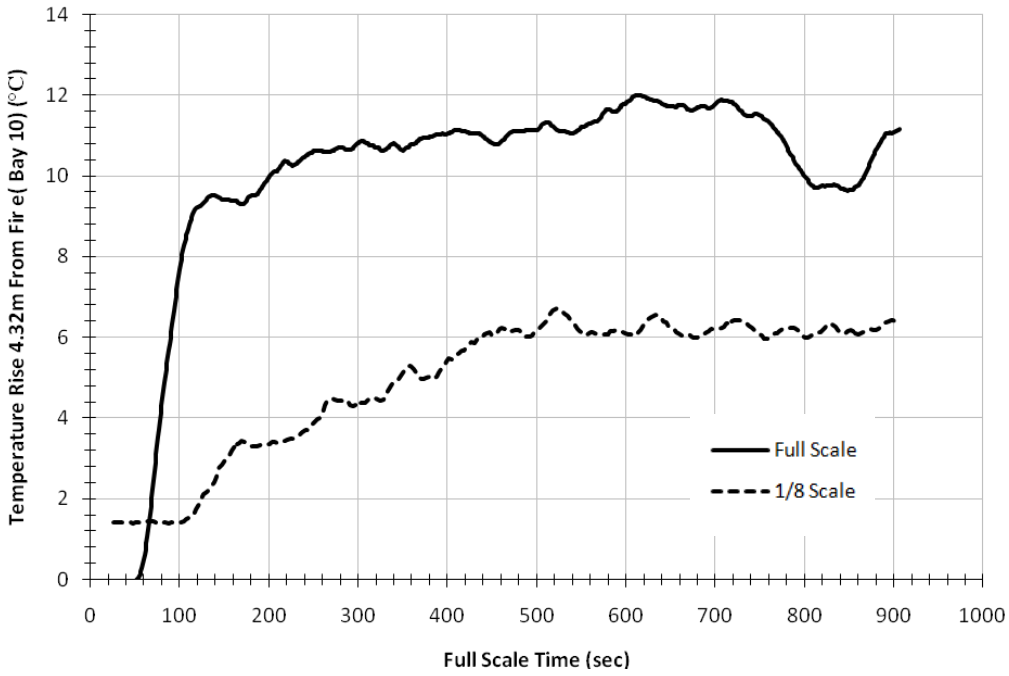

Figure 5.23: Temperature Rise 4.6m from East Wall in Bay 10 for 50 kW Gas Burner.

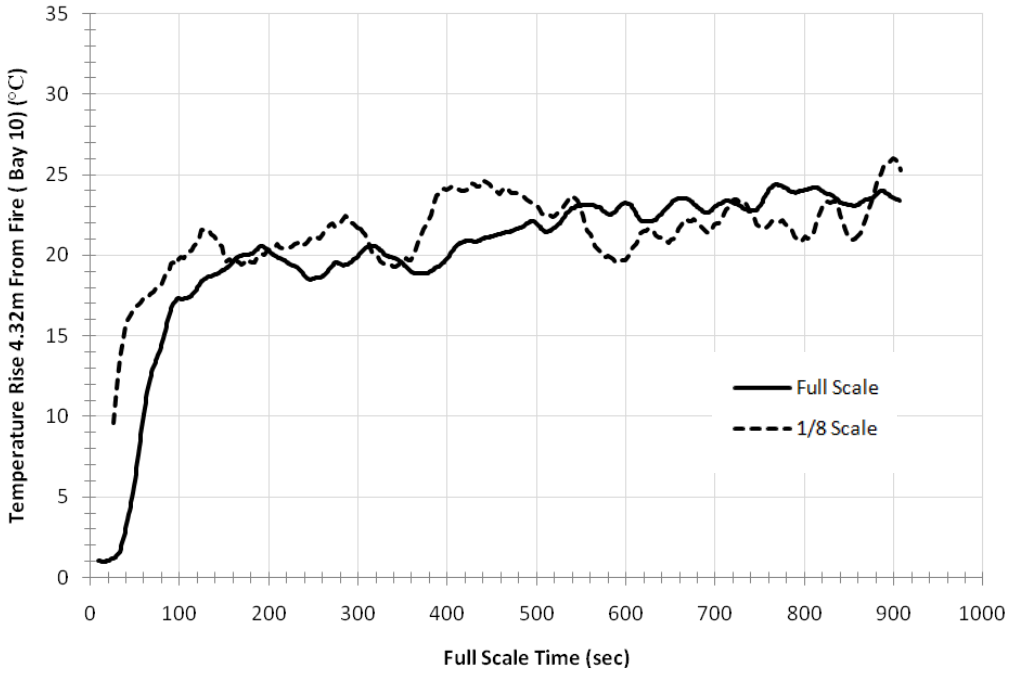

Figure 5.24: Temperature Rise 0.31m from East Wall in Bay 10 for 150 kW Gas Burner.

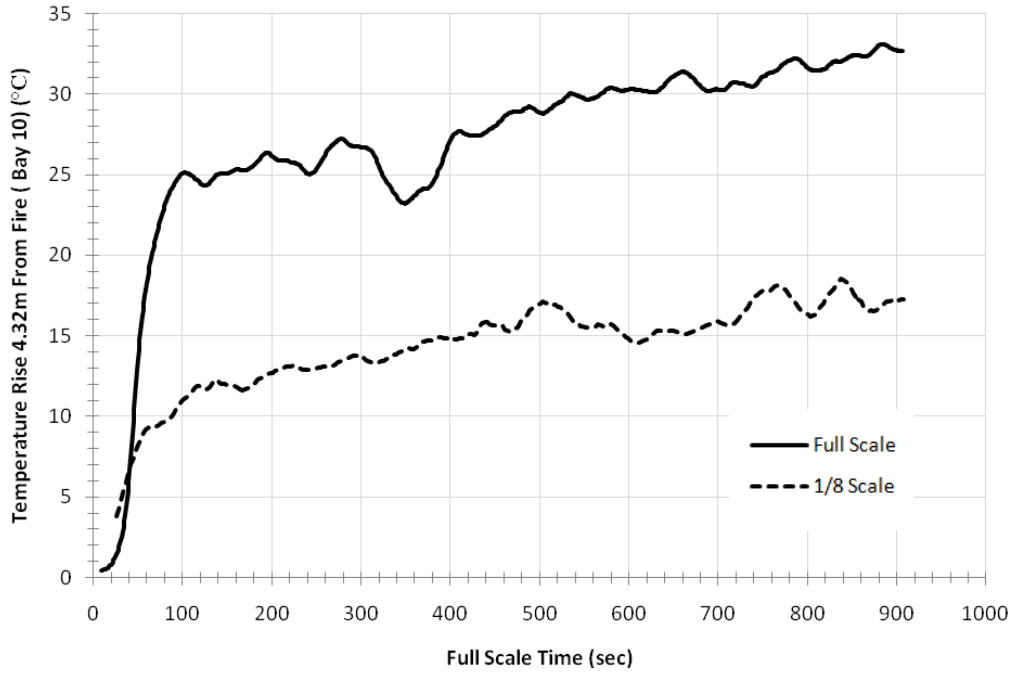

Figure 5.25: Temperature Rise 4.6m from East Wall in Bay 10 for 150 kW Gas Burner.

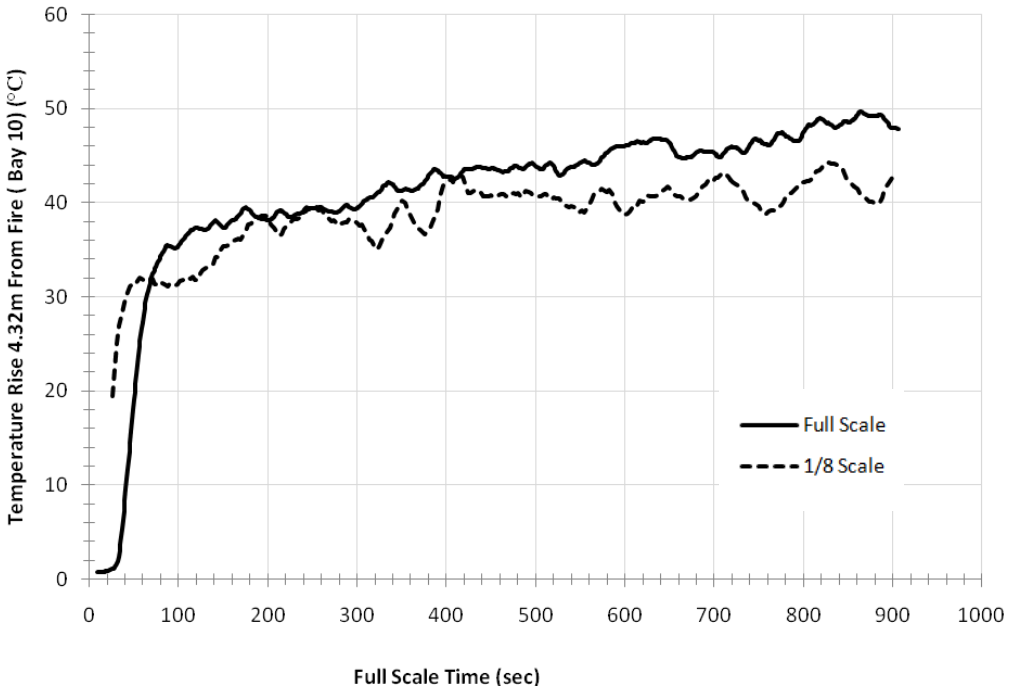

Figure 5.26: Temperature Rise 0.31m from East Wall in Bay 10 for 300 kW Gas Burner.

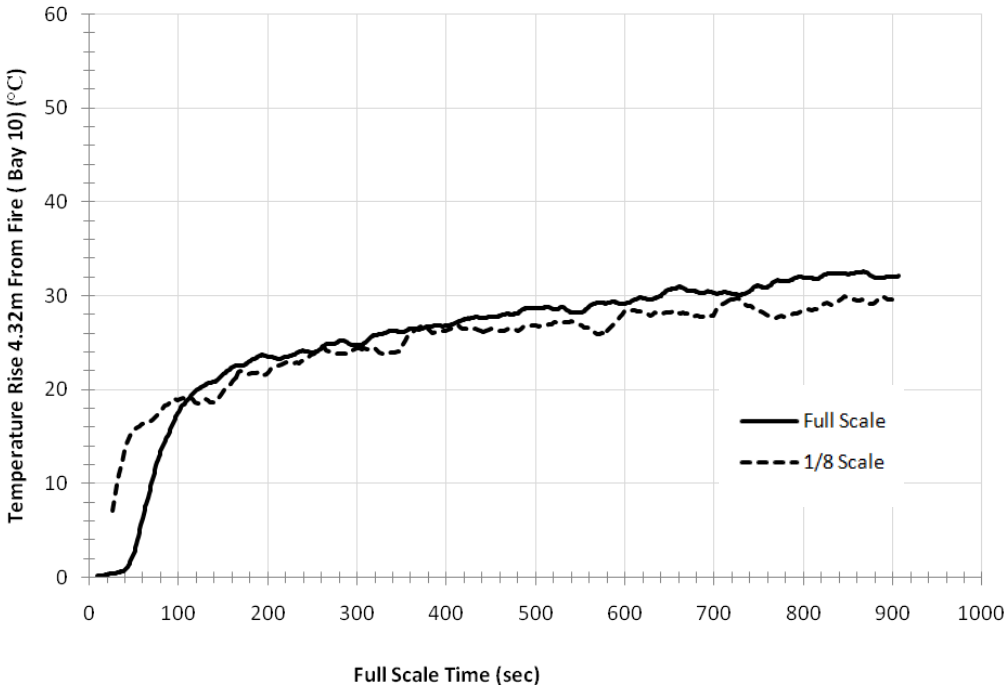

Figure 5.27: Temperature Rise 4.6m from East Wall in Bay 10 for 300 kW Gas Burner.

From these graphs, it is apparent that good results were obtained at all thermocouples located 0.31m from the east wall; the temperature rise between scales is within 10°C of one another. Only the largest fire was accurate at the 4.6m thermocouple location. After the first minute of the 300 kW fire, the temperature rise in the ⅛ scale and the full scale are very close. This shows that effects due to the material boundaries diminish over time for larger fires. The horizontal thermocouple trees in the heptane pool fire experiments were also affected by the heat losses due to the boundary materials. Similar results were achieved where the temperatures at 0.31m from the east wall were within 5°C of the full scale data but the thermocouples 4.6m from the east wall were not as accurate with a temperature difference doubling to ~10°C. Figures 5.28-5.31 shows the temperatures at the 0.31m and 4.6m locations for the small and medium heptane pool fires.

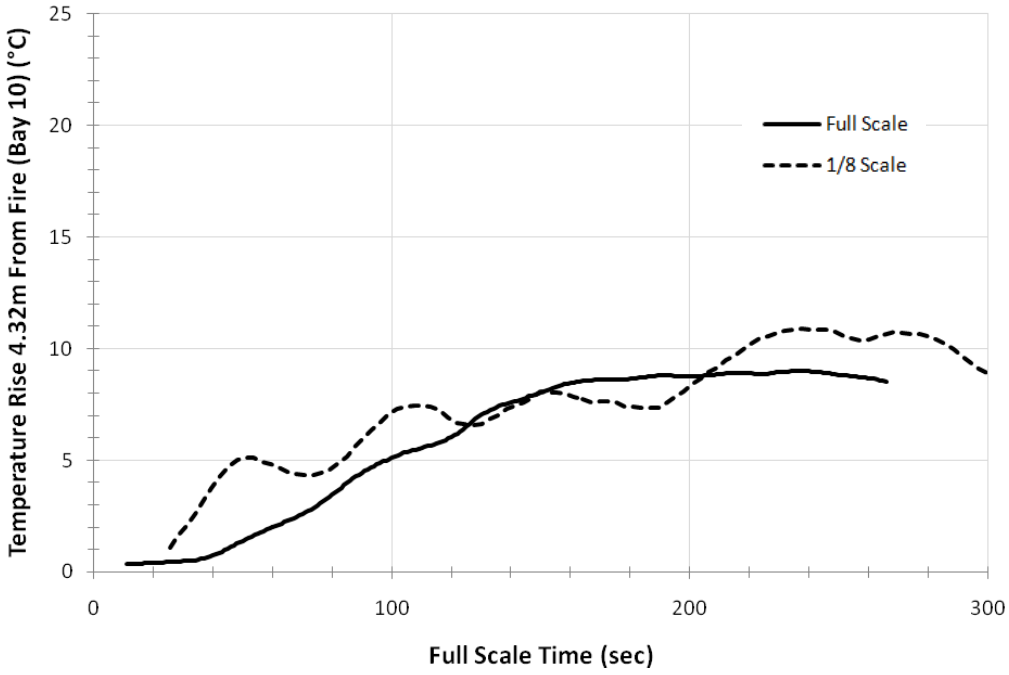

Figure 5.28: Temperature Rise 0.31m From East Wall in Bay 10 for Small Pool Fire.

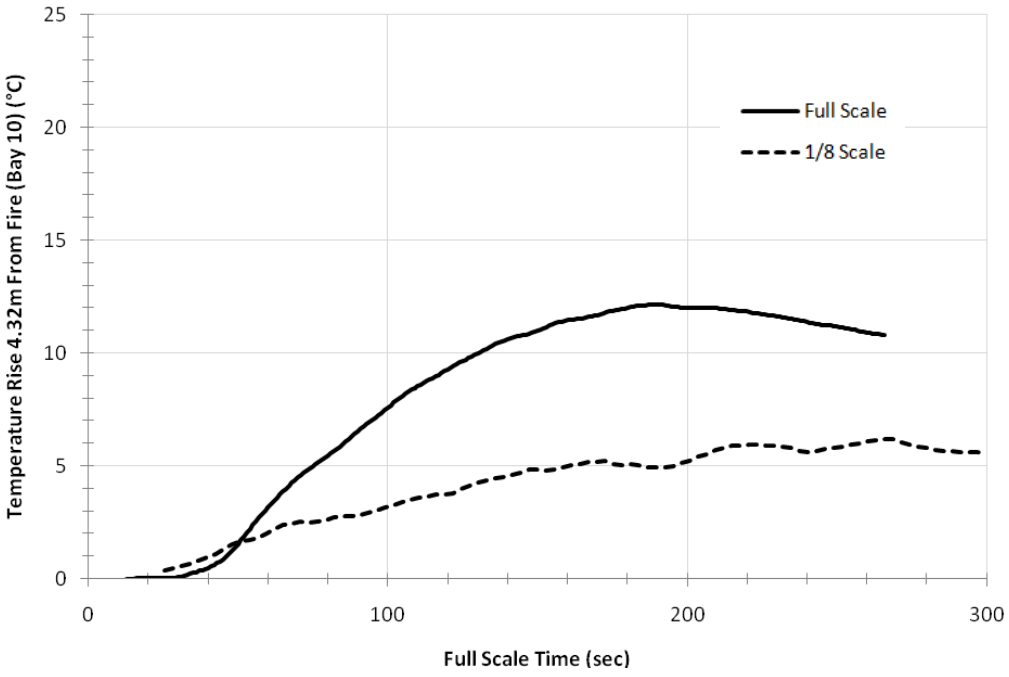

Figure 5.29: Temperature Rise 4.6m From East Wall in Bay 10 for Small Pool Fire.

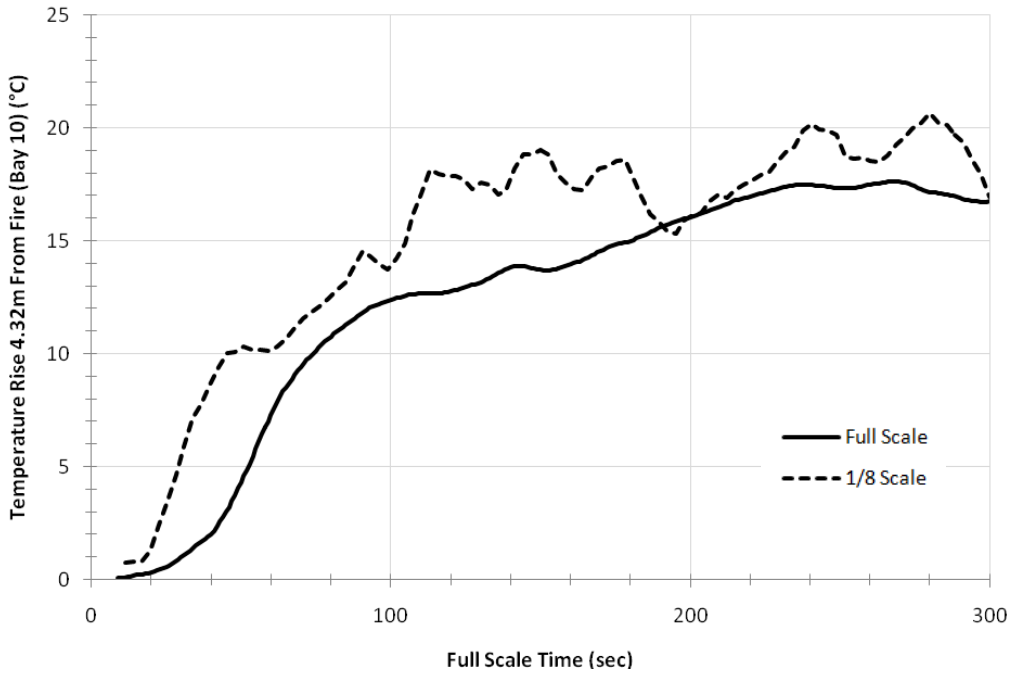

Figure 5.30: Temperature Rise 0.31m From East Wall in Bay 10 for Medium Pool Fire.

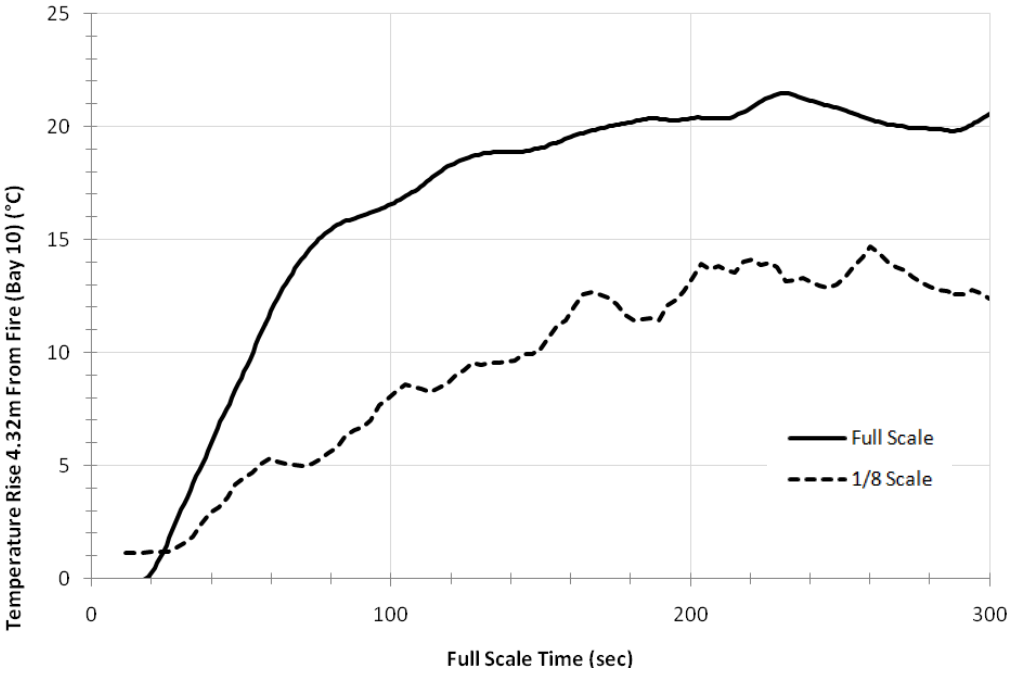

Figure 5.31: Temperature Rise 4.6m From East Wall in Bay 10 for Medium Pool Fire.

It is important to recognize that the bays instrumented with the horizontal thermocouple trees (Bays 2, 4, 10) did not scale as well as the bays closer to the fire. This has a definite impact on the success of the horizontal thermocouple tree scaling.

Future research may want to place additional instrumentation in Bays 13, 15, 16, 17, and 19 since these bays were the most accurate using this scaling methodology.

Temperature Based on Fire Size and Axial Distance from the Fire

Smaller fires for the heptane pool and gas burner have only a few degrees of difference between the ⅛ and full scale data. The larger fires have a much greater discrepancy between scales. For a small burner fire, at 50 kW, the difference in the ⅛ and full scale data is less than 5°C at any given time at 45.7 cm below the ceiling. Figures 5.32-5.34 show the temperatures for the 50 kW fire. Bays 4, 10, and 19 are examined, which provide temperature comparisons both close to and far from the fire. Note that Bay 4 is 8.64 meters from the fire, Bay 10 is 4.32 meters from the fire, and Bay 19 is 2.16 meters from the fire.

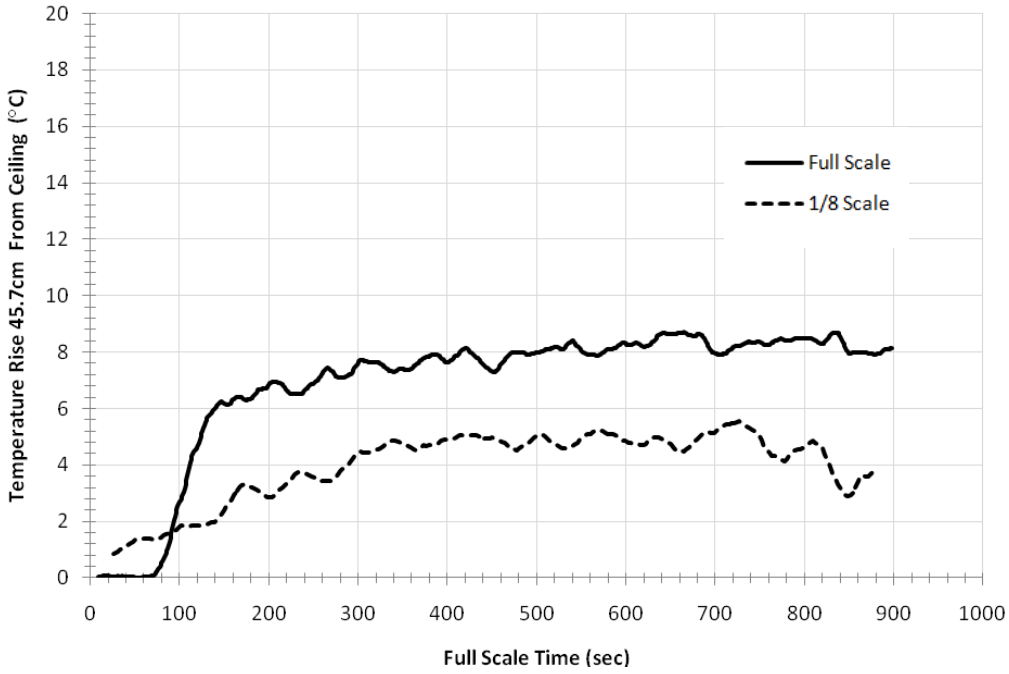

Figure 5.32: Temperature Rise 45.7 cm Below Ceiling in Bay 4 (8.64m away from fire) for 50 kW Gas Burner.

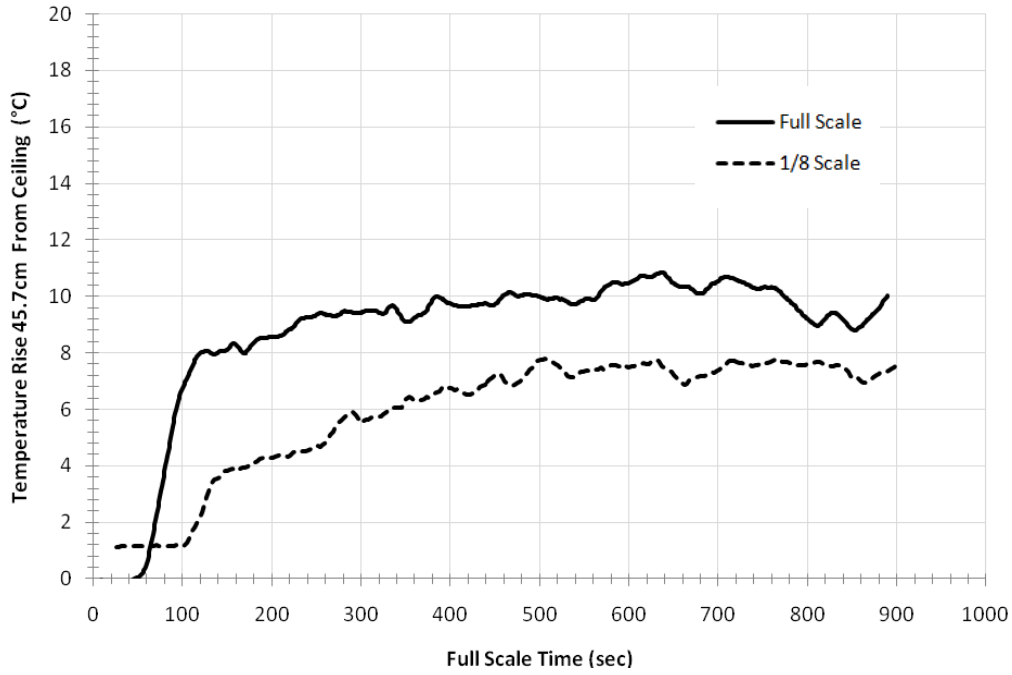

Figure 5.33: Temperature Rise 45.7 cm Below Ceiling in Bay 10 (4.32m away from fire) for 50 kW Gas Burner.

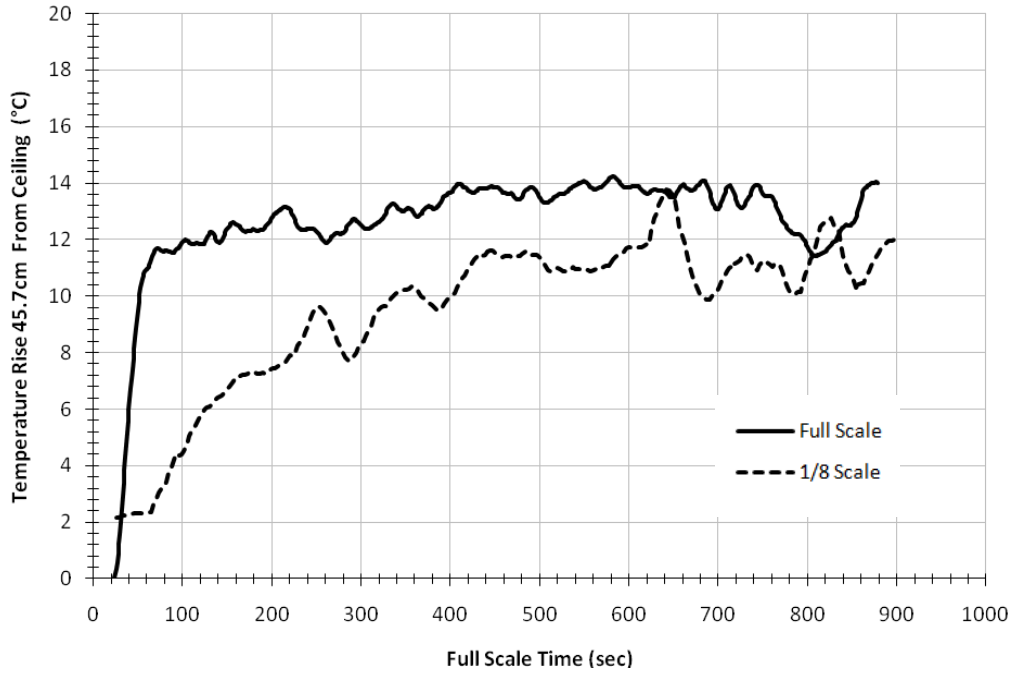

Figure 5.34: Temperature Rise 45.7 cm Below Ceiling in Bay 19 (2.16m away from fire) for 50 kW Gas Burner.

The 250 kW fire had a larger temperature difference between the ⅛ and full scale experiments. Figures 5.35-5.37 shows the temperature differences at these locations

for the 250 kW burner fire. The difference between the full scale and ⅛ scale temperature rise has increased to about 10-15°C.

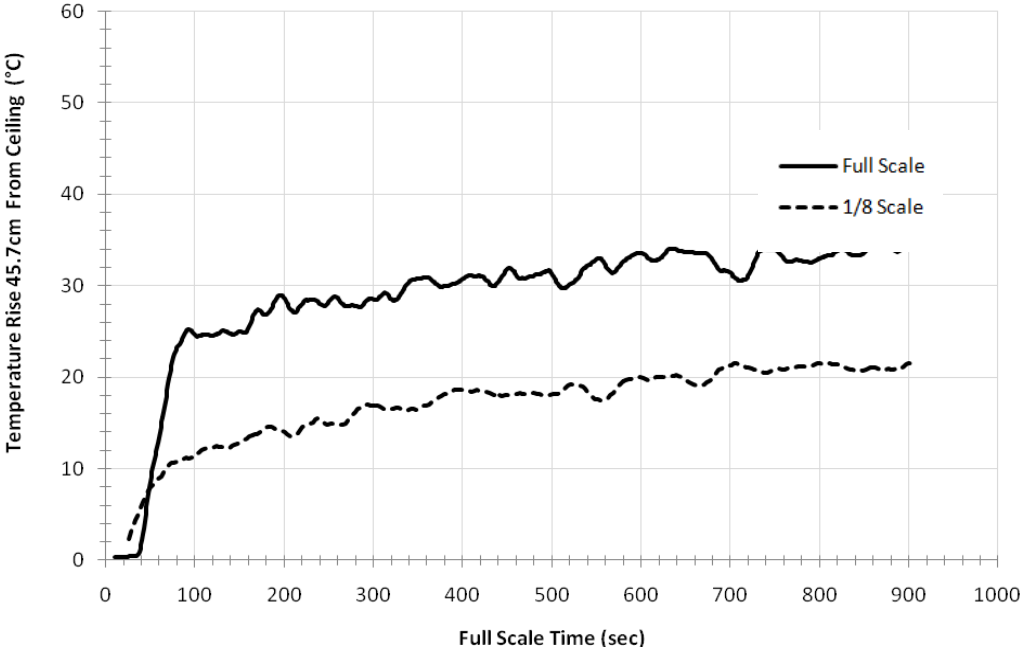

Figure 5.35: Temperature Rise 45.7 cm Below Ceiling in Bay 4 (8.64m away from fire) for 250 kW Gas Burner.

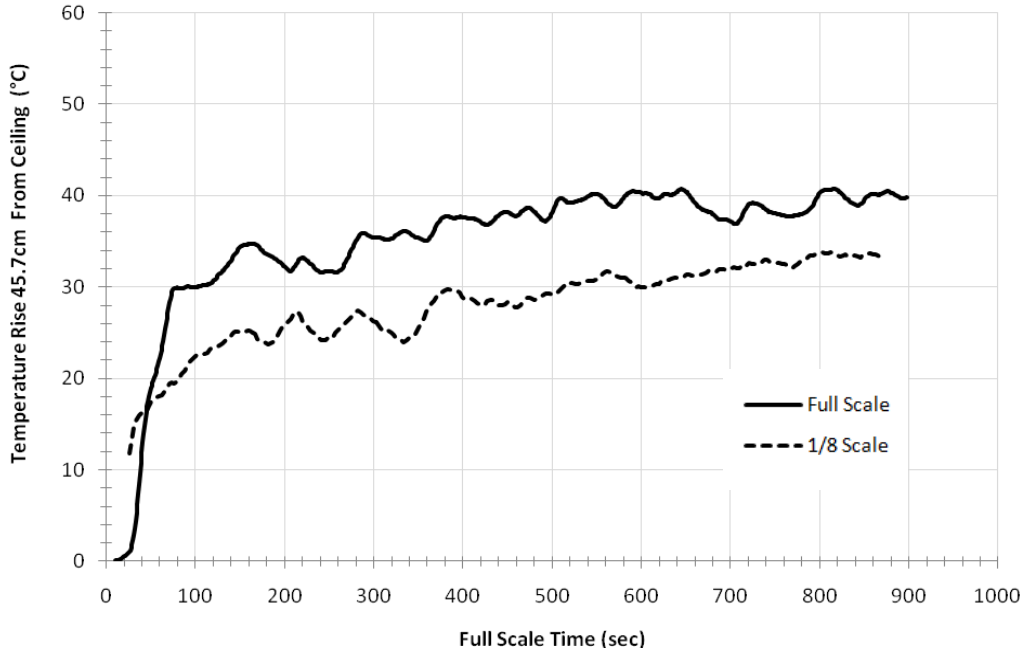

Figure 5.36: Temperature Rise 45.7 cm Below Ceiling in Bay 10 (4.32m away from fire) for 250 kW Gas Burner.

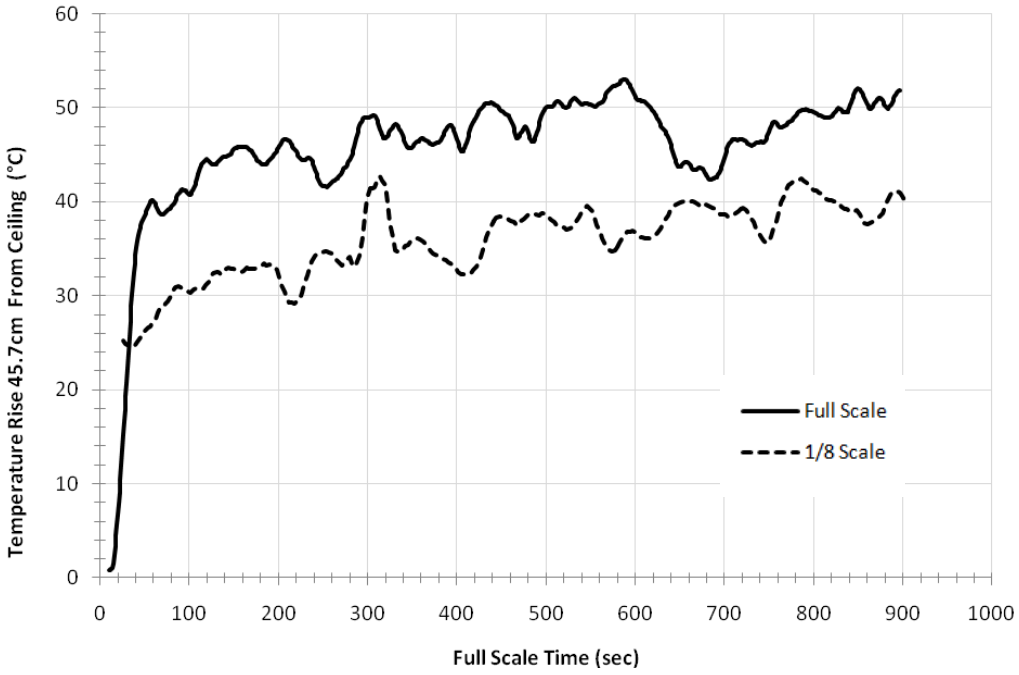

Figure 5.37: Temperature Rise 45.7 cm Below Ceiling in Bay 19 (2.16m away from fire) for 250 kW Gas Burner.

While numerically greater, the temperature differences between scales for larger fires are still relatively close to the differences in temperature for small fires. When the difference is compared to the overall temperature rise, it is seen that the predictive capability of the scale model does not change with fire size.

The accuracy of the model does vary based on the distance from the fire. Some differences exist between the theoretical thermal properties of the boundaries and the actual thermal properties of the boundaries. This causes the heat transfer at the enclosure boundaries to be different between scales. Thermocouples located farther from the fire measure temperatures that have been greatly affected by the numerous partitions. Thermocouples close to the ceiling in bays far from the fire yielded the largest temperature difference between the full and model scale due to heat losses through the boundary materials. While not as accurate as thermocouple measurements closer to the fire, these results still produced values within 20°C of the

full scale data. Figures 5.38-5.42 describe the temperature rise throughout the enclosure for the 250 kW fire. Note: The fire is located in Bay 16.

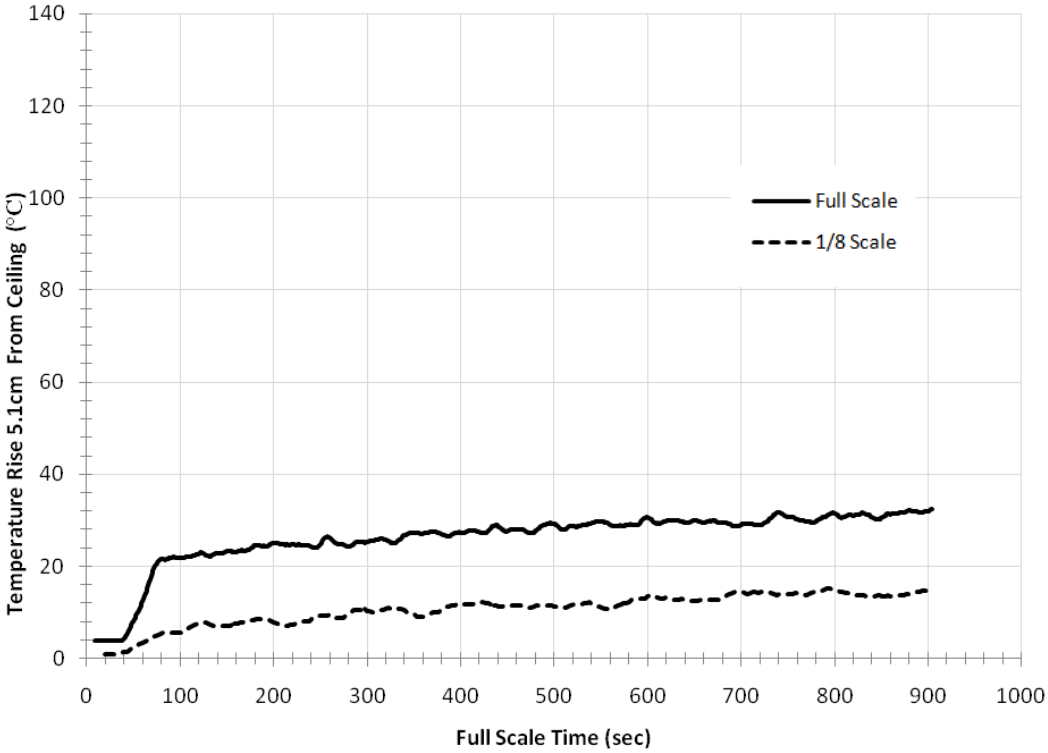

Figure 5.38: Temperature Rise 5.1 cm Below Ceiling in Bay 2 (10.08m away from fire) for 250 kW Gas Burner.

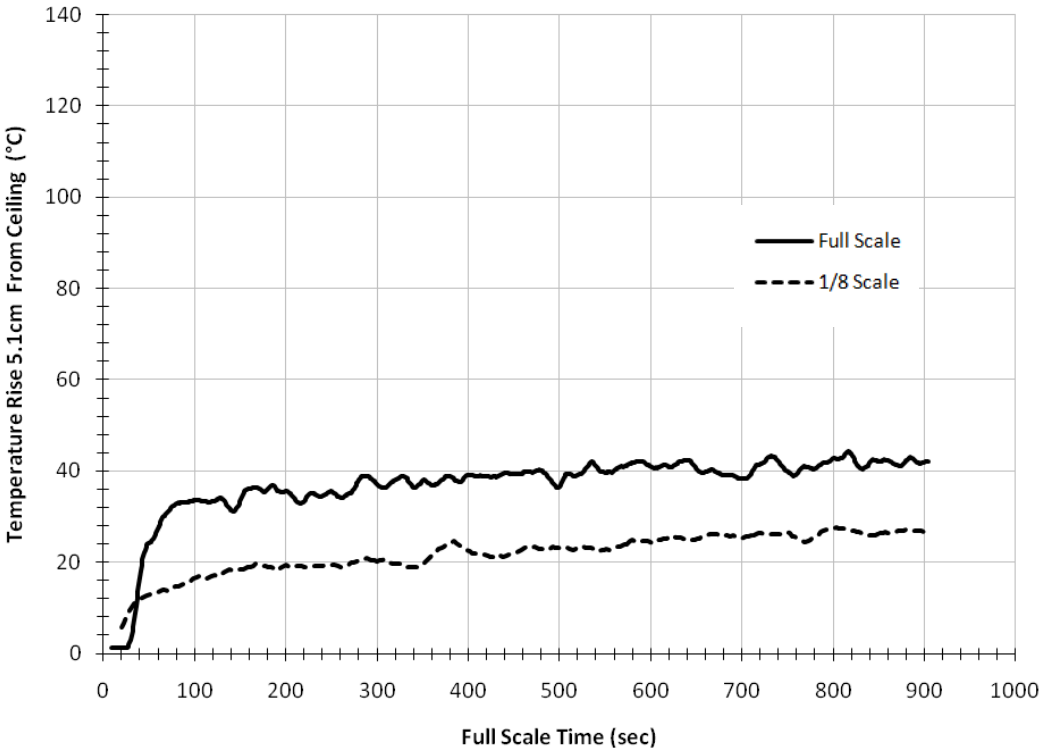

Figure 5.39: Temperature Rise 5.1 cm Below Ceiling in Bay 8 (5.76m away from fire) for 250 kW Gas Burner.

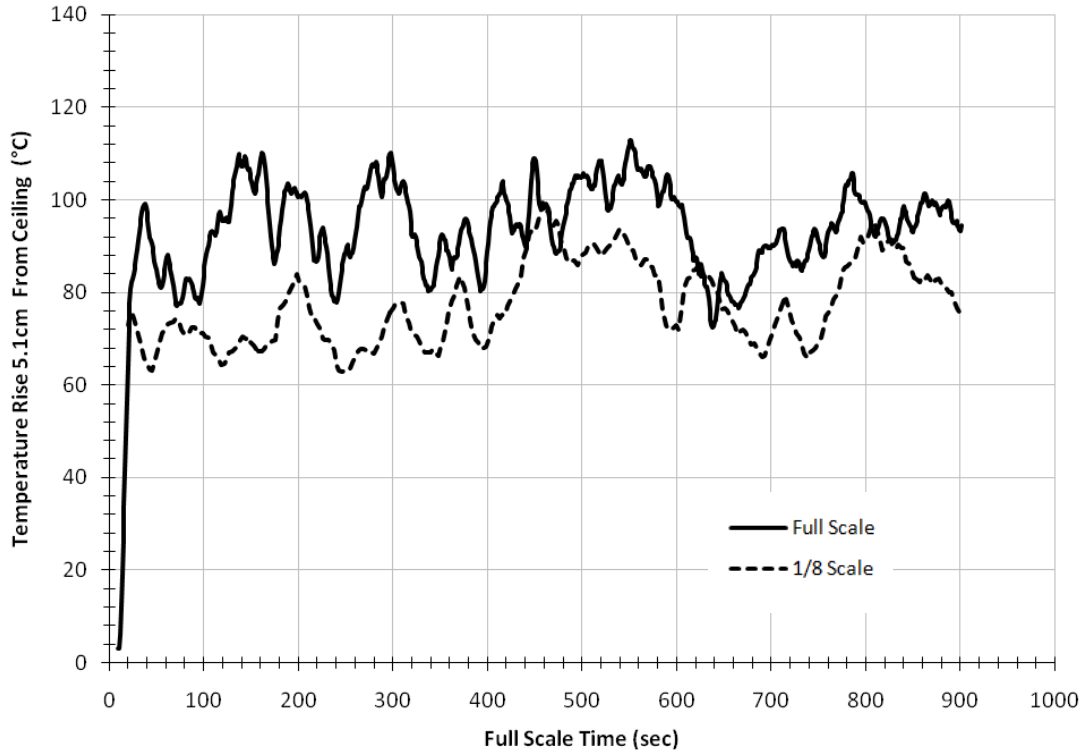

Figure 5.40: Temperature Rise 5.1 cm Below Ceiling in Bay 16 (above fire) for 250 kW Gas Burner.

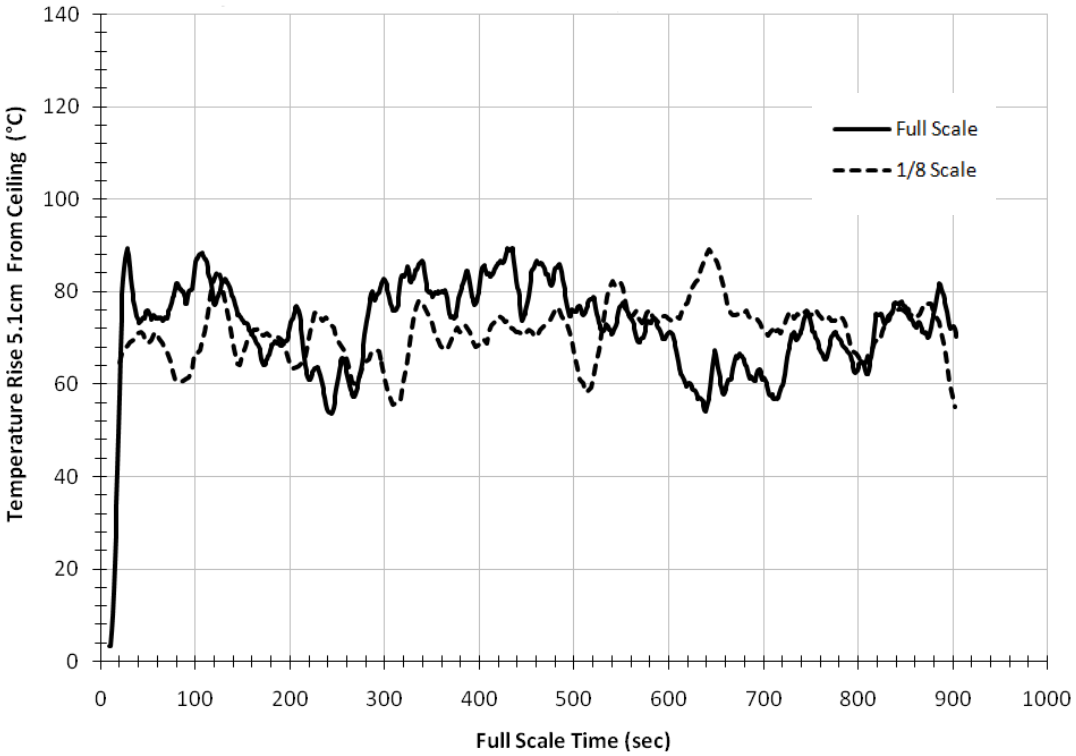

Figure 5.41: Temperature Rise 5.1 cm Below Ceiling in Bay 17 (0.72m away from fire) for 250 kW Gas Burner.

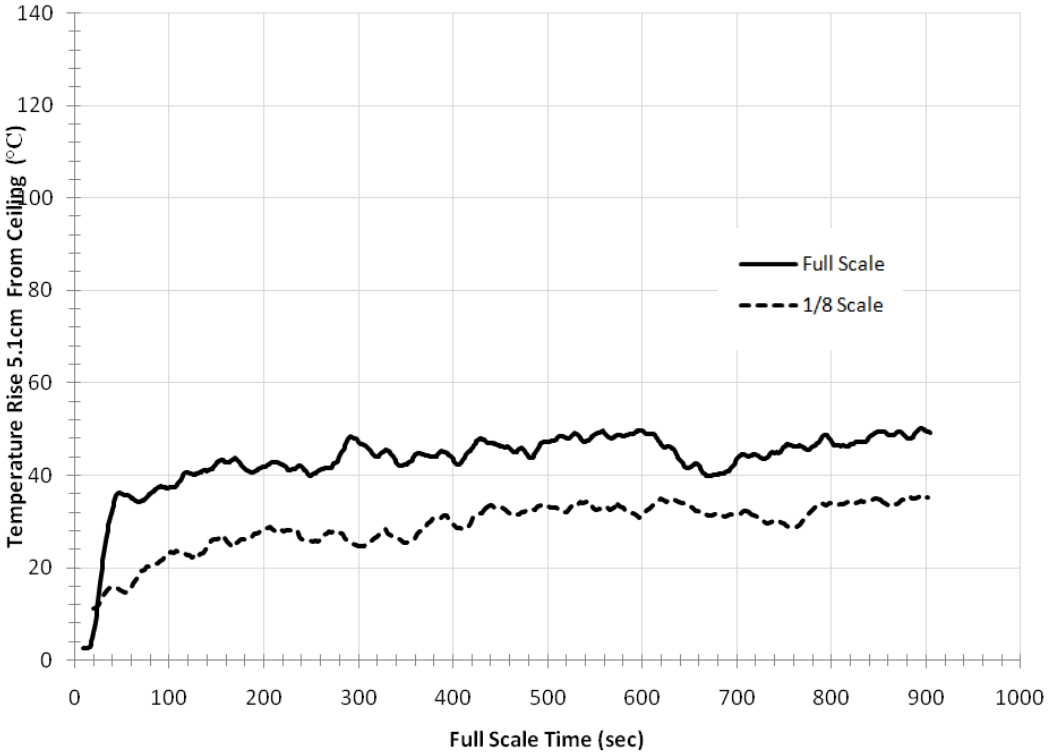

Figure 5.42: Temperature Rise 5.1 cm Below Ceiling in Bay 19 (2.16m away from fire) for 250 kW Gas Burner.

The effect of the material boundaries is seen in these temperature differences. The heptane pool fires followed the same trend; the difference in boundary materials between scales affected the temperature as a function of distance from the fire. This is seen more clearly when the centerline temperatures at steady-state are compared. Figure 5.43 shows the steady-state temperature rise (measured 5.1 cm below the ceiling) in the full scale and the model scale for each instrumented bay in the large pool fire experiments. The fire is located at zero, with the negative distances spanning Bay 2 to Bay 15 and the positive distance spanning Bay 17 to Bay 19. From the differences in these two curves, it is clear that the accuracy of the scale model changes with distance. In other words, the interaction with numerous walls and partitions causes a difference between full and ⅛ scale temperatures due to the scaled boundary materials. As noted in Section 4.3, the scaled density and conductivity of the full scale materials was difficult to match to existing materials. Π_{12} and Π_{13} were compromised slightly in order to construct the scale model. The hot gases in locations close to the fire have not been widely changed by the materials. However, far from the fire, the differences in the heat transfer properties of the material boundaries have affected the hot gas layer for the scale model.

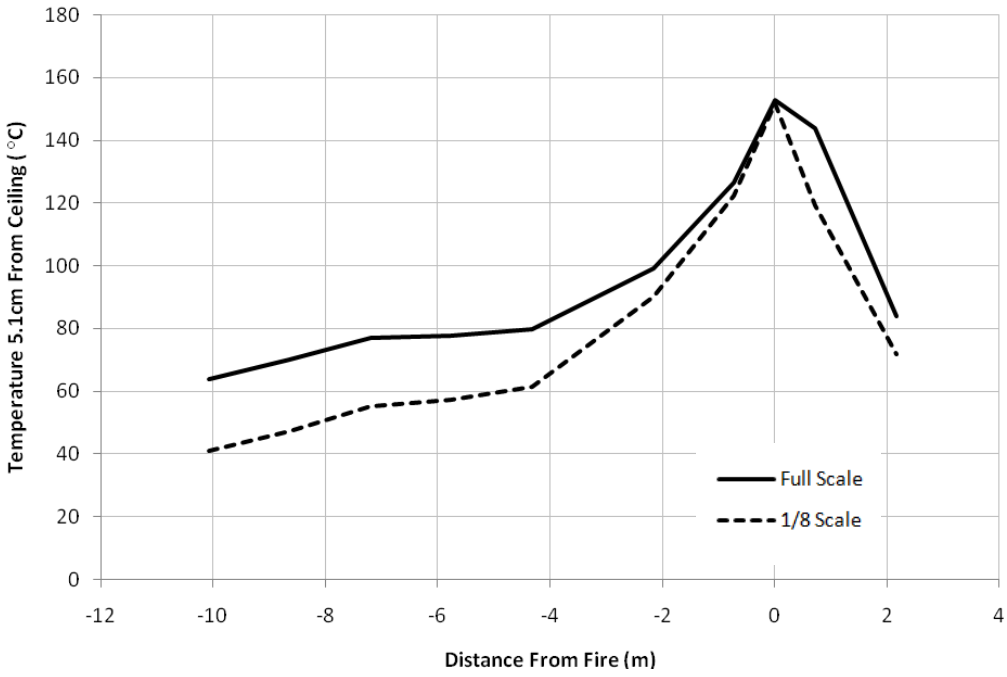

Figure 5.43: Centerline Temperatures for Large Pool Fire at Steady State.

This is also observed for the gas burner, as seen in Figure 5.44. The temperature rise comparison shows the model is accurate close to the fire, but this accuracy decreases with distance from the fire due to material boundaires.

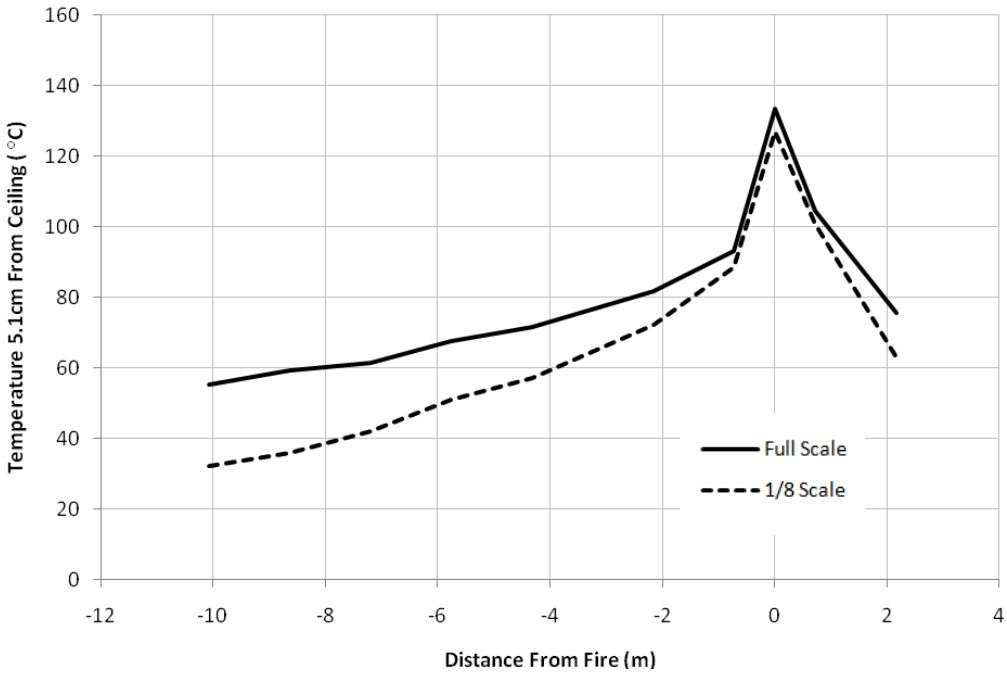

Figure 5.44: Centerline Temperatures for 250 kW Fire at Steady State.

5.2 Fuels

In general, the temperature results were more accurate in the gas burner experiments that in the heptane pool experiments. This is expected since the gas burner has a prescribed burning based on the mass flow of methane. The gas burner was influenced by human error since the mass flow meter used a manually operated value. The burning of heptane is impacted by the characteristics of the pan, the enclosure, and the water in the pan.

5.2.1 Natural Gas Burner

The gas burner was precisely designed to allow the total amount of prescribed flow to be burned evenly across the top surface. In the experiments, the burner was positioned and fixed in order to ensure proper fire locations in each test. It used a mass flow rate determined from the dimensionless heat release rate. This rate, and

therefore the heat release rate of the fire, was accurately modeled for each fire size. As stated earlier, the 25 kW data was not used since a flame could not be sustained with such a low flow (0.214 L/min). The overall success of the gas burner scaling shows that this scaling methodology does work based on the assumptions made in Sections 3 and 4. The model generally resulted in close, but slightly lower temperatures than the full scale model. The difference in temperature rise between the full scale and the ⅛ scale models was a maximum of 10-15°C through all tests and fire sizes. This includes bays at the far end of the enclosure. Some of the slight disparity between scales could be a result of the actual fuel used. Natural gas typically consists of 70-90% methane, with the remainder being a mixture of ethane, propane, butane, carbon dioxide, and other trace gases [27]. Another factor that contributed to the difference in the ⅛ and full scale results is the thermal properties of the enclosure. The difference between the precise density, conductivity, and specific heat calculated by the scaling theory and the actual values of the material used in the scale model result in heat losses over distance. This causes a greater temperature discrepancy in bays farther from the fire. For example, the thermocouples for the model in Bay 2 register temperatures 15°C lower than in the full scale. The flow of hot gases must traverse through 14 bays, causing significant heat losses from the slight differences in boundary materials between the full and ⅛ scale models.

5.2.1.1 Flame Height Comparisons for the Natural Gas Burner

The flame height for the gas burner is modeled accurately for the 250 kW and 300 kW fires (larger fires), but the full scale flames are slightly taller than the ⅛ scale flames for the 50 kW, 75 kW, and 150 kW fires (smaller fires). Figure 5.45 plots the

dimensionless flame height with the dimensionless heat release rate, Q*, for the gas burner.

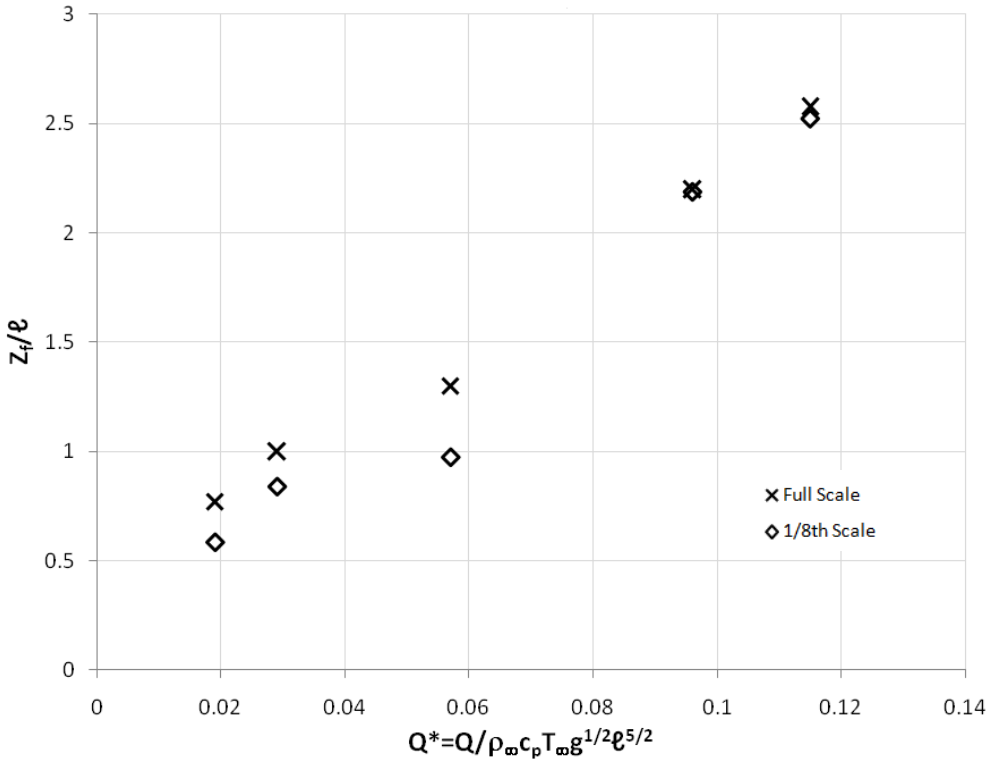

Figure 5.45: Dimensionless Flame Height vs. Q* for Gas Burner.

The flames of the smaller fires in the scale model were very faint and generally laminar (the plume remained turbulent). For a laminar flame, the scaling theory changes slightly. The flame height is proportional to $\dot{Q}$. In a turbulent flame, the flame height is proportional to $\dot{Q}^{2/5}$ [8]. This difference explains the difference in flame height between the model and full scale experiments. The pure methane also contributed to the lower flame height. Figure 5.46 shows the visual flame heights seen in the full scale and the ⅛ scale model. Note that the model flame is difficult to see since it burns so cleanly.

Figure 5.46: Visual Flame Heights for 75 kW Burner in Full and ⅛ Scale.

The actual flame height of the modeled gas burner may have been taller than reported here, but the faint blue flame was difficult to measure.

5.2.1.2 Steady State Temperature Comparisons for the Gas Burner

The transient temperatures for the gas burner experiments have been examined in Section 5.1.6.3. A comparison between the full scale and ⅛ scale model at steady state is provided in Figure 5.47. The graph shows results for 50 kW, 150 kW, and 250 kW at four locations in the enclosure (Bays 2, 13, 16, and 17). The temperatures were averaged over a short period of time during steady state burning. This occurred at 500 seconds since it is during the steady state phase for the gas burner. A perfect scaling theory would result in identical temperatures between the full and ⅛ scales. As seen in Figure 5.47, there is very good agreement between scales in all fires for thermcouples close to the fire. The ⅛ scale temperature measurements from Bay 2 and Bay 13 are slightly off. The full scale temperatures are higher than the model temperatures at these locations. This is due to the differences in the boundary material thermal properties between the full scale and ⅛ model. This can be directly related to the dimensionless group comparison in Section 4.3.1. The boudary Π groups for the

partition material (OSB Chipboard) were both below one, meaning that the model boundary thermal properties are not as high as the full scale boundary themral properties. This results in a difference in temperature measurements in the full and ⅛ scale experiments.

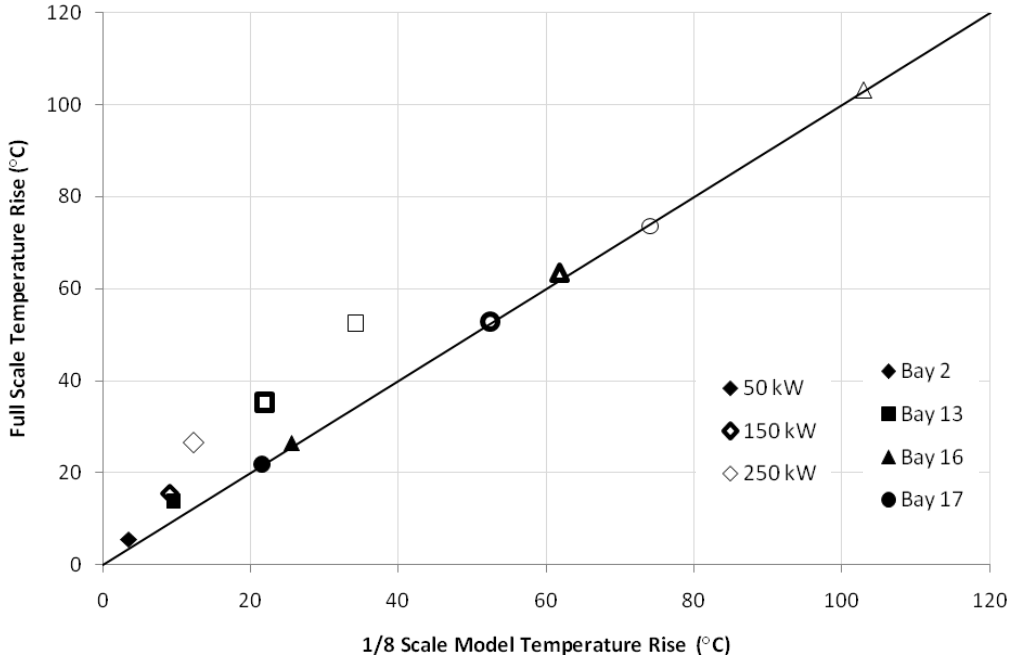

Figure 5.47: Steady State Temperature Comparison for Gas Burner.

5.2.2 Heptane Pool Fire

The ⅛ scale model heptane pools compared reasonably well to the full scale experiment temperature. The pans were constructed out of 0.32 cm thick steel. This may have had an effect on the temperature of the flame and the burning of the heptane due to the high conductivity of steel. The temperature rise in the scale model was slightly faster than the temperature rise in the full scale. This was consistent with each experiment. This was due to the sensitivity of the small gauge thermocouple wire that registered a change in temperature faster than the 28 AWG wire used in the full scale experiments. If a larger wire had been used in the ⅛ scale experiments, a

similar temperature rise growth trend would have occurred between the two scales. The temperature also fluctuates more due to the change in burning rate as a function of time. Unlike the gas burner, the pool fire burning rate is prescribed by the amount of fuel, the thermal properties of the fuel, and the pan dynamics (material, presence of water, etc.). The results of the scale model are still considered a good representation of the full scale experiments.

The temperature discrepancy between models did not vary based on fire size. For the small and medium pool fires, the maximum difference between the small and full scale temperatures was less than 20°C (Bay 17). For the large pool fires, the maximum temperature difference was a factor of two larger, about 40°C (Bay 17). These differences are relative to the overall temperatures reached. Since the large pool fires measured higher overall temperatures, a greater difference between scales is expected. The relative temperature difference was similar for the small, medium, and large pool fires. This is an acceptable representation of the full scale data based on the error associated with the thermal properties of the boundary materials. The scale model generally predicted slightly lower temperatures than the full scale. There are some spikes in the ⅛ scale data due to the fluctuating flame height and the fact that the model time was stretched to full scale by a factor of $\ell^{1/2}$.

The water level in the pan had a significant impact on the burn time, and therefore the mass loss rate, of the heptane fuel. Ideally, the water only provides the heptane with a level burning surface in case of imperfections in the pan. However, burning liquid fuels on water changes the burning characteristics depending on the amount of water present. Unfortunately, there is no current reliable quantification of

the effects of water in burning pools fires. Observations from this experimental series suggest that less water results in a faster burn time since there is less of a heat sink to the fire.

5.2.2.1 Flame Height for Heptane Pool Fire

The flame height for the pool fires is generally accurate for all three fire sizes. Figure 5.48 shows the dimensionless flame height against the dimensionless heat release rate, Q*.

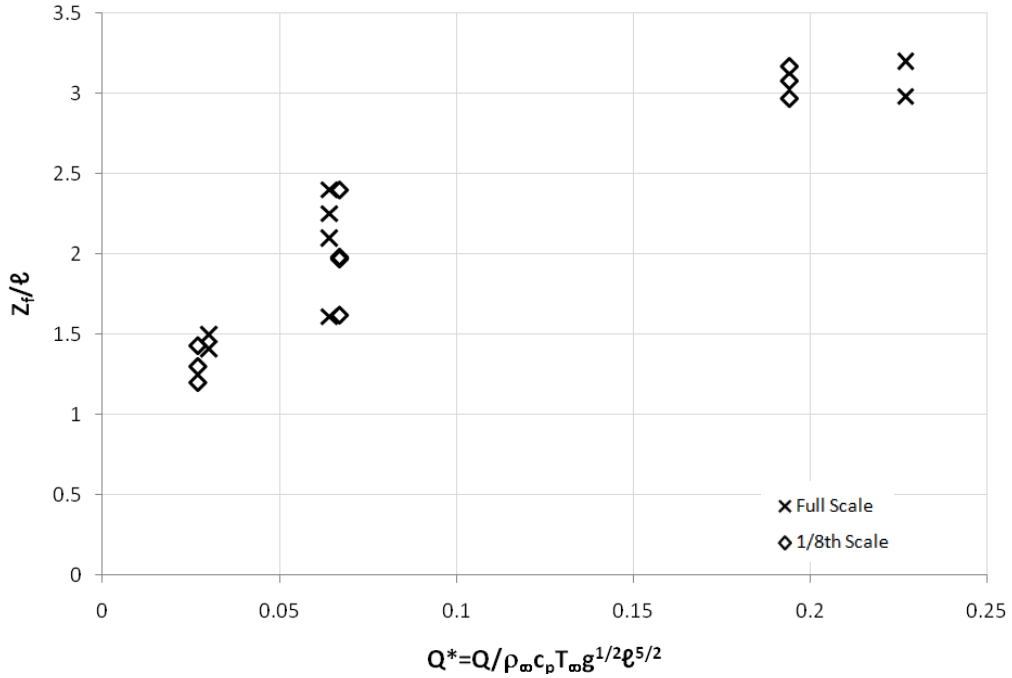

Figure 5.48: Dimensionless Flame Height vs. Q* for Heptane Pool Fire.

This plot displays all the trials from the full and ⅛ scales. The Q* represented in this graph has been calculated based on experimental results. Note that the ⅛ scale fires were designed by matching Q*. The amount of fuel and diameter of the pan were determined before the experiments. Since no load cell was used, the elapsed time and the amount of fuel in the pan were related to a mass loss rate of fuel. From this rough calculation, a heat release rate for the model was estimated. The slight changes in the

Q* values are a result of variations of experiment length and possible human error while measuring the amount of fuel. The small and medium pool fire dimensionless heat release rates were very close to the expected values. The large pool fire had a difference of about 0.03 between the full scale Q* and the scale model Q*. While minor changes are apparent based on the Q* values, the flame height of the full scale experiments is accurately represented by the scaled model.

5.2.2.2 Steady State Temperature Comparisons for Heptane Pool Fire

The transient temperatures for the heptane pool fire experiments have been examined in Section 5.1.6.3. A comparison between the full scale and ⅛ scale model at steady state is provided in Figure 5.49. The graph shows results for small, medium, and large pool fires at four locations in the enclosure (Bays 2, 13, 16, and 17). The temperatures were averaged over a short period of time during steady state burning. This occurred at 150 seconds since it is during the steady state phase for the heptane pool. A perfect scaling theory would result in identical temperatures between the full and ⅛ scales. As seen in Figure 5.49, there is very good agreement between scales for most of the fire sizes and locations. Differences in the boundary material thermal properties between the full scale and ⅛ model account for some discrpancies. This can be directly related to the dimensionless group comparison in Section 4.3.1.

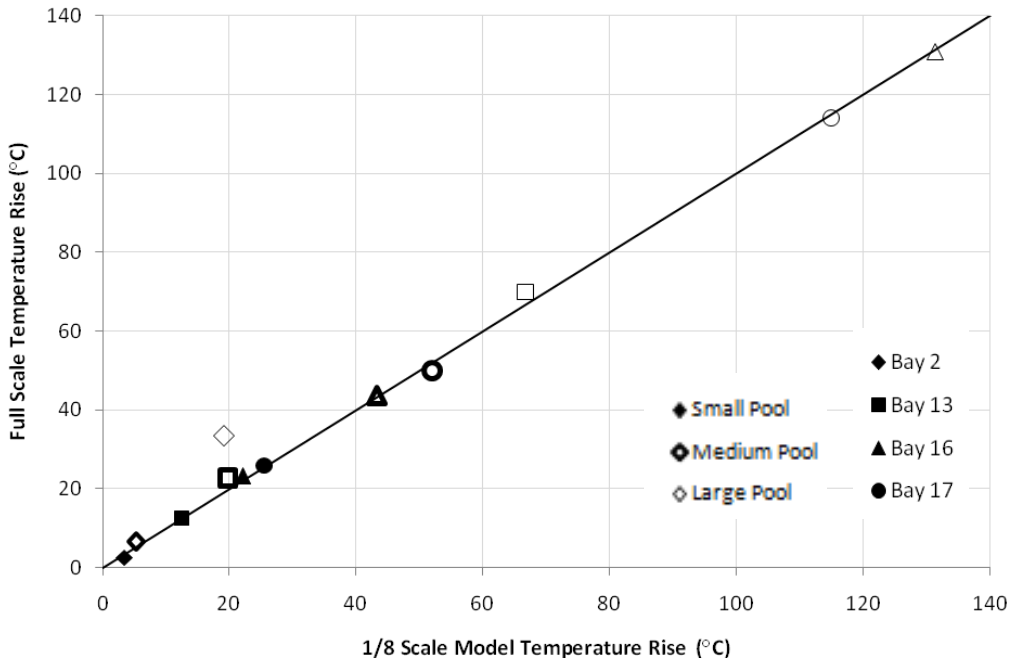

Figure 5.49: Steady State Temperature Comparison for Heptane Pool.

In terms of fire investigation, not all heptane pool fires will be scaled this easily. It is important to note that the surface energy balance for larger turbulent pool fires are driven by radiative feedback [28]. This is very difficult to accurately model since feedback changes based on spatial orientation and temperature of the fire. It has been neglected here since smaller pool fires are convective driven. In cases with larger pool fires, radiation will be a key component in scale modeling and emissivity must be taken into account.

5.3 Consideration of Uncontrolled Independent Variables

The assumptions that are made when deriving the dimensionless groups and constructing the scale model do have an effect on the results presented here. The largest factor that was assumed negligent in the conservation equations was radiation. The two fuels used here reached steady-state quickly; flame spread and fire growth were not the main factors as they are with the wood crib and PU foam. Based on the

fuels, the fires in the enclosure are convection driven fires. In the methodology presented here, radiation is intrinsically accounted for in the scaled heat release rate. This means that the thermocouples above the fire experience comparable radiation to the full scale.

The selected boundaries of the enclosure have an impact on the inside temperatures. In fact, the majority of the temperature discrepancies in this experimental series are related to the imperfect boundary materials. Density, specific heat, and conductivity were scaled independently, yet the availability of materials that meet such specific values limits the accuracy of boundary scaling. The scaled thickness of the boundaries also changes the temperature measured in the enclosure due to thermal penetration. In this research, the boundary materials had a significant impact on temperature measurements far from the fire. This was magnified due to the numerous partitions that affected heat transfer within the enclosure. In every scale model, the limitations of finding the "perfect" boundary materials affect the results. The true art of scaling comes from minimizing the errors associated with such compromise.

The thermocouples were scaled to a 40 AWG wire in order to reduce error of having such a large wire in a ⅛ scale model. The wire diameter prescribed by the dimensionless group was not manufactured, so a slightly larger diameter wire was used. Thermocouples of all sizes have an associated error between the measured bead temperature and the actual gas temperature. This diminishes with smaller thermocouples, but still exists in 40 AWG wire. The thermocouples used in the ⅛ scale model measure a temperature very close to the actual gas temperature. This is

one reason why the model temperature data fluctuates significantly more than the full scale temperature data. If similar flow time of the thermocouple, and therefore similar signal error, is desired in the model, the same size thermocouples are appropriate. Using 28 AWG thermocouples in this scale model may have resulted in a similar response time to temperatures. The sensitivity of the 40 AWG thermocouples caused some ⅛ scale results to have a steeper initial growth than the 28 AWG thermocouples in the full scale experiments.

6. Conclusions

This report is part of a larger research effort to provide fire investigators with the necessary tools to utilize scale modeling. The research examines four fuel sources; a gas burner, liquid pools, wood cribs, and polyurethane foam blocks. These fuels were selected to represent the various fuels that are found in fire investigations. This particular study examined the steady gas burner and liquid pool fires in a complex geometry.

Froude modeling was applied in a ⅛ scale compartment. The design fires were convection driven; therefore radiation was neglected in this research. 40 AWG Type K thermocouples were used to record temperature as a function of time. The thermal response of the enclosure had a significant impact on the overall simulation results. The model was constructed using Kaowool and Marinite products. The conductivity, density, and specific heat of these materials differed slightly from the thermal properties calculated using the scaling theory. The temperatures recorded in the ⅛ model were slightly lower than the full scale values due to this difference. The gas burner and the heptane pans were specially designed and constructed for this research. The burner was scaled geometrically and ensured an even dispersion of the gas. The heptane pans were made to match the Q* from the full scale experiments, which changed with the diameter of the pan.

Gas temperature scaling results for the natural gas burner and heptane pool fire were generally well scaled. Distance was a factor in scaling accuracy due to the material boundaries. The best results were directly above the fire ± 2 bays. The burner scaled better than the heptane pool due to the prescribed mass flow rate of the fuel.

The transient temperature measurements showed similar trends for both fuels. Some discrepancy existed in the model because a more temperature sensitive thermocouple was used.

The heptane pool yielded excellent flame height results. The behavior, shape, color, and turbulence of the flame were also successfully scaled. The smaller gas burner fires produced laminar flames in the scale model, which resulted in a lower flame height. The larger gas burner experiments in the scale model produced flame heights that were in very good agreement with the full scale. Using pure methane instead of natural gas had some effect of the flame height. The steady state comparisons of temperature between the full and ⅛ scale models showed that the scaling laws applied are very accurate close to the fire. In locations far from the fire, the full scale temperatures were higher than the scale model. This is due to the heat transfer differences in the boundary materials.

Future research will include the scaling of the pine wood crib and the PU foam blocks. Porosity, stick spacing, and stick thickness will play a major role in the scaling of the wood crib. The density of the foam, among other thermal properties, will most likely play a role while scaling the PU foam blocks since it impacts the flame spread velocity across the surface. It is important to note that these fuels produce dynamic fires where radiation and flame spread must be considered in the scaling methodology. Accurate wood crib scaling has been accomplished by Perricone [15], whose work would make an excellent starting point for future development on this project. The PU foam must be considered carefully with respect to flame spread. Dr. William Pitts at the National Institute of Standards and

Technology has completed work with foam mattresses that would also benefit future research.

Understanding how to accurately model convection driven fires provides fire investigators with the tools to recreate many fire scenarios. It is especially helpful in fires leading up to flashover or where detection plays a major role in the investigation. The dimensionless groups presented in this thesis are an accurate method to model a full scale fire static fire. Future research will provide investigators with theory to create scale models of fires where flame spread and fire growth play key roles.

Appendix A

Dimensions and Geometry of Full Scale Enclosure (meters)

Plan View: Outer Dimensions

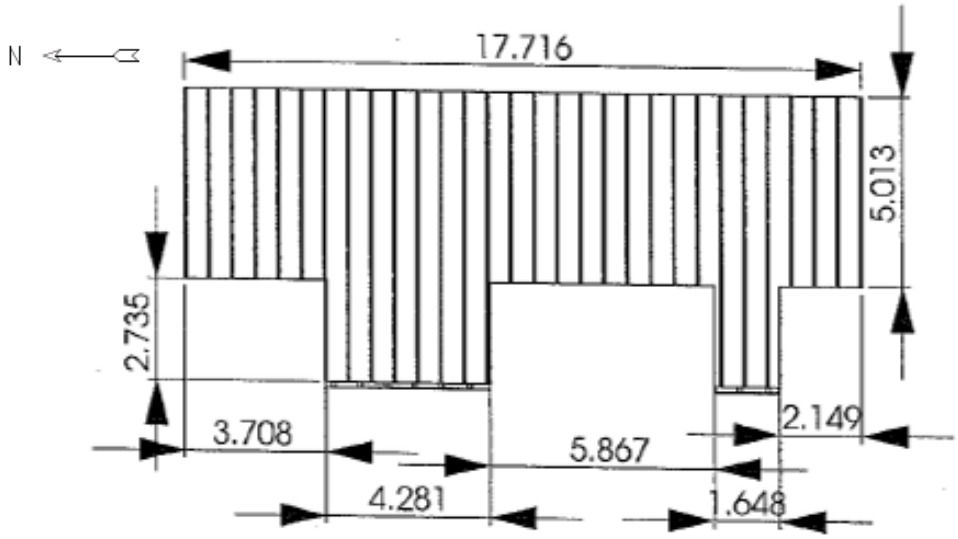

Plan View: Elevation of Enclosure

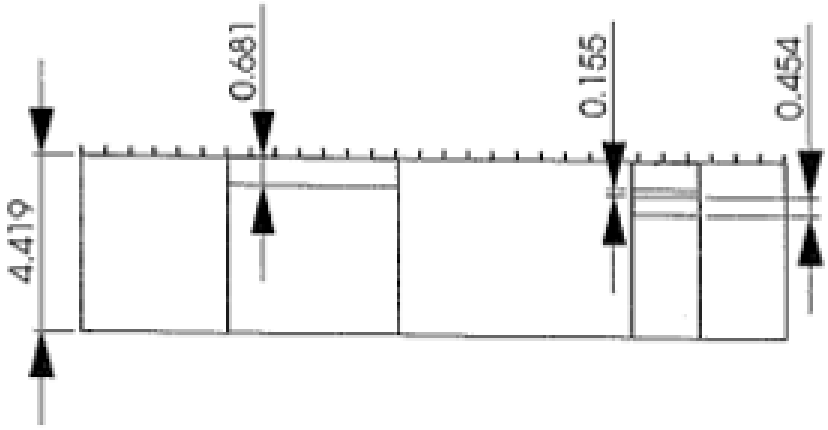

Plan View: Partitions Throughout Enclosure

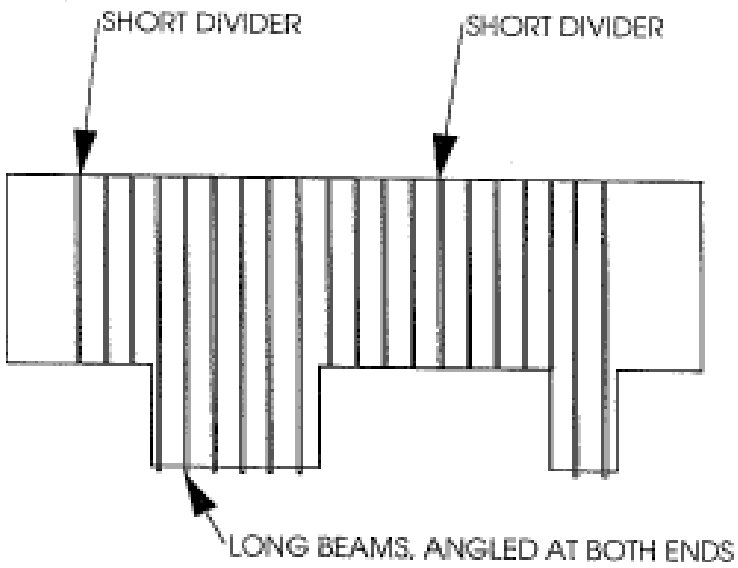

Side View: Partition Locations from Northeast Corner of Enclosure

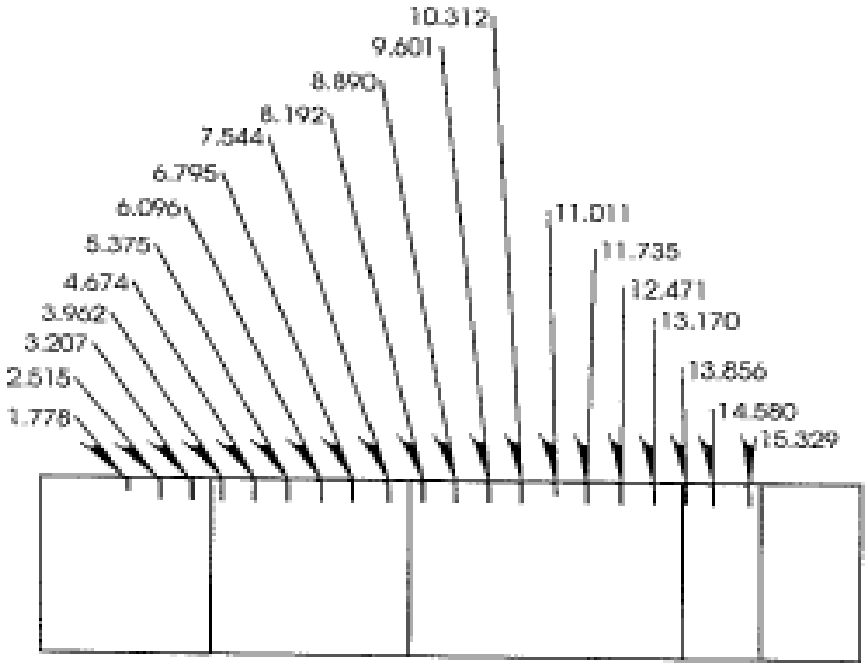

Partition Geometry: Angle and Depth

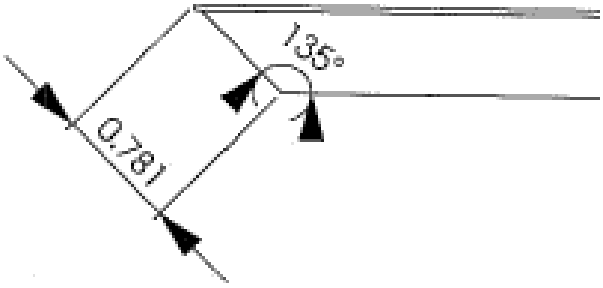

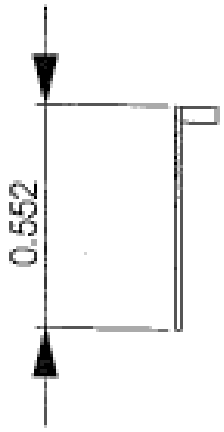

Depth of Long Divider

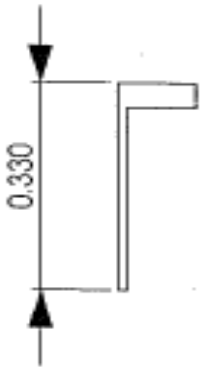

Depth of Short Divider

Instrumentation and Location in Full Scale Enclosure

Temperature: 28 AWG Type K Glass Insulated Thermocouples

- Vertical Thermocouple Trees: All Bays
  5.1cm, 15.2 cm, and 45.7 cm below ceiling
  2 m from East Wall
  Center of Bay
- Horizontal Thermocouple Trees: Bays 2, 4, 10
  0.3 m below ceiling
  15 thermocouples; 1 TC every 0.31 m
  Center of Bay

Velocity: Hot Wire Anemometer

- Bays 2, 6, 13, 19
  15.2 cm below Ceiling
  1.8 m from East Wall
  15.2 cm from South Side

Obscuration: Optical Density Meter

- Bays 2, 6, 13, 19
  Attached to Ceiling (East-West)
  2.3 m from East Wall
  Centered in bay

Detection: Ionization and Photoelectric Smoke Detectors

- Bays 2, 6, 13, 19
  Three Detectors Attached to Ceiling (North-South)
  1.5 m from East Wall
  Order: Ionization, Photoelectric, Ionization
  Centered in bay

Bibliography

1. Saito, K., “Progress in Scale Modeling,” *International Symposium on Scale Modeling*, 1988-2006.
2. Wang, M., Perricone, J., Chang, P.C., Quintiere, J.G. ,“Scale Modeling of Compartment Fires for Structural Fire Testing,” *Journal of Fire Protection Engineering*, **18**, 2008, p.223-240.
3. Samali, B., Kwok, K.C.S, Wood, G.S., Yang, J.N., “Wind Tunnel Tests for Wind-Excited Benchmark Building,” *Journal of Engineering Mechanics*, **130(4)**, 2004, p. 447-450.
4. Rosin, P.O., "The Aerodynamics of Domestic Open Fireplaces", *Journal of the Institute of Fuel*, **12**, 1939, pp. 198-224.
5. Spalding, D.B., “The Art of Partial Modeling,” *Proc. Combustion Inst*., **9**, 1963, p. 833.
6. Williams, F.A., Fire Research Abstracts and Reviews, **11**, 1969, p.1-22.
7. Thomas, P. H., “Dimensional Analysis: A Magic Art in Fire Research”, *Fire Safety Journal*, **15**, 1989, p. 3-29.
8. Quintiere, J.G., Private Communications, University of Maryland, 2009.
9. Gross, A.F., and Robertson, D., “Experimental Fires in Enclosures,” *Combustion Institute Symposium on Combustion*, 1965, p.931-942.
10. Quintiere, J.G., McCaffery, B.J., and Kashiwagi, T., “A Scaling Study of a Corridor Subject to a Room Fire,” *The 17th National Heat Transfer Conference*, 1977.

11. Heskestad, G., "Similarity Relations for the Initial Convective Flow Generated by Fire," *The American Society of Mechanical Engineers, Heat Transfer Division*, 1972.
12. Heskestad, G., "Modeling of Enclosure Fires," *The Combustion Institute- 14th Symposium on Combustion*, 1973, p. 1021-1030.
13. Croce, P.A. and Xin, Y., "Scale Modeling of Quasi-steady Wood Crib Fires in Enclosures," *Fire Safety Journal*, **40**, 2005, p. 245-66.
14. Block, J.A., "A Theoretical and Experimental Study of Non-propagating Freeburning Fires," *The Combustion Institute- 13th Symposium on Combustion*, 1971, p.971-978.
15. Perricone, J., Wang, M., Quintiere, J., "Scale Modeling of the Transient Thermal Response of Insulated Structural Frames Exposed to Fire," *Fire Technology*, **44**, 2008, p. 113-136.
16. Quintiere, J. G., *Fundamentals of Fire Phenomena*, Wiley, p. 377-403, 2006.
17. Incropera, F. P., Dewitt, D. P., *Fundamentals of Heat and Mass Transfer*, *4th Edition*, Wiley, 1996, p. 374, p. 398.
18. Quintiere, J. G., "Scaling Applications in Fire Research," *Fire Safety Journal*, **15**, 1989, p. 3-29.
19. Batchelor, G.K., "An Introduction to Fluid Dynamics," *Cambridge University Press*, 1967.
20. "Thermal Conductivity of Common Materials," August 2009, < http://www.engineeringtoolbox.com/thermal-conductivity-d_429.html>.

21. “Kaowool ® High Temperature Boards,” *Thermal Ceramics*, August 2009, <http://www. thermalceramics.com/pdfs-uploaded/datasheets/americas/514-715.pdf>.
22. “Structural Insulations Summary Data,” *BNZ Materials Inc*., August 2009, <http://www.bnzmaterials.com/datasi.html>.
23. “2640A/2645A NetDAQ Fluke User’s Manual,” Fluke Corporation, 1996.
24. Linteris, G.T., and Rafferty, I., “Scale Model Flame for Determining the Heat Release Rate from Burning Polymers,” *National Institute of Standards and Technology*, 2008.
25. Hill, K., Dreisbach, J., et al., “Verification and Validation of Selected Fire Models for Nuclear Power Plant Applications: Volume 2: Experimental Uncertainty,” *U.S. Nuclear Regulatory Commission*, NUREG-1824, 2007.
26. Trochim, W.M.K., “The T-Test,” 2006, March 2010, <http://www.social researchmethods.net/kb/stat_t.php>.
27. “Background of Natural Gas,” *Natural Gas Supply Association*, March 2010, < http://www.naturalgas.org/overview/background.asp>.
28. Orloff, L., and De Ris, J., “Froude Modeling of Pool Fires,” *The Combustion Institute- 19th Symposium on Combustion*, 1982, p. 885-895.